Doctoral Dissertation

Development of Polygonal Buffer Rods for Ultrasonic Pulse-Echo Measurements with High Signal-to-Noise Ratio

高いＳＮ比を有する超音波パルスエコー計測のための多角形バッファーロッドの開発

Farhana Binti Mohd Foudzi
(12700386)

Materials Science Course
Graduate School of Nagaoka University of Technology
Nagaoka University of Technology
Supervisor: Prof. Ikuo Ihara

Abstract

In ultrasonic pulse-echo measurements with a long cylindrical buffer rod, it has been known that spurious echoes (also known as trailing echoes) are often generated due to diffraction and mode conversion of ultrasonic waves within the rod of a finite diameter. From the cross-sectional view of a cylindrical buffer rod, it is found that such trailing echoes are generated when the mode converted waves are parallel to each other and propagate to the side wall of the rod perpendicularly. Such trailing echoes are considered as noise and therefore, they deteriorate the signal-to-noise ratio (SNR) in the pulse-echo measurements because of their possible overlapping with the main echo while a pulse-echo measurement is being performed. Although tapering or cladding for the cylindrical buffer rod may be effective to reduce such trailing echoes, they are not always sufficient for practical uses of the buffer rod. In this work, a new idea of using polygonal buffer rods has been proposed as an alternative method to reduce the trailing echoes and result in improving the SNR. The idea is basically to use a polygonal rod whose normal sectional shape is a polygon such as a triangle, square, pentagon, hexagon or heptagon. The effectiveness of such polygonal rods is examined numerically and experimentally. It is found from a three-dimensional numerical simulations based on a finite difference method that ‘odd polygons’ having sides any one of which is not parallel to any of the other sides, such as triangle, pentagon and heptagon, are effective to reduce the trailing echoes because of less interferences among mode converted waves in the rod. However, there still exists a certain amount of trailing echoes even in the odd polygonal rods where such trailing echoes are generated by the possible interference of the waves due to the bilateral symmetry shape of the odd polygons. In order to eliminate such remaining trailing echoes, the idea of using irregular polygons is proposed. Since the symmetry shape of the polygons results in generating trailing echoes, such generation can be prevented by distorting one vertex of the regular polygon. By such distortion, the influence of symmetry is eliminated. The effectiveness of such irregular polygonal buffer rods on restraining the generation of trailing echoes is numerically and experimentally

investigated. It is found that the trailing echoes are completely eliminated with the irregular pentagon and the SNR is five times higher than the regular pentagon. Furthermore, cladding effect on the reduction of the trailing echoes is also investigated. It is found that the trailing echoes are reduced when the velocity of cladding layer is faster than that of the core and the highest SNR can be obtained when V_{clad} = 120% V_{core} and ρ_{clad} = 70% ρ_{core}. Based on such investigation, it has been demonstrated numerically that polygonal buffer rods with an optimum cladding layer provide higher SNR as expected. Thus, it is highly expected that the polygonal buffer rods proposed in this work can be promising tool for advanced ultrasonic measurements and evaluations.

Acknowledgement

I would like to say thank you to my supervisor, Prof. Ikuo Ihara for his endless guidance, advice, helpful discussions and support throughout my studies in Nagaoka University of Technology. To my examiners; Prof. Hideo Koguchi, Associate Prof. Yukio Miyashita, Associate Prof. Hiroo Taura and Associate Prof. Takahiko Kurahashi, a heartful appreciation and thank you for the endless opinions and benefit discussions during my first and second defenses. To Assistant Prof. Iwao Matsuya and my laboratory members, thank you for the endless help regarding studies, lab works and living in Japan, despite of the language barrier. In addition, a special appreciation to my fellow doctoral lab mates, Akira Kosugi and Muhammad Nur Farhan for their endless motivation and morale support throughout my journey in obtaining a doctoral degree. In addition, thank you to Majlis Amanah Rakyat (MARA) for giving me the opportunity to further my study in Japan. Finally, thank you to my beloved mother; Umi Kathom Shafii, aunt; Mazni Buyong and sister; Hazwani Foudzi for their endless prayers for my success.

Table of Contents

Table of Contents

Chapter 1

Introduction

Ultrasound, due to its ability that can probe any surface or object nondestructively, makes it a promising candidate for the material characterization or process monitoring of industrial processes at elevated temperature. In this chapter, the principle of ultrasound is presented. In addition, the common measurement methods using ultrasound are presented.

1.1 Introduction of ultrasound

Increasing demands of high quality end products enhance the needs to monitor the production of the industrial processes that are normally conducted at high temperature. Although the conventional method such as thermocouple is capable for such monitoring, however, thermocouple is sometimes not stable, non-repeatable, and gives a slow response. For a precise measurement and monitoring of a manufacturing process, a fast response, robustness, repeatable and does not disturb the production line is desired. For such approach, ultrasound is a suitable tool for measuring material properties or process monitoring due to its capability to interrogate the internal parts of materials nondestructively [1-7]. Ultrasound, also known as sound waves, propagates at a frequency greater than 20,000Hz and sensitive to any disturbance in the elastic mediums such as solids, liquids and gases. When the ultrasonic waves encounter any boundary or medium that has different acoustic impedance, the ultrasonic waves will be reflected. The degree of reflection depends on the acoustic impedance of a medium.

1.2 Acoustic impedance

Acoustic impedance is a product of density and velocity of a material. The sound waves with high frequency (ultrasound) travel through material under the influence of sound pressure that is caused by the molecules in the medium. The acoustic impedance is given in Equation 1.1,

$$Z = \rho V \tag{1.1}$$

where Z, ρ and V are acoustic impedance (Pa.s/m^3), density (kg/m^3) and velocity (m/s), respectively. Since each material has its distinctive velocity and density, the acoustic impedance for each material can be calculated.

1.3 Reflection and transmission

1.3.1 Normal angle

When an ultrasonic wave perpendicularly impinges on an interface between two mediums, as shown in Figure 1-1, a part of the wave is reflected back into medium I at

normal angle. While, the remaining part of the incident wave is transmitted into medium II. Such phenomenon is because the incident wave encounters an interface with different acoustic impedance (impedance mismatch). The amount of ultrasonic waves (energy) that are reflected at a boundary can be calculated in percentage (%). The greater the impedance mismatch, the greater the percentage of energy that will be reflected at the boundary between one medium or more. The degree of reflection is given by Equation 1.2,

$$R = \left[\frac{Z_2 - Z_1}{Z_2 + Z_1}\right]^2 \text{ x } 100\% \qquad (1.2)$$

where R, Z_1 and Z_2 are reflection, acoustic impedance for the first medium and acoustic impedance for the second medium, respectively. The reflected amount of reflected energy plus with the transmitted energy must equal to the amount of incident energy. Therefore, the amount of transmitted energy can be simply calculated by Equation 1.3 where T and R are transmission and reflection, respectively.

$$T = (1 - R) \text{ x } 100\% \qquad (1.3)$$

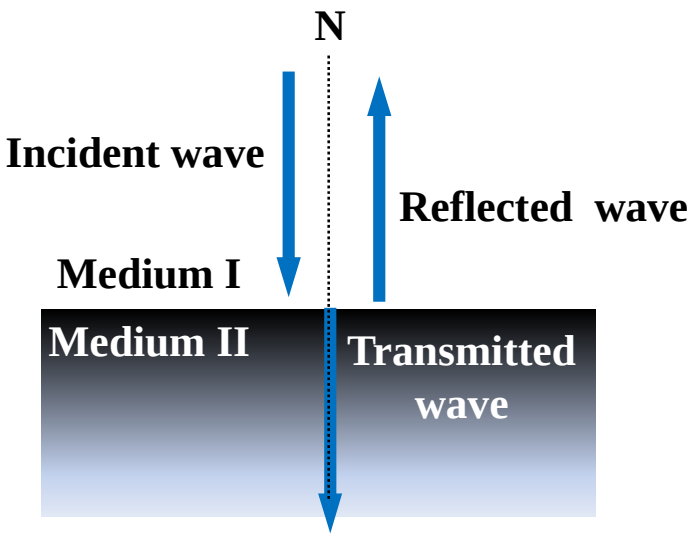

Figure 1-1: Normal reflection and transmission of waves at an interface between two mediums

1.3.2 Oblique angle

Meanwhile, when an ultrasonic wave passes through an interface between two different mediums at an oblique angle, as shown in Figure 1-2, depending on the index of refraction of the materials, the ultrasonic waves will be reflected and refracted. Such reflection and refraction are strongly influenced by Snell's Law, as given in Equation 1.4, where V_L and V_S are longitudinal wave velocity and shear wave velocity, respectively.

$$\frac{\sin\theta}{V_L} = \frac{\sin\theta}{V_S} \tag{1.4}$$

Figure 1.1 shows the behaviors of wave reflection on two different mediums. As the incident wave (θ_1) with longitudinal velocity of V_{L1} reached the interface between medium 1 and medium 2, the incident wave is reflected and refracted. The angle for both incident and reflected waves are same due to the same velocity. However, the refracted angle is different from both incident angle and reflected angle due to velocity difference. Since the refracted angle (θ_2) is bigger than the incident angle (θ_1), the velocity for the second medium is faster than that of medium 1.

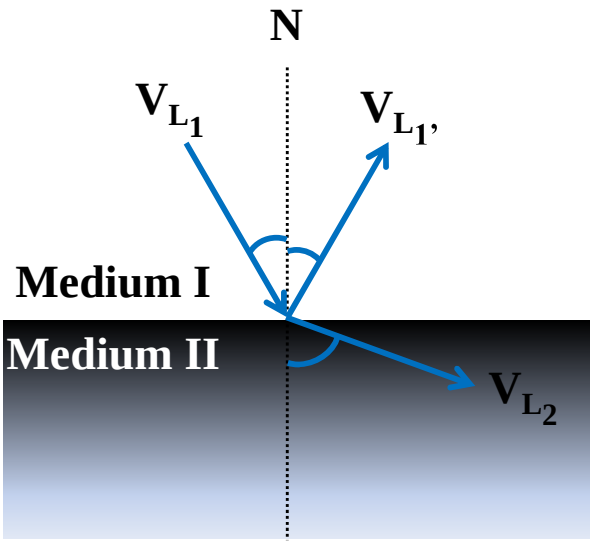

Figure 1-2: Oblique reflection and refraction of waves at an interface between two mediums.

1.4 The principle of ultrasonic testing

Ultrasonic testing can be carried out either in pulse-echo mode or through transmission mode. Such testing is based on vibration in materials which consists of atoms that are forced to move in a vibrational motion. Such movement is not possible in a vacuum state. Therefore, ultrasonic testing is possible in solid, liquid and gas state. In solid, the sound waves can propagate in four modes; longitudinal wave, shear wave, surface wave and plane wave. Based on these four waves, longitudinal wave and shear wave are the commonly used in ultrasonic testing. Figure 1.3 shows the difference between a longitudinal wave and a shear wave. It is observed that for longitudinal wave, the oscillations occur is the direction of the wave propagation. It is also called as pressure or compression waves due to compression and expansion forces that occur in such direction. Longitudinal wave can be generated in all states; solids, liquids and gases since the wave energy travel through the atomic structure of a material. Unlike longitudinal wave, the shear wave propagates at direction perpendicular to the wave propagation. For an effective propagation of shear wave, the material should be in solid. In addition, shear wave is weaker than longitudinal wave because shear wave is usually generated from the reflection of longitudinal wave. Ultrasonic testing, due to its nondestructive ability, has a higher accuracy compared to other nondestructive testing such as liquid penetrant and magnetic particle, in terms of defect detection and thickness measurement. In addition, the size, location and shape of such defects can be obtained from ultrasonic testing. It also provides deep penetration so that defects or material properties in narrow places can be measured at fast time response. However, there are some limitations with ultrasonic testing. One of the common disadvantages is that in order to carry a precise and accurate testing using ultrasound, an experienced and skilled examiners are required. Besides that, the test objects must be smooth and not rough for precise measurement. Adequate amount and suitable type of couplant are also necessary for an effective transfer of ultrasonic wave energy between the transducer and a test object (for contact method).

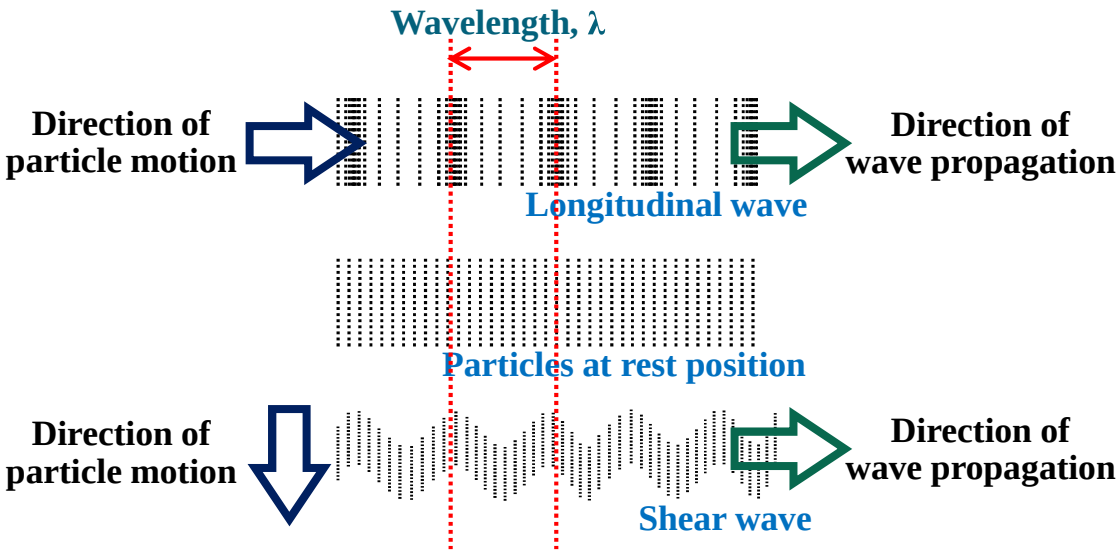

Figure 1-3: Difference between longitudinal and shear waves

1.4.1 Pulse-echo mode

The principle of a pulse-echo is shown in Figure 1-4. It is observed that only one ultrasonic transducer is used for the measuring. That means such ultrasonic transducer act as the transmitter and receiver as well. From the ultrasonic transducer, due to vibration in the piezoelectric element embedded in the transducer, an ultrasonic wave is generated and propagates into the specimen. Since no transducer is located at the bottom of the specimen, due to impedance mismatch, the ultrasonic wave is reflected at the normal angle. Such reflected ultrasonic wave is then propagates back to the upper side of the specimen and received at the ultrasonic transducer. Pulse-echo technique is wide applied in many applications due to its simplicity of aiding only one transducer during the measurement is being conducted. One of the common examples of using the pulse-echo technique is measuring the water depth [8]. The depth of the water can be calculated by dividing into half the time the reflected wave arrived. Take note that the pulse-echo method is also possible to be applied on a specimen that has many layers. Since each material has their own acoustic impedance, the ultrasonic waves will be

reflected at each boundary (interface). Therefore, the thickness of the layers in a specimen can be obtained easily [9]. A typical pulse-echo testing consists of pulser/receiver, transducer and a display device. A pulser-receiver, which is connected to the ultrasonic transducer, is an electronic device that can produce high voltage electrical pulses. Based on such pulses, the transducer generates high frequency ultrasonic waves (energy). Such high frequency sound waves are then introduced and propagate through the material in the form of waves. When there are some defects such as voids or cracks, some of the ultrasonic waves will be reflected and received at the transducer. The received waves are then converted to an electrical signal by the transducer and later displayed on the screen. Since the velocity of the ultrasonic wave and the time it was received are known, the distance for such defects can be calculated.

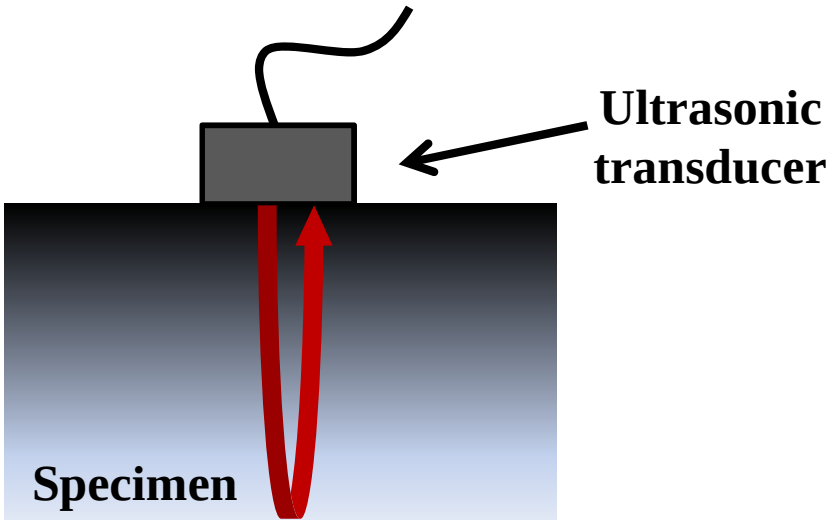

Figure 1-4: A pulse-echo mode

1.4.2 Through-transmission mode

The principle for conducting an ultrasonic measurement using the through-transmission mode is also similar with the pulse-echo mode, expect, two transducers are used where one transducer is employed for transmitting and another transducer is for receiving the wave signal. Figure 1-5 shows the schematic of a through-transmission mode. It is observed that the two ultrasonic transducers are located on the same vertical line. Such placement is important so that the ultrasonic waves can be transmitted to the receiver precisely.

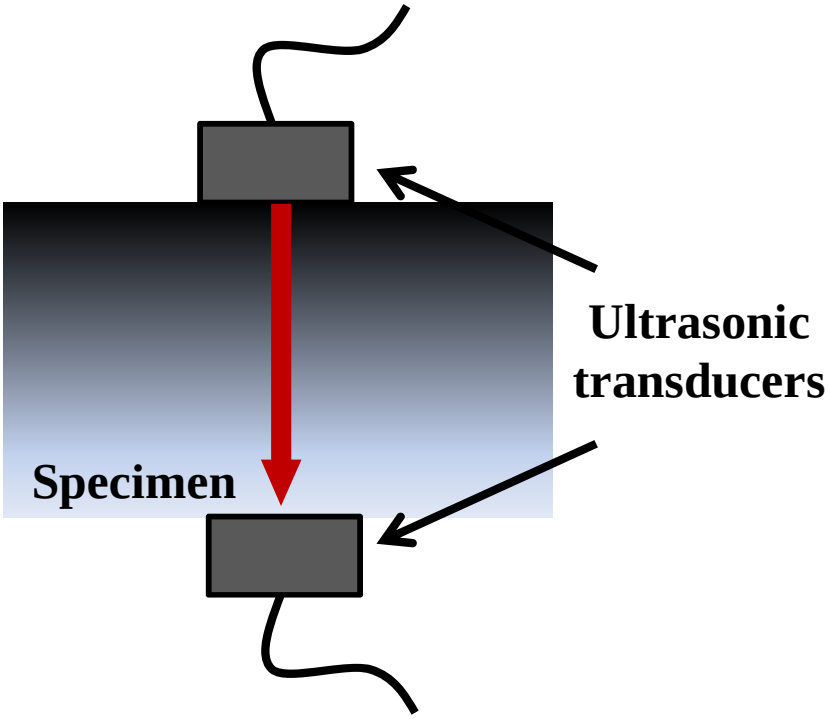

Figure 1-5: A through-transmission mode

1.5 Types of ultrasonic testing (non-contact methods)

There are several ultrasonic methods for material characterizations and process monitoring where such methods are divided into non-contact and in-contact techniques. The common non-contact methods are laser ultrasound and electromagnetic acoustic transducer (EMAT).

1.5.1 Laser ultrasound

Laser ultrasound uses lasers to generate and detect ultrasonic waves in any medium such as solid, liquid or gas. Laser ultrasound, which is a non-contact method, can generate any types of waves such as longitudinal, shear, surface and plate at desired frequency [8-13]. It is widely used to measure thickness, detect cracks or flaws and also material characterizations [14].The basic principle of laser ultrasound method would be a generation laser, a detection laser and a detector. Figure 1-6 shows the basic experimental set-up for laser ultrasound. The pulsed generation laser will hit on a material or workpiece, where such workpiece will absorb the pulsed laser. The absorbed pulsed laser in a workpiece is then converted to heat, which results to rapid localized temperature increase. Such rapid temperature increase leads to a rapid thermal expansion of a local region, which leads to generation of ultrasound waves into the medium. The ultrasonic waves are generated either by thermoelastic or ablative. The difference between these two (thermoelastic and ablate) is that the tendency to melt the workpiece or material. If the material does not melt, the generation mechanism is called thermoelastic and if the material does melt, such regime is called ablate.

The unique features of laser ultrasound are:

1) Couplant-free method since it is a non-contact method
2) Can be carried out in a far distance
3) Can be carried out in moving conditions where speed can be up to 20 m/s
4) The generated waves with high bandwidth enhances spatial resolution rather than the conventional contact transducer, so that the defect detection is more reliable
5) Can be operated on curved complex surfaces
6) Can probe macrostructures to very thin films because the broadband systems provide information from kHz to GHz.

However, there are some limitations with laser ultrasound where it has lower sensitivity rather than conventional contact piezoelectric transducer (PZT) transducer. Besides that, the experimental set up for laser ultrasound can be very expensive compared to other conventional ultrasonic techniques.

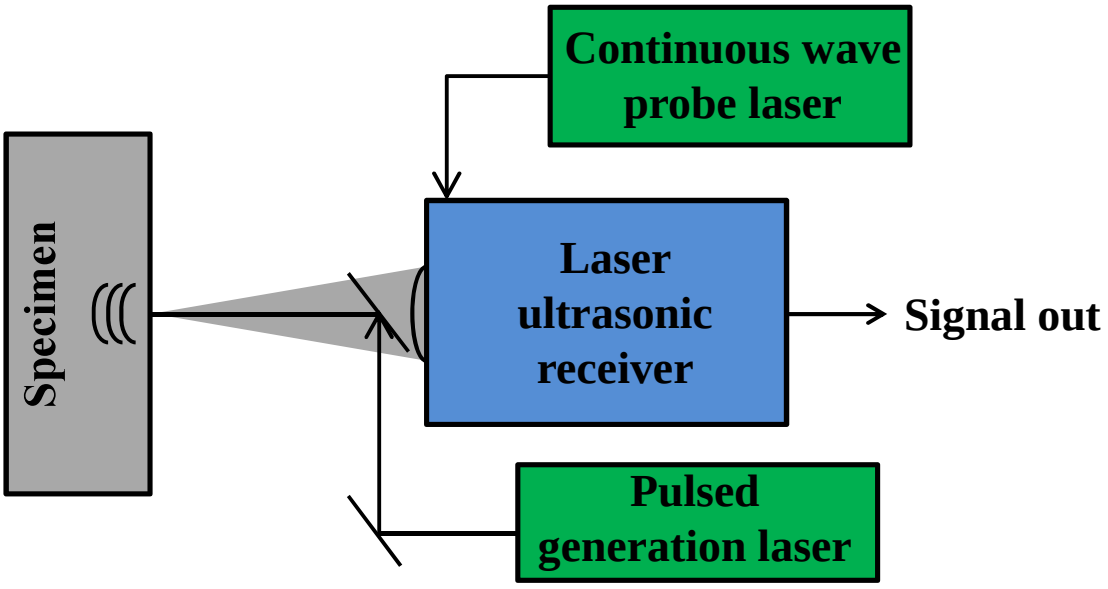

Figure 1-6: Schematic diagram of a laser ultrasound set-up

1.5.2 Electromagnetic acoustic transducer (EMAT)

Another non-contact method, is electromagnetic acoustic transducer, also eliminates the use of couplant [15,16]. This technique has been applied in many industrial processes such as manufacturing, automotive and pressure vessels This transducer is commonly generates shear horizontal bulk wave mode, surface wave, lamb wave and other guided-wave modes in metallic and/or ferromagnetic materials [17]. Figure 1-7 below shows the difference between a conventional piezoelectric transducer and an electromagnetic acoustic transducer. The basic component for a conventional piezoelectric transducer is crystal while EMAT consists of a magnet and an electric coil. The ultrasonic waves are generated and received by the coil and magnet in the EMAT where the measured object is made from a conductive material. Therefore, the ultrasonic waves are transmitted through magnetic field interaction. There are two mechanisms to generate such ultrasonic waves; Lorentz force and magnetostriction. Lorentz force is

used when the material is conductive while magnetostriction is used when the material is ferromagnetic. The alternating current (AC) current supplied for the coil generates eddy current on the surface of the object. Such current, which is generated at a very thin layer of the object, reduces its thickness as the frequency of AC increases. The eddy current in the magnetic field experiences Lorentz force where it is applied on the surface region of an object due to the interaction between the electrons and atoms. Such interaction and distribution of Lorentz force can be controlled by the design of the magnet and coil, location of transducer and object and material properties.

For ferromagnetic material, when the alternating current (AC) is applied on the electric coil, it induces an AC magnetic field and therefore, produces magnetostriction at ultrasonic frequency in the material. Such magnetostriction is defined by a dimensional change in the ferromagnetic material when an external magnetic field is applied. The flux field of a magnet expands or collapses depends on the voltage in the coil while the amount of change (dimension) depends on the magnitude and direction of the field [18]. The similarity between piezoelectric and electromagnetic acoustic transducer is that both of them can be used in pulse-echo, pitch-catch and through-transmission methods. However, there are some advantages and disadvantages between these two transducers. As stated earlier, electromagnetic acoustic transducer (EMAT) eliminates the use of couplant compared to piezoelectric transducer. Due to such couplant-free, ultrasonic testing with EMAT can be conducted in a dry environment. In addition, since EMAT is a non-contact method, it will be less sensitive to the condition of the object surface. Unlike piezoelectric transducer, the surface object must be smooth for a precise measurement. Therefore, the surface for EMAT testing can be in a rough surface. Besides that, it is easier to generate shear waves with EMAT compared to piezoelectric transducer. Although EMAT is better than piezoelectric transducer due to non-contact and couplant-free, however, the ultrasonic waves generated by EMAT is weaker compared to that generated by piezoelectric transducer. In addition, since the ultrasonic waves are transmitted through a magnetic flux region between the test objects, which means the test objects must be magnetic and metallic. EMAT has been used in many applications such as flaw detection in steel products, thickness measurements, defect

inspection on plates [19] laser weld inspection on automotive components, railway inspection [18,20].

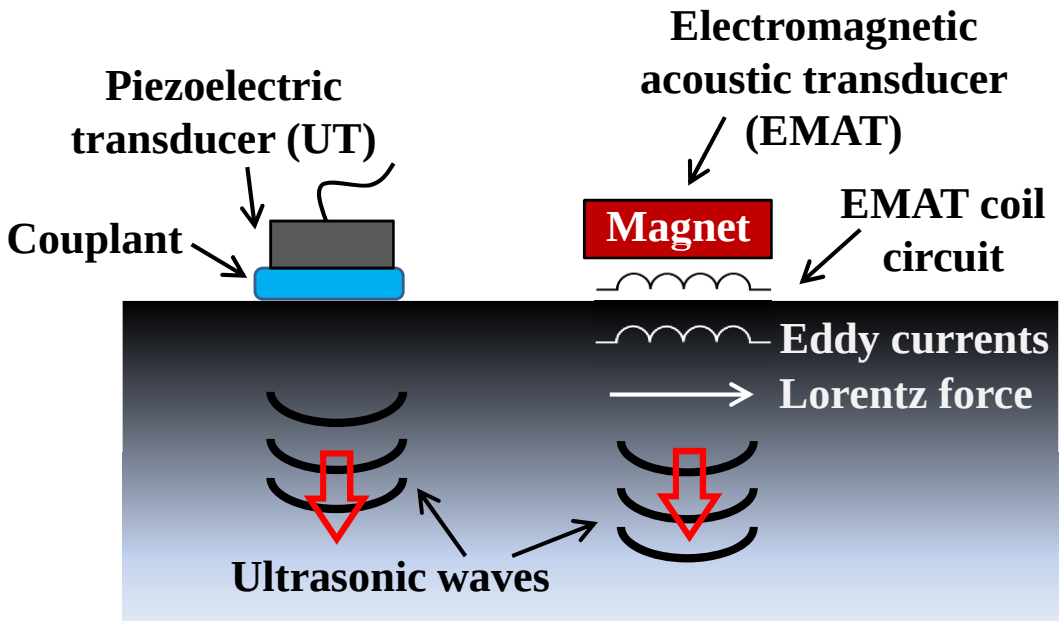

Figure 1-7: Difference between a piezoelectric transducer and an electromagnetic acoustic transducer.

1.6 Types of ultrasonic testing (contact methods)

For contact methods, the common techniques used in ultrasonic testing are high temperature ultrasonic transducer and buffer rod.

1.6.1 High temperature ultrasonic transducer

For the application at high temperature, it is impossible to employ the conventional piezoelectric transducers due to their temperature limitation. Due to such problem, high temperature ultrasonic transducer is used. The use of high temperature ultrasonic transducer is very necessary in material characterization and process monitoring at high temperature, particularly in the industrial processes that deals with hot metal pipes or

tanks. Since the conventional ultrasonic transducer is limited to such high temperature, it is very necessary to use the high temperature ultrasonic transducer. The common piezoelectric materials for a high temperature ultrasonic transducer bismuth titanate, BIT (Bi4Ti3O12), modified BIT, lead metaniobate, and BIT/PZT film (sol-gel technology) [21]. Although most of the commercialized high temperature ultrasonic transducers can withstand up to 400^{o}C, however, due to thermal cycle [22,23], such transducer is limited for higher temperature application (>400^{o}C). Therefore, the material selection for a high temperature transducer is very important. It is reported that lithium niobate ($LiNbO_3$) which is well known for its high Curie temperature is used as the piezoelectric material for a high temperature transducer. The $LiNbO_3$ single crystal was bonded on a stainless steel substrate. Such transducer was heated in an electric furnace with temperature ranging from room temperature up to 1000^{o}C.

1.6.2 Buffer rod

Buffer rod (also known as waveguide) act as a medium to transmit and receive the ultrasonic signals from the measured materials that are located in harsh environments such as narrow places and high temperature. The common type of a buffer rod is usually associated with a long cylindrical buffer rod, as shown in Figure 1.8 [24]. It is observed that the wave propagates along the axial direction of the buffer rod. The rod material should have low ultrasonic loss so that the energy (ultrasonic waves) can be confined in the core properly with less attenuation along the long rod [30,55,56]. Materials such as sapphire and quartz have very low of ultrasonic loss; therefore, less diffraction of wave will occur and minimized the generation of trailing echoes. However, such materials have several limitations such as expensive, mechanical and thermal properties that are not compatible with the measurement condition and easy to generate cracks during thermal cycle. Therefore, metals such as steel and aluminum are usually selected as the buffer rod material since they are machinable and have high melting points. Ceramic and polymer buffer rods are also available depending on the probed material. Acoustic impedance which is the product of density and velocity influences the material selection for the buffer rod [30,56]. Such selection is important for a precise measurement of the

probed parts. Metal buffer rods are known for their robustness and high melting temperature, however, for the process monitoring related to polymer, the measured signals are found to be weak. This is due to the acoustic impedance mismatch between polymer (sample) and metal (buffer rod). Therefore, the reflection coefficient at the interface of metal buffer rod and polymer is large. This leads to less amount of the guided ultrasonic waves (energy) in the metal buffer rod transmitted into the molten polymer, leading to poor SNR [56] In order to overcome this, polyetheretherketone (PEEK) has been proposed as the core of a clad polymer buffer rod [30]. The cladding layer is made of heat-resistant epoxy. As the result, high SNR is obtained and the application of such proposed clad polymer buffer rod is applicable up to 350^{o}C. In addition, since polymer has a poor thermal conductivity, the length of polymer buffer rod can be short. This reduces the attenuation waves in the rod, leading to better received signal at the ultrasonic transducer. Unlike polymer, the thermal conductivity of metal is high; therefore, the metal buffer rod must be sufficiently long enough so that during the cooling process at UT, it will not reduce the temperature of the measured sample.

Figure 1-8: A typical uniform cylindrical buffer rod

1.7 Applications of buffer rod

Since the buffer rod act as a waveguide in probing the surface or the interior part of a material or an object nondestructively, it can be applied in a room temperature as well as high temperature. One of the common applications of a buffer rod technique is crack or defect detection. In this measurement, some of the cracks may be located in narrow places which are hard to be reached by the examiner. Such problem can be overcome with the aid of a buffer rod. Figure 1-9 shows the application of a buffer rod in a narrow place in the middle of a material. Take note that the pulse-echo measurement is usually used where one end of the buffer rod is applied with the conventional ultrasonic transducer (UT) while the other end is contacts the samples directly. For a sufficient transmission of the ultrasonic waves from the buffer rod into the die, a couplant is used between the buffer rod and the die. It is noted that a longer rod leads to wave attenuation along the rod; therefore, the selection of rod material is important [51]. From the buffer rod, the ultrasonic waves that are generated by the ultrasonic transducer are transmitted into the material. Take note that the material for both buffer rod and the material are preferably to be the same, so that the impedance mismatch is small. Therefore, almost all the ultrasonic waves will be transmitted into the material efficiently. As the ultrasonic wave reached the end of the material, due to the impedance mismatch between the material and its surrounding (air), it is reflected at a normal angle and will be received at the UT. However, if the ultrasonic wave arrived at any cracks that are within the axial direction of the buffer rod, such wave will then be reflected at received at the UT. Take note that the reflected wave from the crack surface will arrive first at the UT rather than the reflected wave from the end surface of the material. The location of the crack can also be calculated if the thickness of the material is known.

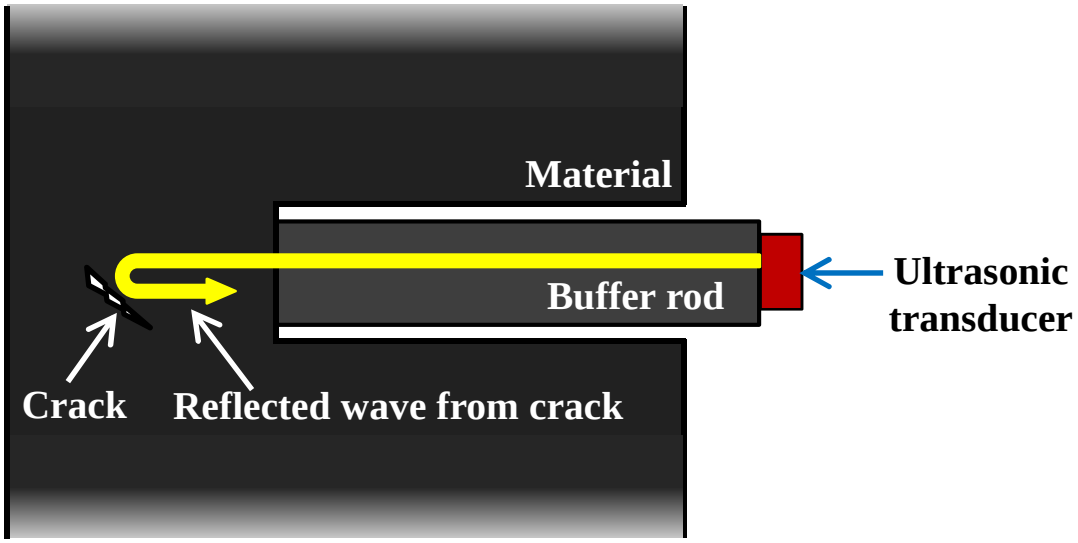

Figure 1-9: Crack detection in a narrow place of a material using a buffer rod

In order to measure the material properties while the material is being heated, a buffer rod is applied as the waveguide with a conventional piezoelectric UT. Although it has been mentioned that the high temperature UT is commercially available, but due to some limitations, the use of the conventional type of UT with a buffer rod is preferable. Figure 1-10 shows how a buffer rod is employed at one end of the material while it is heated. Such measurement, which is in a pulse-echo mode, is possible to be conducted without damaging the conventional UT that can only withstand up to 50^{o}C.

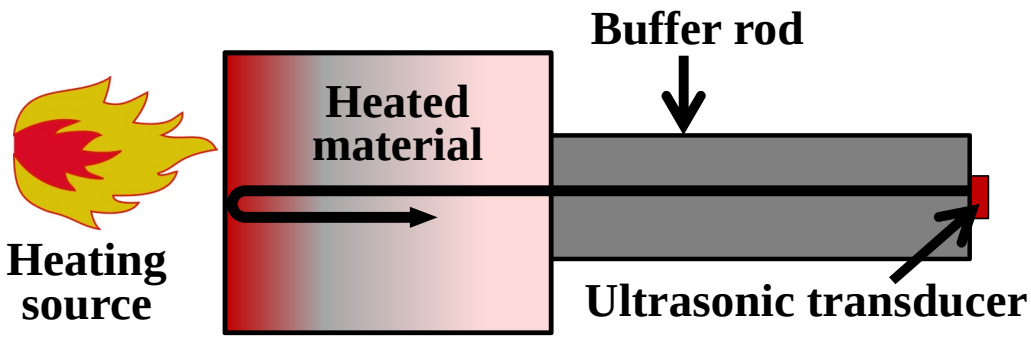

Figure 1-10: Measuring a heated material using a buffer rod

Since it is very attractive fact that the buffer rod technique is applicable for measuring the material properties at high temperature, it is widely applied in many industrial processes such as die casting [25,26], polymer extrusion [27-36], molten metals [37-44], particle detection [45-47] and injection molding [48-50]. However, in such industrial processes, the operating temperature is very high around ~700^{o}C. Therefore, a cooling system is usually installed near the UT. Such cooling system which is aided by water or air is usually installed with coils. Figure 1-11 shows a buffer rod that is installed with a cooling system. With such cooling system, the application of buffer rod at high temperature is more reliable.

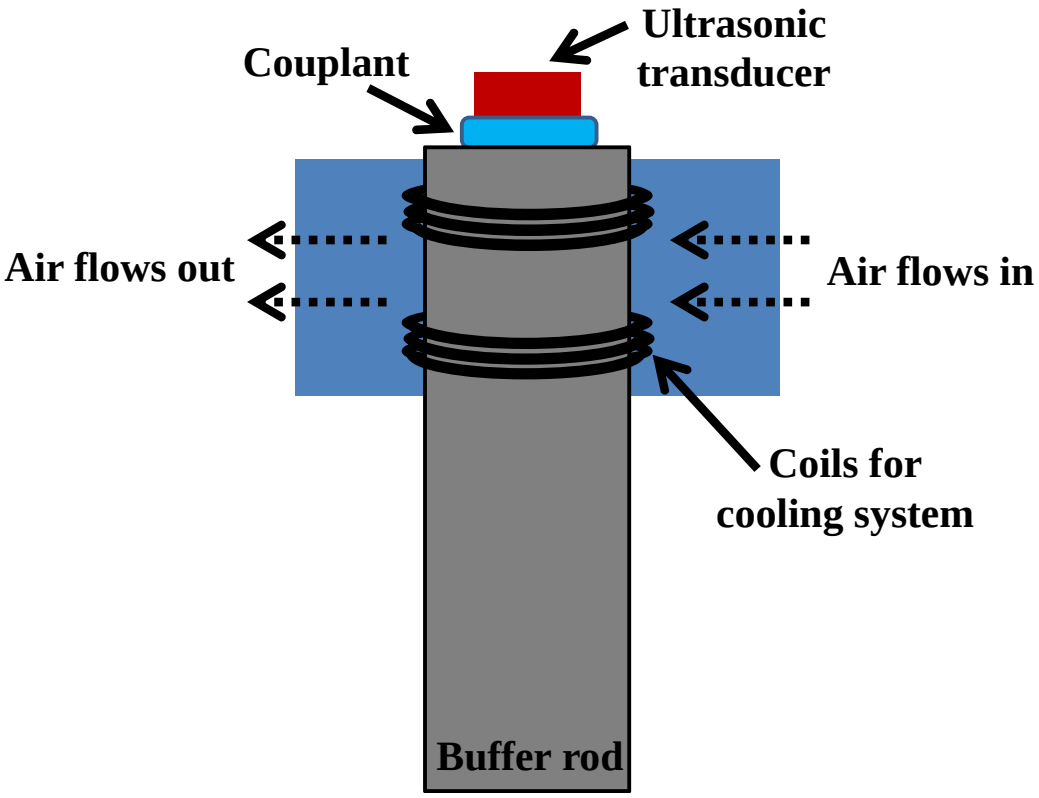

Figure 1-11: Buffer rod with a cooling system for high temperature applications

The application of buffer rod in industrial processes such as die casting and particle detection in molten aluminum is presented. In die casting, it is hard to measure the molten metal in a die that consists of several layers of steel. Such layers make the pulse-echo measurement complicated where the ultrasonic waves will be reflected at the boundary of different media [33]. Therefore, the buffer rod technique is the appropriate solution for such measurement since it can be attached directly onto external surface or even mounted in the die. In addition, the solidification process of a cast metal can be measured with the buffer rod technique. Solidification is the stage where the molten metal that is subjected into a mold is fully solidifies. With the aid of the buffer rod, the time when the metal has fully solidified can be measured by the buffer rod. Figure 1-12 shows the stages for detecting the solidification of a metal [26]. From the top image of Figure 1-12, no molten metal is filled between the dies, therefore, such gap between the two dies is called cavity. Since the acoustic impedance between the buffer rod and air (cavity) is huge, almost all the ultrasonic waves that are generated by the UT will be reflected back to the UT. However, as the molten metal fills in the die, due to small impedance mismatch between the buffer rod and the molten metal, the ultrasonic waves are transmitted into the molten metal, as shown by the middle image. Therefore, only small amount of the ultrasonic waves will be reflected at the interface between the end of the buffer rod that is in contact with the molten metal and the molten metal. That means, only weak signal will be received at the UT. After the cast metal has fully solidified, it will shrink where such shrinkage results to the formation of cavities between the cast metal and the surface of the two dies. Therefore, the ultrasonic wave will be reflected due to such cavity where such reflected wave indicates that the cast metal has been solidified, as shown by the last image in Figure 1-12. In molten metal industries, the cleanliness of a molten particle is very important since many unwanted impurities or particles are presented. By using such buffer rod with a cooling system as shown in Figure 1-11, a buffer rod is immersed into a container containing molten metal. The buffer rod is clamped by a jig outside of the container. The measurement mode is in pulse-echo since only one UT is installed. It has been reported that when two buffer rods are used for detecting the particles in a molten metal, it is called as a pitch-catch mode [41].

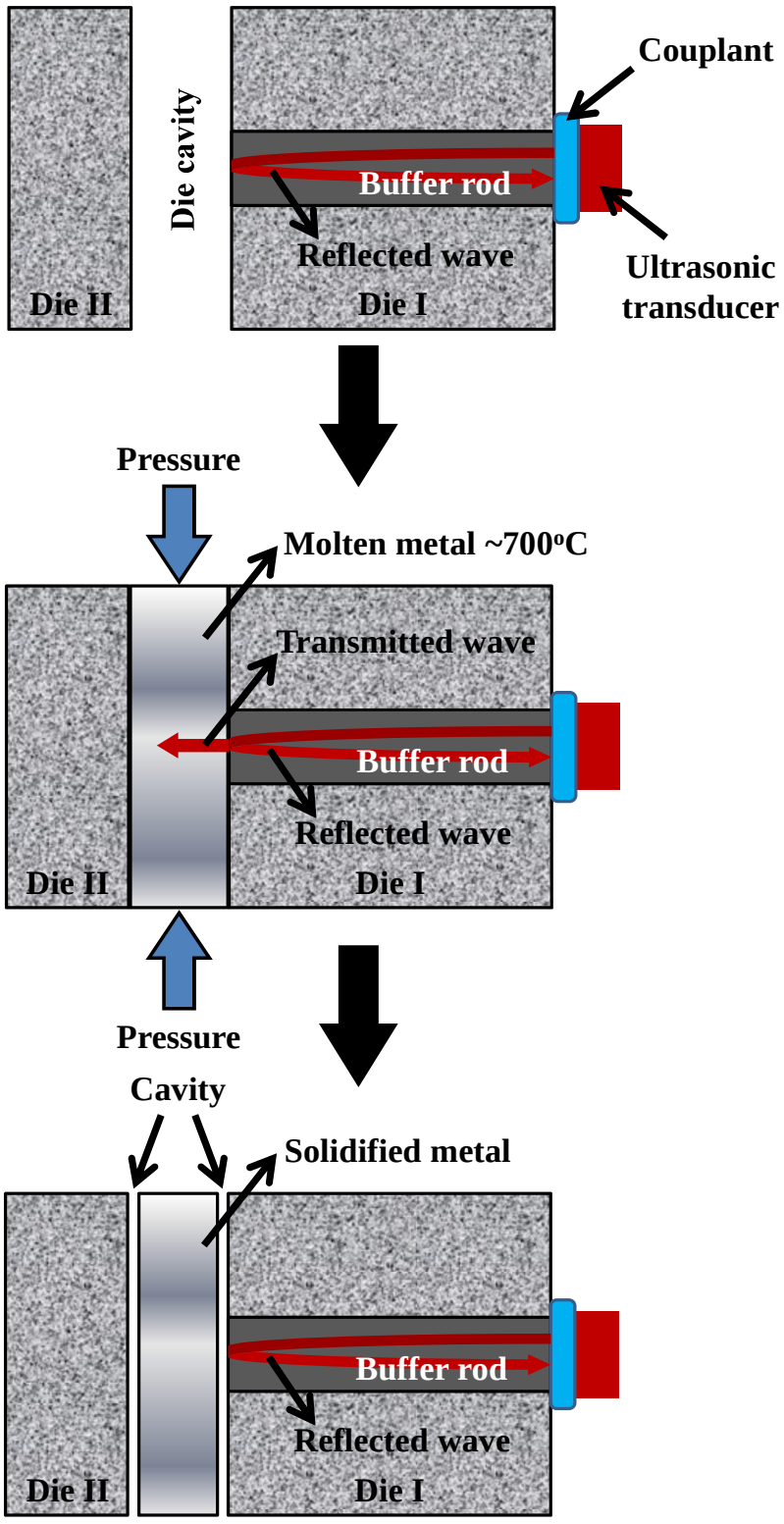

Figure 1-12: Monitoring a solidification process using a buffer rod.

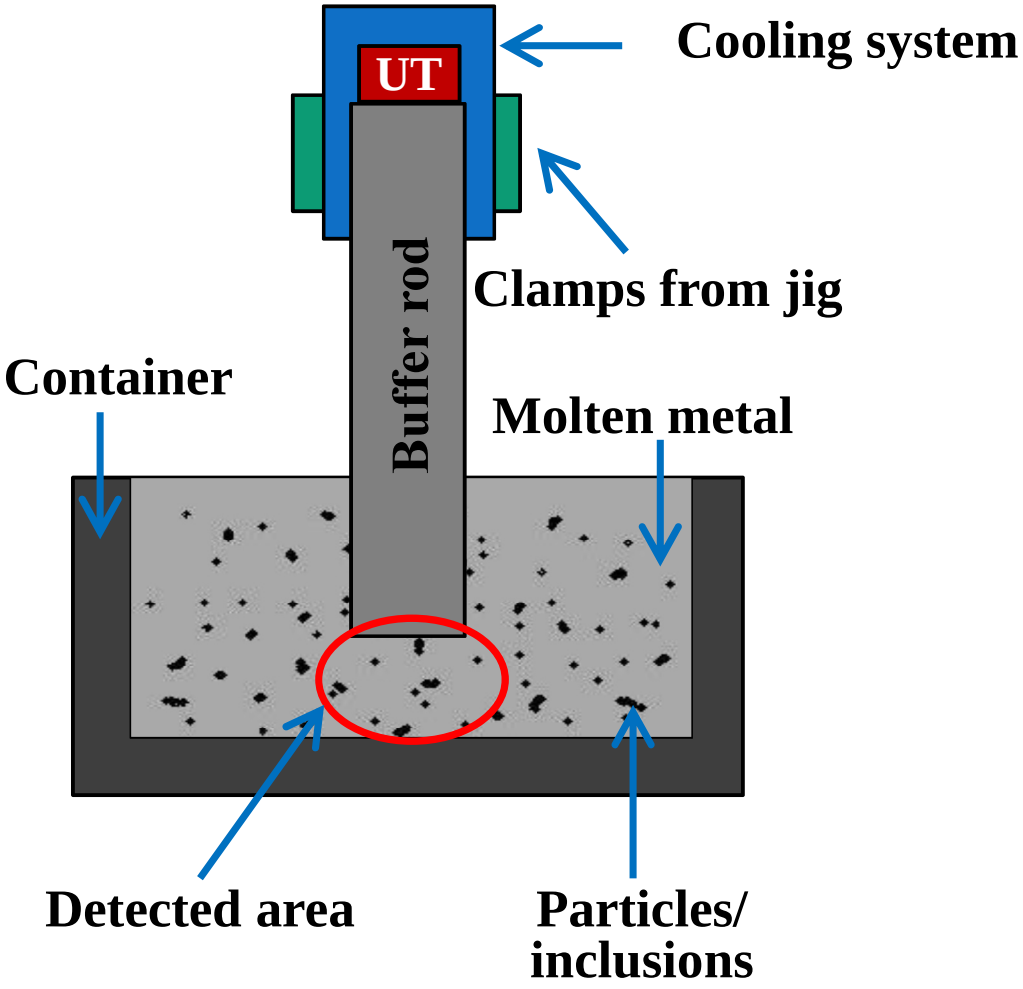

Figure 1-13: Particle detection in a molten metal using a buffer rod

Although buffer rod technique is well known for its simplicity, robustness and fast response, this technique is commonly associated with the generation of spurious echo (also known as trailing echoes) that are generated due to wave diffraction and mode conversion within a rod having finite diameter.

1.8 Generation of trailing echoes by buffer rod

Buffer rod technique is commonly associated with the generation of spurious echo (also known as trailing echoes) that is generated due to wave diffraction and mode conversion within a rod having finite diameter. Figure 1-14 shows such generation that is clearly observed between the first echo and second echo. Such generation is unwanted due to possible overlapping with the first echo and deteriorates the signal-to-noise ratio (SNR). There are several methods to reduce such generation such as taper and cladding.

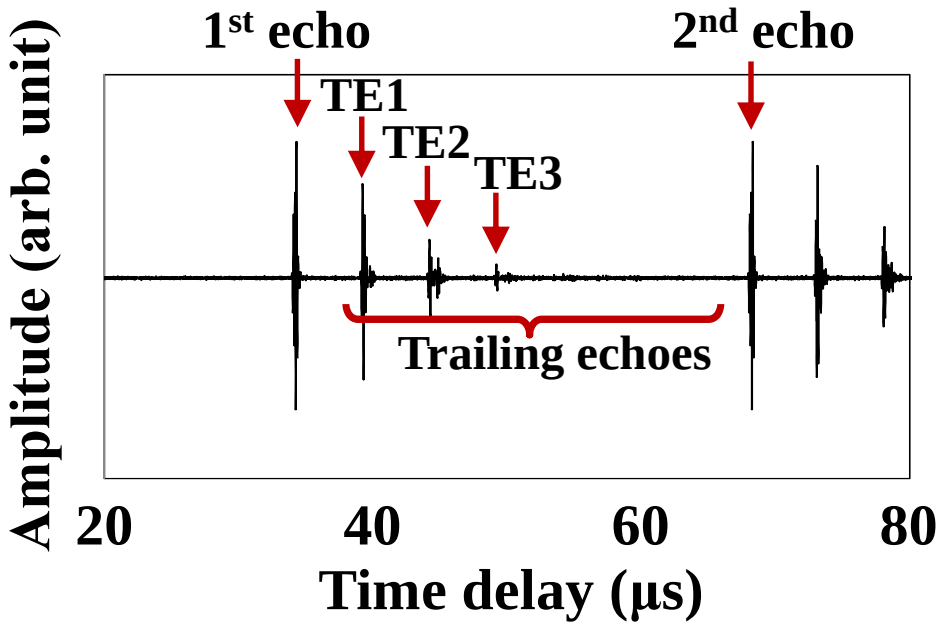

Figure 1-14: Generation of trailing echoes between the first and second echoes

1.8.1 Threading effect

Threading is basically a screwed surface that is fabricated onto the outer surface of the uniform rod, as shown by Figure 1-15. The function of threading is to disturb the mode conversion that occurred at the rod-air boundary. By such disturbance, the mode converted shear waves will be out of phase, therefore, the UT will not detect the generated trailing echoes.

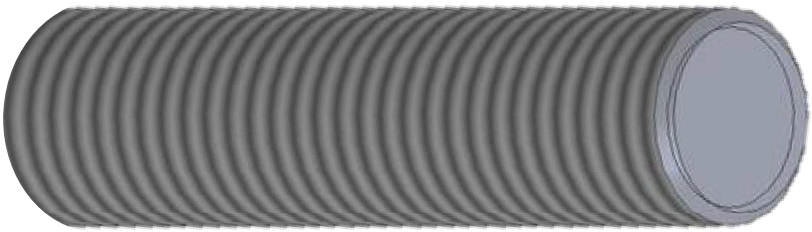

Figure 1-15: A threaded uniform cylindrical buffer rod

1.8.2 Tapering effect

Taper is defined by reducing the diameter of one or both ends of the buffer rod so that it disturbs the rod periphery. Figure 1-16 shows a taper buffer rod where one end rod has a smaller diameter than the other end rod. The difference between these two diameters is defined by the taper angle, θ. Such angle prevents the detection of trailing echoes at the ultrasonic transducer since the echoes are not in phase [14-16]. The larger the tapering angle, the better the SNR of the received signal. However, such approach requires bigger diameter of buffer rods and will not be practical for the applications at narrow places. It was found that taper angle of 1^{o} is adequate for reducing trailing echoes [14]. In addition, double taper was found to be better than the single taper since it has the advantage of small access and small thermal mass which makes the cooling process efficient [3,14,23].

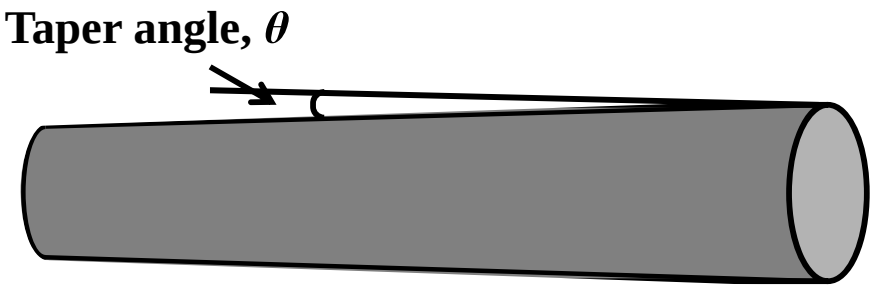

Figure 1-16: A taper cylindrical buffer rod

1.8.3 Cladding effect

Although tapered buffer rods with short length and thick diameter are proven to reduce the trailing echoes effectively, however, such rods are difficult to apply for the production monitoring where the buffer rods should be mounted. Such mounting will disturb the rod periphery and weakens the measured signals [14]. Therefore, the use of cladding is widely applied on uniform or taper buffer rod. Cladding is introduced by applying another layer on the outer surface of the rod except the end surfaces of the rod. Figure 1-17 shows a schematic of a clad cylindrical buffer rod. Thermal spray and electroplating are some of the methods to produce the cladding layer [18]. It is noted that thermal spray produces a porous state of cladding layer that enhances the dispersion of trailing echoes into the cladding layer; therefore thin layer of cladding is possible [1,13,19]. The function of cladding is to guide the ultrasonic waves in the core so that strong signal can be maintained throughout the measurement [1,11,20] Although the mode conversion still occur, the propagation of the generated trailing echoes is on the interface between the core and the clad. Therefore, the trailing echoes will not be received at UT and great SNR is obtained. In order to achieve such performance of clad buffer rods, the velocity of clad should be higher than that of core.

The selection of clad material depends on the core material so that the energy of the ultrasonic waves is strongly confined in the core.

The benefits of cladding are:

1) High performance where the trailing echoes are greatly reduced
2) High amplitude of the desired signal
3) Can be applied in transmission or reflection measuring mode
4) Low ultrasonic loss since the ultrasonic waves are properly guided in the core
5) Machinable where metals are usually used as the cladding layer
6) No energy loss during immersion in molten metal
7) Additional layer of cladding is possible for mounting purpose

Figure 1-17: A clad cylindrical buffer rod

1.8.4 Other methods to reduce trailing echoes

Besides taper and cladding, the SNR can be improved by introducing a focused lens at one end of buffer rod. By using such rods, the ultrasonic waves can be focused onto small area of about one wavelength [19]. Figure 1-18 shows a double taper clad buffer rod where one of the end rod has a spherical concave ultrasonic lens. Although long buffer rods are commonly used where such length leads to wave attenuation, it was found that the resolution of the received image in ultrasonic imaging is still adequate. Such focused buffer rod is also able to monitor the alumina particles with the size of 160 μm suspended in molten aluminum successfully. Another approach of making a focused buffer rod is by introducing a conical tip with the angle of 45^{o} as shown by Figure 1-19, so that the trapping of air bubbles on the tip surface during the immersion of sample is prevented [21,22,24]. Such angle is also ensures all the reflected waves (the direction of such waves is depicted by arrows) are received in phase at the transducer, thus forming a strong amplitude signal [25].

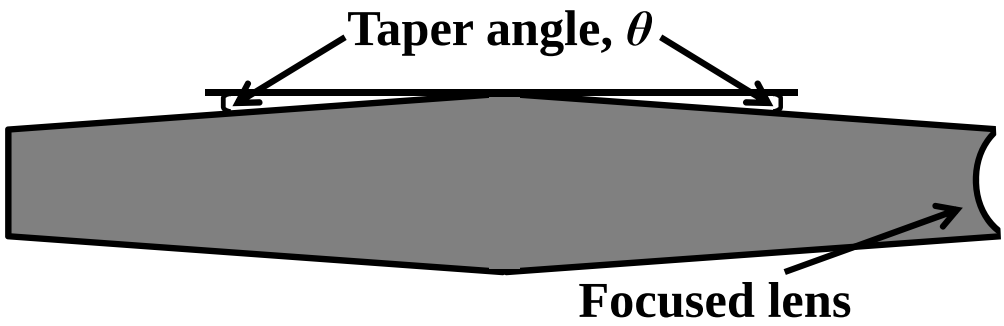

Figure 1-18: A double taper cylindrical buffer rod with one focused lens

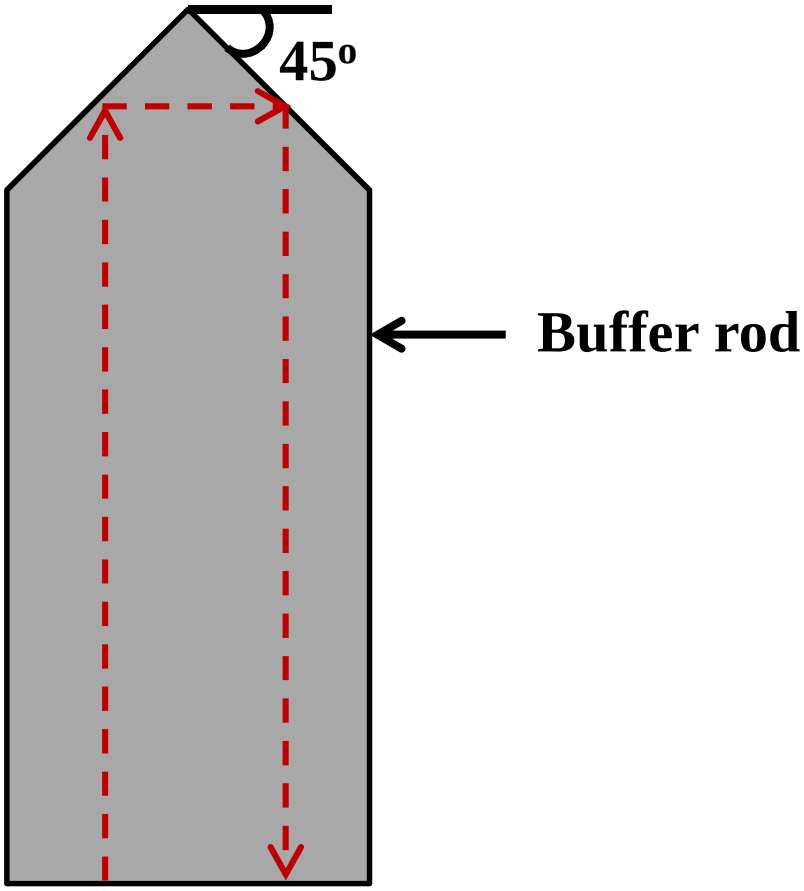

Figure 1-19: A buffer rod with a conical tip of 45^{o}.

1.9 Problem statements

1) Based on the discussion made on laser ultrasound, electromagnetic acoustic transducer, high temperature ultrasonic transducer and buffer technique, it is noted that each technique has its own benefits and limitations. In this work, the buffer rod is chosen as the measuring tool due to its fast response, simplicity, cost effective (in terms of the experimental setups), robustness, safety and strong signal.

2) Although the trailing echoes can be reduced by using the tapering or cladding effects, the fabrication and machining process of these methods on the buffer rods may be difficult for some materials that are hard to machine and brittle.

3) In addition, although the cladding effect seems promising for reducing the trailing echoes significantly, very few works have been conducted on finding the appropriate

condition for a cladding layer. Such condition is very important for the future use so that the optimum clad buffer rod with high SNR can be designed and fabricated.

1.10 Objectives of research

1) To reduce trailing echoes and improve the signal-to-noise ratio (SNR) so that strong signal can be obtained from any ultrasonic measurements.
2) To propose geometrical shapes as the cross-sectional shapes of the buffer rods since the current methods such as threading, tapering and cladding only focus on the outer surface of a cylindrical buffer rod. In this work, the geometrical shapes are polygons.
3) To investigate the appropriate condition of a cladding layer since less work has been reported on investigating the optimum condition for such layer.

1.11 Construction of thesis

Chapter 1

In chapter 1, the fundamentals of ultrasound are presented. Also this chapter reviews the literature study and related works on ultrasonic pulse-echo technique. In addition, some applications of buffer rod method in the pulse-echo measurements and some problems of using the buffer rod are described extensively. Based on such background, the scope of the present study is addressed.

Chapter 2

In chapter 2, the generation of trailing echoes in a cylindrical buffer rod is numerically and experimentally investigated. Such generation is verified from the numerical simulation where a three-dimensional finite difference method is employed. It is found that the generation of trailing echoes can be illustrated from the cross-sectional shape itself. A trailing echo can be generated when the mode converted shear waves propagate to the side wall of the rod perpendicularly and constructive interferences between the waves occur effectively. Thus, the generation mechanism of such trailing echoes is theoretically described. In addition, the validity and effectiveness of using the numerical simulation has been demonstrated experimentally.

Chapter 3

In chapter 3, the cladding effect to reduce the trailing echo is examined numerically. It is found that the SNR changes drastically with the material combination for the cladding and core and the highest SNR is appeared when the velocity and density of the cladding are approximately 120% and 70% of the core, respectively. It should be noted that an appropriate SNR is obtained when the velocity of cladding is approximately 110% of the core regardless of the density value of the cladding on the condition that the density value is within the range from 75% to 150% of the core. This fact obtained here could be useful for reducing trailing echoes that are appeared in polygonal buffer rods developed in this work.

Chapter 4

In chapter 4, polygonal buffer rods have been proposed to reduce the trailing echoes and result in improving the SNR in ultrasonic pulse-echo measurements. The idea is basically to use a polygonal rod whose normal sectional shape is a polygon such as a triangle, square, pentagon, hexagon or heptagon. The effectiveness of such polygonal rods is examined numerically and experimentally. It is found from a three-dimensional numerical simulations based on a finite difference method that 'odd polygons' having sides any one of which is not parallel to any of the other sides, such as triangle, pentagon and heptagon, are effective to reduce the trailing echoes, because of less interferences among the mode converted waves in the rod. It should be noted that there still exist a certain amount of trailing echoes even in the odd polygonal rods where such trailing echoes are generated by the possible interference of the waves due to the bilateral symmetry shape of the odd polygons.

Chapter 5

In chapter 5, to eliminate such remaining trailing echoes existing in the odd polygonal rods, an effective idea of using irregular polygons is proposed. Because the symmetry shape of the polygons results in generating trailing echoes, such generation can be prevented by distorting the half side of a polygon. The effectiveness of such irregular polygonal buffer rods on restraining the generation of trailing echoes is numerically and

experimentally investigated. It is found that the trailing echoes are almost completely eliminated with the irregular pentagon and the SNR of the pulse-echo is approximately five times higher than the regular pentagon.

Chapter 6

General conclusions and future prospects of the research are summarized in chapter 6. It is highly believed that the proposed method; polygonal buffer rods are effective to reduce the trailing echoes and improve the SNR. The mechanism presented in this work is also beneficial for designing the optimum buffer rod with high SNR.

1.12 Conclusions

1) The existing methods to reduce the trailing echoes and improve the signal-to-noise ratio (SNR) such as threading, tapering and cladding are proven to be effective. However, all of these methods only focus on the external surface of the buffer rod rather than the cross-sectional shape itself. In addition, such existing methods have their own disadvantages such as machining (threading and tapering) and material selection (cladding).

2) New idea which focuses on the cross-sectional shape is proposed in this work. Since the common buffer rod is in the shape of a cylindrical buffer rod where the cross-sectional shape is in the shape of a circle, such circle is changed to a geometrical shape which is a polygon.

1.13 References

[1] Y Ono, Y Zhang, JF Moison, CK Jen and CY Su: Simulation experiments in water for U detection of inclusions in molten metals, The 4th Inter. Conference on control and automation (ICCA 2003) Montreal Canada, pp. 927 – 931.

[2] CK Jen, JG Legoux and L Parent: Experimental evaluation of clad metallic buffer rods for high temperature ultrasonic measurements, NDT & E International 33 (2000) pp. 145 – 153.

[3] CK Jen, B Cao, KT Nguyen, CA Loong, JG Legoux: On-line ultrasonic monitoring of a die-casting process using buffer rods, Ultrasonics 35 (1997) pp. 335 – 344.

[4] Y Ono, M Kobayashi, CK Jen, CC Cheng, A Derdouri and Y Simard: Real time non-intrusive and non-destructive ultrasonic monitoring of injection and co-injection molding processes, SPE ANTEC (2004) pp. 556 –560

[5] I Ihara, H Aso and D Burhan: In-situ observation of alumina particles in molten aluminum using a focused ultrasonic sensor, JSME International Journal Series A 47(3) (2004) pp. 280 – 287.

[6] CK Jen, C Neron, EL Adler, GW Farnell, J Kushibiki, K Abe: Long acoustic imaging probes, Proceedings of IEEE ultrasonic symposium (1990) pp. 875 – 880.

[7] H Wang, B Cao, CK Jen, KT Nguyen, M Viens: On-line ultrasonic monitoring of the injection molding process, Polymer Engineering & Science 37(2) (1997) pp. 363 – 376.

[8] PR Hoskins, K Martin, A Thrush: Diagnostic Ultrasound: Physics and Equipment, 2nd Edition, Cambridge, July 2010, p. 2.

[9] G Wrobel and S Pawlak: A comparison study of the pulse-echo and through-transmission ultrasonics in glass/epoxy composites, Journal of Achievements in Material and Manufacturing Engineering 22(2) (2007) pp. 51 – 54.

[10] B Audoin, C Bescond: Measurement by LASER-generated ultrasound of four stiffness coefficients of an anisotropic material at elevated temperatures, Journal of Nondestructive Evaluation 16(2) (1997) pp. 91 – 100.

[11] CA Calder, EC Draney, WW Wilcox: Noncontact measurement of the elastic constants of plutonium at evaluated temperature, J. Nucl. Mater. 27 (1981) pp. 126 – 136.

[12] JD Aussel, JP Monchalin: Precision laser-ultrasonic velocity measurements and elastic constant determination, Ultrasonics 27 (1989) pp. 165 – 177.

[13] S Krishnasway, Theory and Applications of Laser-Ultrasonic Techniques, Ultrasonic Nondestructive Evaluation: Engineering and Biological Material Characterization, Edited by Tribikram Kundu, CRC Press, Dec 29 2003, pp. 435 – 494.

[14] CB Scruby and LE Drain, Laser Ultrasonics (Adam Hilger: Bristol) 1990.

[15] M Hirao and H Ogi: EMATs for science and industry, Kluwer Academic Publishers, Boston (2003).

[16] HM Frost, Electromagnetic-ultrasonic transducers: Principle, practice and applications: Physical Acoustic XIV, edited by WP Mason and PN Thurston, Academic Press, New York pp.179 – 270.

[17] RB Thompson: Physical Principle of Measurements with EMAT Transducer, Ultrasonic Measurement Methods, Physical Acoustics Vol XIX, Edited by RN Thurston and Allan D Pierce, Academic Press, 1990.

[18] M Hirao and H Ogi: An SH-wave EMAT technique for gas pipeline inspection, NDT & E International 32 (1999) pp. 127 – 132.

[19] M Gori, S Giamboni, ED Alessio, S Ghia and F Cernuschi: EMAT transducers and thickness characterization on aged boiler tubes, Ultrasonic 34 (1996) pp. 339 – 342.

[20] H Gao, B Lopez, SM Ali, J Flora and J Monks (Innerspec Technologies): Inline testing of ERW tubes using ultrasonic guided waves EMATs in 16th US National Congress of Theoretical and Applied Mechanics (USNCTAM2010-384), State College, PA, USA, June 27 – July 2, 2010.

[21] R Kazys, A Voleisis and B Voleisiene, High temperature ultrasonic transducers: review, Ultragarsas (Ultrasound) Vol.63 No.2 pp. 7 -17.

[22] M Kobayashi, CK Jen, JF Bussiere and KT Wu: High temperature integrated and flexible ultrasonic transducers for nondestructive testing, NDT & E International 42 (2009) pp. 157 – 161.

[23] CK Jen, JG Legoux and L Parent: Experimental evaluation of clad metallic buffer rods for high temperature ultrasonic measurements, NDT & E International 33 (2000) pp. 145 – 153.

[24] CA Balanis: Circular Waveguide, Advanced Engineering Electromagnetic, Wiley, Solution Manual Edition, (May 9 1989), pp. 643 – 644.

[25] LC Lynnworth, V Magori,: Industrial process contril sensors and systems, in Physical Acoustics vol XXIII, RN Thurston, AD Pierce and EP Papadakis, Eds. New York: Academic (1999) pp. 275 – 470.

[26] CK Jen, B Cao, KY Nguyen, CA Loong, JG Legoux,: On-line ultrasonic monitoring of a die casting using buffer rods, Ultrasonics 35(5) (1997) pp. 335 – 344.

[27] R Edwards, and C Thomas: On-line measurement of polymer orientation using ultrasonic technology, Polymer Engineering Science vol 41 (2001) pp. 1644 – 1653

[28] Z Sun, CK Jen and CK Shih: Application of ultrasound in the determination of fundamental polymer extrusion performance, Monitoring of melting and mixing processes, in Proceeding of Polymer Processing Society Conference (2002) pp. 1- 6.

[29] TF Chen, KT Nguyen , SSL Wen and CK Jen: Temperature measurement of polymer extrusion by ultrasonic techniques, Meas. Sci. Tech, vol 10 (1999) pp. 139 – 145.

[30] CK Jen, DR Franca, Z Sun and I Ihara: Clad polymer buffer rods for polymer process monitoring, Ultrasonics 39 (2001) pp. 81 – 89.

[31] L Piche, A Hamel, A Gendron, MM Dumoulin, J Tatibouet: Ultrasonic characterization of polymer melts under processing conditions, US Patent 5,433,112 (18 July 1995)

[32] A Sahnoune, L Piche, A Hamel, R Gendron, LE Daigneault LM Caron: Ultrasonic monitoring of foaming in polymers, Proceedings of SPE ANTEC (1997) pp. 2259 – 2263.

[33] CK Jen, JY Chen, SV Hoa, KT Nguyen, JG Legoux, H Hebert: Clad buffer rods for in-situ process monitoring, Proceeding of IEEE Ultrasonic Symposium (1997) pp. 801 – 806.

[34] Z Sun, CK Jen, DR Franca, JW Liaw: Polymer extrusion and cure monitoring using clad polymer buffer rods Proceedings of IEEE Ultrasonics Symposium 1 (2000) pp. 489 – 494

[35] N Legros, CK Jen, I Ihara: Ultrasonic evaluation and application of oriented polymer rods, Ultrasonics 37 (1999) pp. 291 – 297

[36] LC Lynnworth: Ultrasonic Measurements for Process Control (New York: academic, (1989)

[37] TL Manfield: Ultrasonic technology for measuring molten aluminum quality, materials evaluation, vol 41 (1983) pp 743-747

[38] NDG Mountford, ID Sommerville, A Simionescu and C Bai: Sound pulses used for online visualtion of liquid metal quality, AFS Transactions vol 10 (1997) pp 939 – 946

[39] RS Young and DE Pitcher: Methods of the apparatus for testing molten metal, US Patent 3,444,726 May 20 1969

[40] I Ihara, CK Jen and DR Franca: Detection of inclusion in molten metal by focused ultrasonic wave Jpn. J. Appl. Phys. vol 39 (2000) pp 3152-3153

[41] Y Ono, JF Moisan, CK Jen and DR Franca: Development of ultrasonic technique with buffer rod in molten aluminum, in Proc IEEE International Ultrasonics Symposium 1 (2002) pp. 805 – 810

[42] CK Jen, JG legoux, and L parent: Experimental evaluation of clad metallic buffer rod for high temperature ultrasonic measurement, NDT & E Inter. Vol 33 (2000) pp. 145-153.

[43] Y Ono, Y Zhang, JF Moison, CK Jen, CY Su: Simulation experiments in water for U detection of inclusions in molten metals, The 4th Inter. Conference on control and automation (ICCA 2003) Montreal Canada, pp . 927 – 931.

[44] OGH Nygaard and KS Mylvanganam: Ultrasonic time-domain reflectometry for level measurement in molten metals, Technisches Messen Vol 60 (1) (1993) pp 4-14

[45] I Ihara, H Aso, D Burhan: In situ observation of alumina particles in molten aluminum using a focused ultrasonic sensor, JSME Int. J. Ser. A 47(3) (2004) pp. 280 – 286.

[46] RC Stiffler, RC Wojnar MFA Warchol LW Cisko and JM Urbanic: Apparatus and method for ultrasonic particle detection in molten metal, US patent 5,708,209 (Jan 13 1998)

[47] Y Ono, JF Moisan, CK Jen: Ultrasonic techniques for imaging and measurements in molten aluminum, IEEE Trans. Ultrason. Ferroelectr. Freq. Control 50 (2003) pp. 1711 – 1721

[48] Y Ono, CK Jen, CC Cheng and M Kobayashi: Real-time monitoring of injection molding for microfluidic devices using ultrasound, Polymer Engineering and Science 45(4) (2005) pp. 606 – 612.

[49] DV Rosato and DV Rosato: Injection Molding Handbook, 2nd edition, Chapman & Hall, New York (1995)

[50] H Wang, B Cao, CK Jen, KT Nguyen, M Viens: On-line ultrasonic monitoring of the injection molding process, Polymer Engineering & Science 37(2) (1997) pp. 363 – 376

[51] V Rajendran, N Palanivelu and BK Chaudhuri: A device for the measurement of ultrasonic velocity and attenuation in solid materials under different thermal condition, Measurement 38 (2005) pp. 248 – 256.

[52] CK Jen, L Piche, J Bussiere: Long isotropic buffer rods, J. Acoust. Soc. Am. 88(1) (1990) pp. 23-25

[53] DR Franca, CK Jen, KT Nguyen, R Gendron: Ultrasonic in - line monitoring of polymer extrusion, Polymer Engineering & Science 40(1) pp. 82 – 94

[54] E Papadakis: Ultrasonic diffraction loss and phase change in anisotropic materials, J. Acoust. Soc. Am. 40 (1966) pp. 863 – 876.

[55] N Hoppe, A Puttmer, P Hauptmann: Optimization of buffer rod geometry using MATLAB, IEEE Ultraosnics Symposium (2001) pp 365 – 368

[56] CK Jen, JG Legoux: Clad ultrasonic waveguides with reduced trailing echoes, US Patent 5,828,274 (May 28 1996)

Chapter 2

Generation of Trailing Echoes in a Cylindrical Buffer Rod

It is known that trailing echoes are often generated in a long cylindrical buffer rod due to diffraction and mode conversion of waves along the rod having a finite diameter. In order to understand such generation, in this chapter, the generation of trailing echoes in a cylindrical buffer rod is examined by a numerical simulation based on a finite difference method. The mechanism to generate a trailing echo in a cylindrical buffer rod is presented. The validity of the simulation results is then verified with experiment.

2.1 Mechanism to generate trailing echoes

It is known that trailing echoes are often generated with long cylindrical buffer rods where such generation is due to wave diffraction and mode conversion of waves along a finite diameter of rods [2-15].

2.1.1 Wave diffraction

Wave diffraction is the bending of waves around obstacles and openings. There are two principles in wave diffractions; axial pressure profile and polar coordinate diffraction-type presentation. In this work, the first principle which is the axial pressure profile is used in this work. This is because of the pressure subjected on the rod by the transducer that is located at the center of the cross-sectional shape of buffer rod. In addition, this principle is correlated with the mechanism of the first principle where the pressure is emitted from the center line of the transducer. The definition of axial pressure profile is the diffraction plots the maximum pressure of an ultrasonic waveform as a function of the axial coordinate emanating from the center line of a transducer. Since the diffraction occurs at any obstacles or openings, which means the waves are diffracted from the edge of a transducer, as shown by Figure 2-1. The ultrasonic transducer is located at the center of the cross-sectional shape. There are two types of waves generated from the ultrasonic transducer (source) which are edge wave and plane wave, respectively. The plane wave propagates along the axial direction of the buffer while the edge wave propagates to the side wall of the rod at oblique angle. The plane wave is the fastest to be reflected at the rod end and received at the source compared to edge wave.

2.1.2 Mode conversion

The second stage for generating a trailing echo is mode conversion. The mode conversion means that a wave changes its type from longitudinal to shear waves and vice versa when it reached a rod boundary due to the acoustic impedance mismatch. The angle for such conversion can be calculated from Snell’s Law, if the incident angle for the longitudinal wave and velocity for both medium are known. Figure 2-2 shows the

mode conversion between two medium.. The angle for such conversion is shown by Equation 2.1,

$$\frac{\sin\theta_1}{V_{L_1}} = \frac{\sin\theta_2}{V_{L_2}} = \frac{\sin\theta_3}{V_{S_1}} = \frac{\sin\theta_4}{V_{S_2}} \tag{2.1}$$

where V_L and V_S are longitudinal wave velocity and shear wave velocity, respectively. As shown in Fig 2-22, the reflected angle for S_1 is smaller than that of L_1. This is because shear waves travel slower than longitudinal waves.

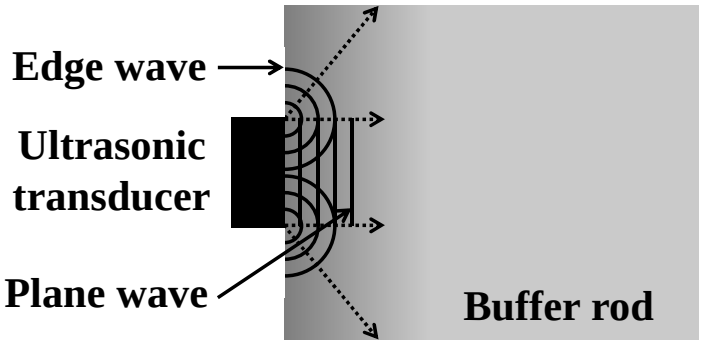

Figure 2-1: Wave diffraction where two types of waves are generated from the ultrasonic transducer.

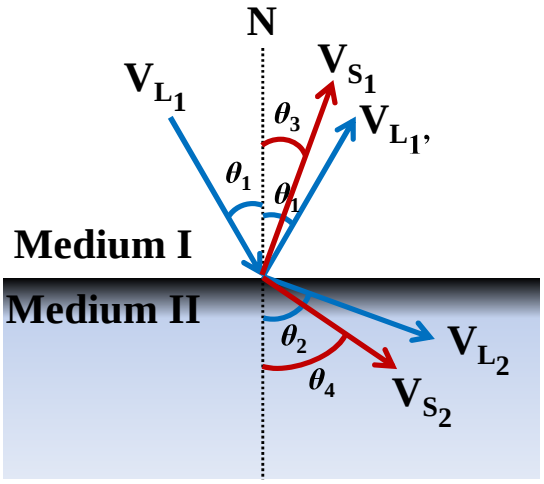

Figure 2-2: Mode conversion between two mediums.

2.1.3 Mechanism to generate trailing echoes in a cylindrical buffer rod

Figure 2-3 shows the mechanism to generate the first and second trailing echoes for a cylindrical buffer rod from side view (top figure) and cross-sectional view (bottom figures), where UT, L and S are ultrasonic transducer, longitudinal wave and shear wave, respectively. The UT which is located at the center of the cross-sectional shape is a longitudinal type and the number (0,1,2..) for each wave denotes the number of reflection and mode conversion of waves, i.e., the first reflected longitudinal wave is depicted as L_1. From the source (UT), a pair of longitudinal waves (L_0) with critical incident angle (θ_c) propagates to the rod boundary separately and each L_0 is reflected to L_1. Such oblique propagation is due to the wave diffraction where L_0 is an edge wave. Due to such critical angle, the reflected angle for both L_1 is 90^o. It is noted that there are many incident angles of L_0 emitted by the UT, however, in order for a UT to receive a wave, the wave direction must be in a perpendicular direction to the UT. During the reflection of L_0 to L_1, L_0 is also partially converted to shear wave (S_1) due to mode conversion. As shown in Figure 2-3, the reflected angle for S_1 is smaller than that of L_1. This is because shear waves travel slower than longitudinal waves. It is noted that the angle for such conversion is calculated by Snell's Law. Each of S_1 is then propagates to their opposite rod boundary and converted again to L_2. The propagation of S_1 to its opposite rod boundary is depicted in the first and second figures from left in the cross-sectional view of Figure 2-3. It is observed that both S_1 are parallel to each other and propagate to the side wall of the rod perpendicularly. Such parallelism and the arrival of S_1 perpendicular to the rod boundary (from cross-sectional view) result to the conversion of S_1 to L_2, where the propagation of L_2 is perpendicular to UT. Such perpendicular direction will then interfere at UT and generate an echo. Such echo can be either main echoes or trailing echoes. These echoes (main and trailing echoes) can be distinguished by their time delay. The same mechanism is also true for generating the second trailing echoes where L_3 arrived at UT in a perpendicular direction. Therefore, from the cross-sectional view, a trailing echo can be generated if the mode converted shear waves propagate to the side wall of the rod perpendicularly. In addition, in order to generate a trailing echo, three stages are involved; wave diffraction, mode conversion

and interference at UT. In order to verify the mechanism, a cylindrical buffer rod is numerically investigated.

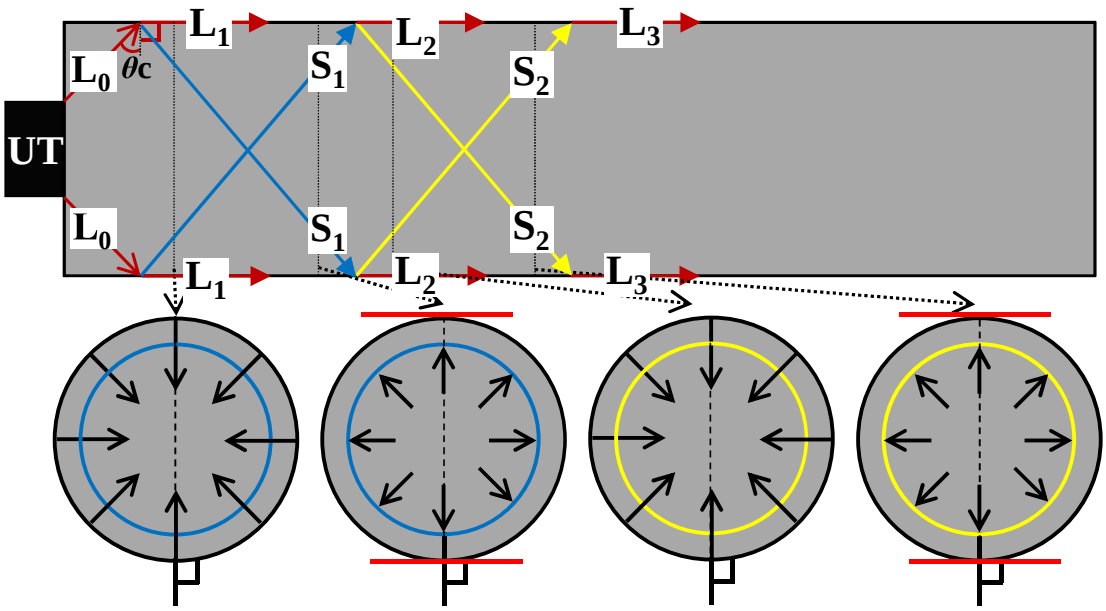

Figure 2-3: Mechanism to generate the first and second trailing echoes for a cylindrical buffer rod, from the side view (top figure) and cross-sectional view (bottom figures), respectively.

2.2 Three-dimensional numerical simulation

In this work, a commercially available three-dimensional numerical simulation based on a finite difference analysis called Wave3000 from CyberLogic, Inc. (New York) is used to investigate the behavior of ultrasonic waves propagating in any 3D objects. This software uses a three-dimensional isotropic model made by a discrete grid [20]. Equation 2.2 shows a hyperbolic partial differential equation for the general wave equation with a constant wave velocity, c.

$$\frac{\partial^2 w}{\partial t^2} = c^2 \nabla^2 w \tag{2.2}$$

If the simulation is in two-dimensional (2D), there are two different axis which are *x* and *y* where;

$$\nabla^2 w = \frac{\partial^2 w}{\partial x^2} + \frac{\partial^2 w}{\partial y^2} \tag{2.3}$$

But since the finite difference method is in three-dimensional simulation, an additional axis which is *z* is added where;

$$\nabla^2 w = \frac{\partial^2 w}{\partial x^2} + \frac{\partial^2 w}{\partial y^2} + \frac{\partial^2 w}{\partial z^2} \tag{2.4}$$

In an isotropic medium, the elastic wave equation in 3D is shown by Equation 2.5 where λ and μ are the Lame parameters, ρ is the density, *f* is the source function of the driving force and *w* is the displacement vector [21].

$$\rho \ddot{w} = f + (\lambda + 2\mu) \nabla (\nabla . \mathrm{w}) - \mu \nabla \mathrm{x} (\nabla \mathrm{x} w) \tag{2.5}$$

The divergence operator, $\nabla(\nabla.\mathrm{w})$ shown in Equation 2.5 can be elaborated as shown in Equation 2.6.

$$\nabla(\nabla . w) = \left(\frac{\partial}{\partial_x}, \frac{\partial}{\partial_y}, \frac{\partial}{\partial_z}\right)\left(\frac{\partial_w}{\partial_x} i + \frac{\partial_w}{\partial_y} j + \frac{\partial_w}{\partial_z} k\right) \tag{2.6}$$

For longitudinal waves, the propagation direction is assumed to be along the *z*-axis, which is the axial direction of the rod. The equation (Equation 2.2) is used to calculate the displacements of u_x, u_y and u_z at each spatial grid point at every time step that the user defined. Such displacements at each spatial grid point also occur under the boundary conditions at every interface that impose continuity of stresses and displacements. The wave behavior such as propagation motions for both longitudinal and shear waves in the medium can be obtained at every time step, as long as the stability requirement for the finite difference equations is satisfied. In order to make a stable calculation, the time step was chosen according to the von Neumann stability equation, as shown by Equation 2.7, where V_L, V_S and ε are the longitudinal wave velocity, shear wave velocity and grid spacing, respectively. The grid spacing, ε should be smaller than the shortest wavelength related to the highest frequency in the pulse and the lowest wave velocity in the medium, so that the sufficient accuracy in the calculation can be achieved.

$$\Delta t = \frac{\varepsilon}{\sqrt{V_L^2 - V_S^2}} \tag{2.7}$$

2.2.1 Three-dimensional simulation model

In order to create such 3D objects, there are several shape commands that are provided in Wave3000 such as block, cylinder or ellipsoid. However, since the 3D objects are polygonal buffer rods, it is a time consuming process to create such buffer rods using these shape commands. In order to overcome such problem, another command in Wave3000 is used to create the 3D models for the polygonal buffer rods where such command is “Create 3D object by slices”. This command allows the user to create any 3D model from a set of 2D slices or images in the file format of PCX, DICOM or RAW. These 2D slices or images will be transferred and defined as 3D models in Wave3000. In this work, PCX file format is used for the 2D image since such file format is commonly available in any graphic software. In order to create the 2D slices,

commercially available graphic software called CorelDRAW Graphic Suite X4 is used. Take note that in this work, the length of the buffer rod is 100 mm. Therefore, in order to design an adequate rod, the diameter of the circle is 20 mm. That means that the area of the designed circle is 314 mm^2. The circle is then export as PCX type so that it can be run in Wave3000. By using the 'Create 3D object by slices' command, since the resolution is 10 voxel/mm and the rod length is 100 mm, the value for the slice thickness is set to be 1000. The current file format which is in 2D image is changed to WHF when it is in 3D object. The material for the 3D cylindrical buffer rod is defined as mild steel. During defining the material for a 3D object, the material properties such as density, longitudinal wave velocity, shear wave velocity, wavelength, acoustic impedance and others are given. The longitudinal velocity, shear velocity and density for mild steel are 5900 m/s, 3200 m/s and 7800 kg/m^3, respectively. The values for each parameter (material properties) can be changed since the values for density, ρ (kg/m3), lambda, λ (MPa) and mu, μ (MPa) influence the material properties. In this simulations, the lambda, λ is defined as the 1st Lame constant while mu, μ is defined as the 2nd Lame constant. These two constants are the variables used to calculate the material properties such as Young's Modulus, Poisson's ratio, bulk modulus, longitudinal velocity and shear velocity of the 3D objects. The equation for each material property is presented below.

$$\text{Young's modulus} = \frac{\mu(3\lambda+2\mu)}{(\lambda+\mu)} \tag{2.8}$$

$$\text{Poisson's ratio} = \frac{\lambda}{[2(\lambda+\mu)]} \tag{2.9}$$

$$\text{Bulk Modulus} = \lambda + \frac{2}{3}\mu \tag{2.10}$$

$$\text{Longitudinal wave velocity} = \left[\frac{(\lambda+2\mu)}{\rho}\right]^{0.5} \tag{2.11}$$

$$\text{Shear wave velocity} = \left[\frac{\mu}{\rho}\right]^{0.5} \tag{2.12}$$

The value for lamba, λ and mu, μ can also be calculated where the equations are:

$$\lambda = \rho\left(V_L{}^2 - 2\,V_S{}^2\right) \tag{2.13}$$

$$\mu = \rho\,V_S{}^2 \tag{2.14}$$

Take note that the range of the gray level is 0 to 255, where 255 is defined as vacuum. It is observed that the 3D model changed its color to red when the gray level is defined as 178. Therefore, such value depends on which gray color that has been defined during creating the 2D image. In order to transmit ultrasonic waves into the 3D model, an ultrasonic transducer (UT) is defined at one end of the rod. The location for the UT is defined by the center of mass of the cross-sectional shape. Since the center of mass for a circle is at the center, the offset values for *x*-axis (H center offset) and *y*-axis (V center offset) are set at 0 (zero). Take note that in this work, the UT diameter is 6.35 mm; therefore, the UT radius is set to 3.175 mm. The UT type is defined as a Sine Gaussian longitudinal and the measurement type is in pulse-echo mode. Such measurement mode means that only UT will be used that act as a transmitter and also a receiver. By clicking the time function for the Sine Gaussian pulse, the waveform can be defined by defining the values for duration, amplitude, frequency and time constant '*a*', respectively. In this simulation, the equation for the Sine Gaussian is given by:

$$p(t) = \left[\frac{-\left(t-\frac{Duration}{2}\right)^2}{a^2}\right] sin\,2\pi f t \tag{2.15}$$

Take note that the time constant, *a* is inversely proportional to the bandwidth. That means by decreasing the time constant, the bandwidth will be increased. In this work, the value for duration, amplitude, frequency and time constant are 0.6 μs, 1, 5 MHz and 0.15 μs. Such values are chosen so that the waveform is almost similar with the waveform that is expected to be obtained in the experimental works. Figure 2-4 shows the waveform of the Sin Gaussian Pulse that is defined by these values.

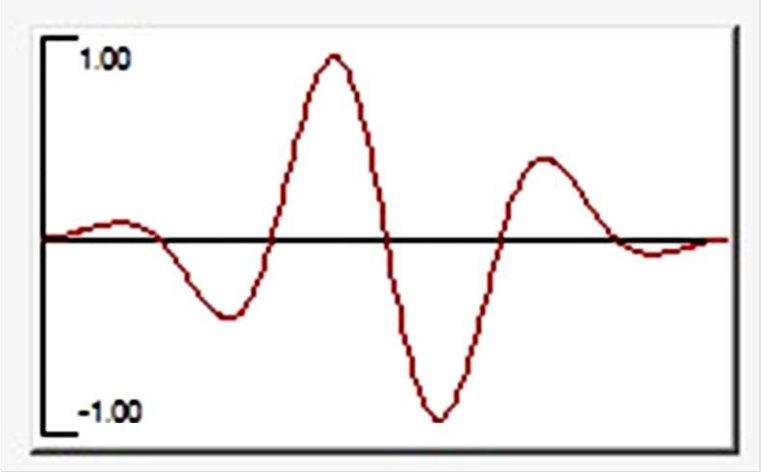

Figure 2-4: Waveform for the Sine-Gaussian Pulse.

Next, the output parameters for the pulse-echo measurement are defined in the 'Receiver Configuration' section where the user can choose which types of wave as the output. In this work, the output type of wave is chosen as longitudinal wave. The measurement data is then saved in txt. file format. Finally, the parameters such as frequency, wavelength, simulation time and others are manually defined in the 'Job Parameter' section in the software. The frequency is defined by the operating frequency of the UT that the user used. The value of resolving wavelength is chosen based on the lowest velocity in the pulse. That means the value for the resolving wavelength must be lower than the wavelength for the shear velocity. The wave propagation can also be

recorded using the 'Save Image Frequency' function. However, take note that since the 3D model takes a huge computational time, a huge memory size is needed for such recording function. Therefore, in this work, free recording software called CamStudio, is used to record the wave propagation. Before running the simulation, the parameters and values that have been defined for the 3D model is checked. In this work, since the mode resolution and the resolving wavelength are 10 voxel/mm and 0.6 mm, respectively, the grit size for each axis (x, y and z) is given. Since there are 10 voxels for every 1 mm, that means the length for each grit 0.06 mm. The total grit for each axis is 10 times from the defined length. That means when the diameter of rod is defined as 20 mm, it means that there are 200 voxels in such diameter. The total step is 0.9, based on equation 2.3 where such time step gives the value of the total step of 13084. For grid/voxel, if the value is more than 1, it means that the calculation is more accurate where additional grid is added into the calculation so that the simulation process is smoother, rather than that when the value of the grid /voxel is less than 1. The value of grid/voxel can simply calculated by resolution/wavelength. In addition, the user can also view their 3D model by 'View' → '3D Viewer' during and after the simulation. The simulation is conducted using a 64-bit workstation with multi-core Intel ® Xeon ® 2.4 GHz processors and 28 GB RAM (Precision T7500, Dell, Austin, Texas).

2.2.2 Simulation results and discussion

Figure 2-5 shows the simulated waveform for a cylindrical buffer rod where the formation of the first, second and third trailing echoes depicted as TE1, TE2 and TE3 are clearly observed between the first echo (E1) and second echo (E2). In this work, in order to measure the performance of buffer rods, SNR is used where it is defined as a ratio of the amplitude of the first echo (E1) relative to that of the largest trailing echoes accompanying the main echo: SNR = A_0/A_1 [5, 16,17]. Poor value of SNR is obtained due to big amplitude of the first trailing echo (TE1). Since the numerical simulation is carried out in three-dimensional, the wave propagation studies are possible from the side view and the cross-section view of the simulation model. Figure 2-6 shows the captured images of one round-trip of ultrasonic pulsed echo propagating through the 100 mm length cylindrical buffer rods, from side view (top image) and cross-section

view (bottom images), respectively. The brighter in the image means the higher amplitude in the ultrasonic waves. From the side view, the desired signals such as first echo and trailing echoes can be identified by the bright lines that are almost parallel to the UT surface, depending on the time delay. Therefore, from left, the first, second and third bright lines are identified as E1, TE1 and TE2, respectively. Meanwhile from the cross-section view, the desired signals such as main echo and trailing echoes are identified by the bright cross-section. Based on the simulation results, the mechanism to generate such trailing echoes in cylindrical buffer rods has been verified. In order to confirm the validity of the simulation results, experiment is conducted on a 100mm length cylindrical buffer rod using the same condition used in the simulation.

2.3 Experiment

2.3.1 Experimental setup

The experimental setup is shown in Figure 2-7 where the buffer rod is connected to the pulser receiver. It is observed that a layer of couplant (usually liquid type) is employed between the ultrasonic transducer and the end of one rod. The pulser receiver is connected with a computer for displaying and analyzing the received signals. A steel (S45C) cylindrical buffer rod having the same dimension as the three-dimensional cylindrical simulation model is fabricated. Figure 2-8 shows the fabricated buffer rod having the rod length of 100 mm and rod diameter of 20 mm. The fabricated cylindrical buffer rod is paired with a longitudinal UT as shown in Figure 2-9. The operating frequency and diameter of UT are 5 MHz and 6.35 mm, respectively. Since the measurement is a pulse-echo mode, only one transducer is used for transmitting and receiving the ultrasonic pulsed waves. Although it has been reported that diameter of UT should be 75% of diameter rod, the tendency of trailing echo does not change drastically as long as the size of UT is smaller than the rod so that all energy can be launched and coupled out of the core efficiently [10]. Operating frequency of 5MHz is chosen due to its efficiency and acceptable loss (in terms of attenuation) in the probed parts [18].

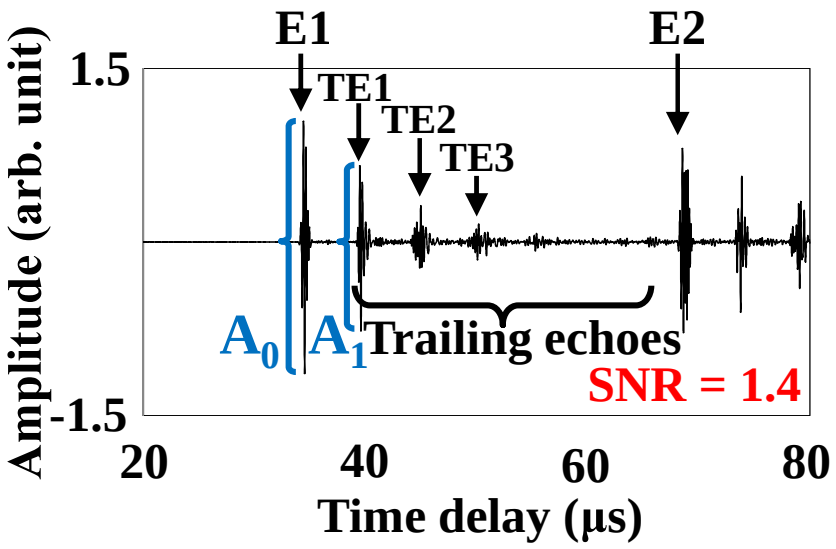

Figure 2-5: Simulated waveform for the 100 mm length cylindrical buffer rod

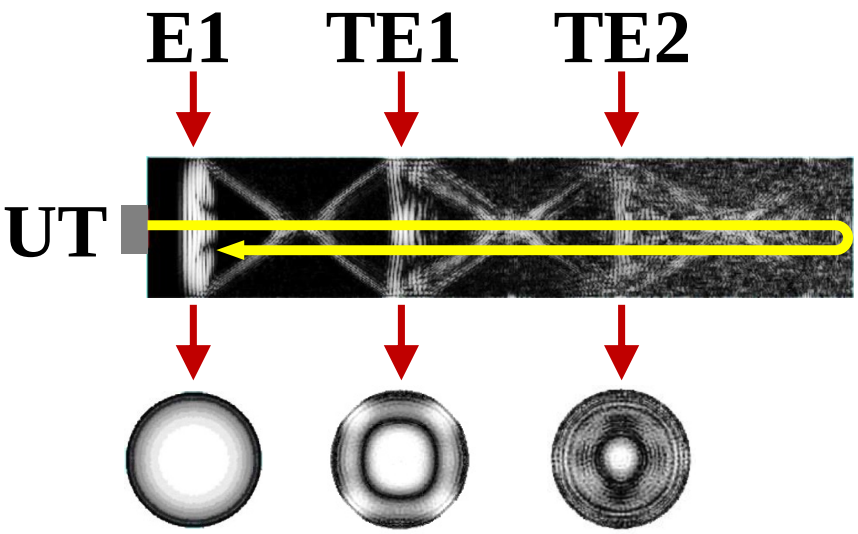

Figure 2-6: Captured images of one-round trip ultrasonic pulsed echo propagating through the 100mm length cylindrical buffer rod, from side view (top image) and cross0section view (bottom images), respectively.

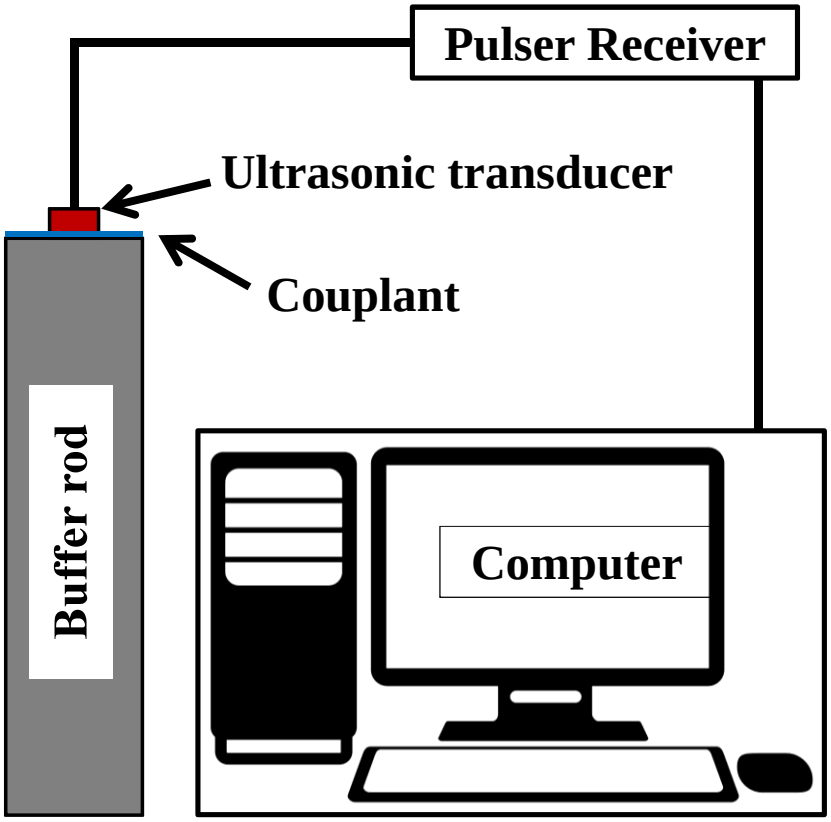

Figure 2-7: Experimental set-up for a pulse-echo measurement with a buffer rod

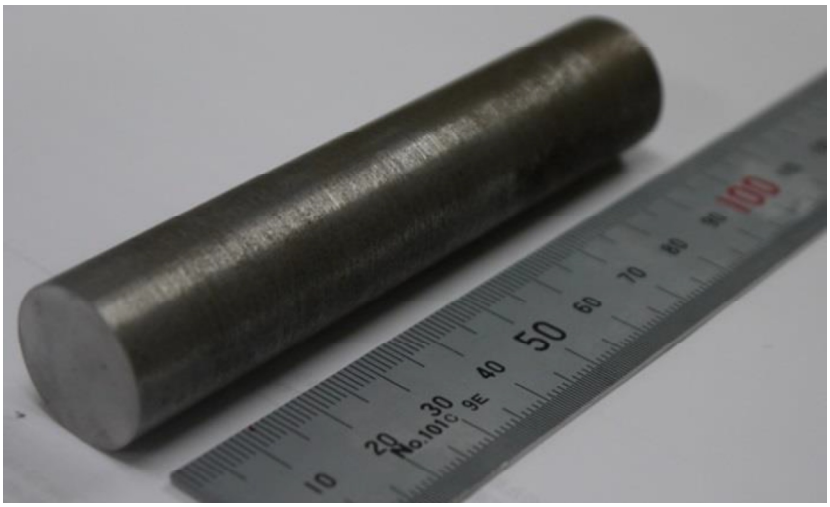

Figure 2-8: 100 mm length cylindrical buffer rod

The couplant which was not defined in the numerical simulation is applied between the UT and one end of the rod. In order to eliminate the influence of gripping on buffer rods during the pulse-echo measurement, a jig is used to hold the buffer rod, as shown in Figure 2-10. Such approach is to prevent any energy loss where the ultrasonic pulsed waves may be transferred into the hand grip of the examiner. Besides that, the pressure subjected by the transducer on the surface of rod is constant. Next, the ultrasonic transducer is connected to a pulser-receiver (Olympus 5073PR) as shown in Figure 2-11. In order to receive the ultrasonic pulse waves, the pulser-receiver is connected to a computer where the LabView program is used to analyze the received signals, as shown in Figure 2-21. The received signals are then saved in an Excel file format. By using the LabView program, several precise measurements such as distance, velocity can be calculated on the received signal using the cross-correlation method [19].

Figure 2-9: A longitudinal ultrasonic transducer with operating frequency of 5MHz

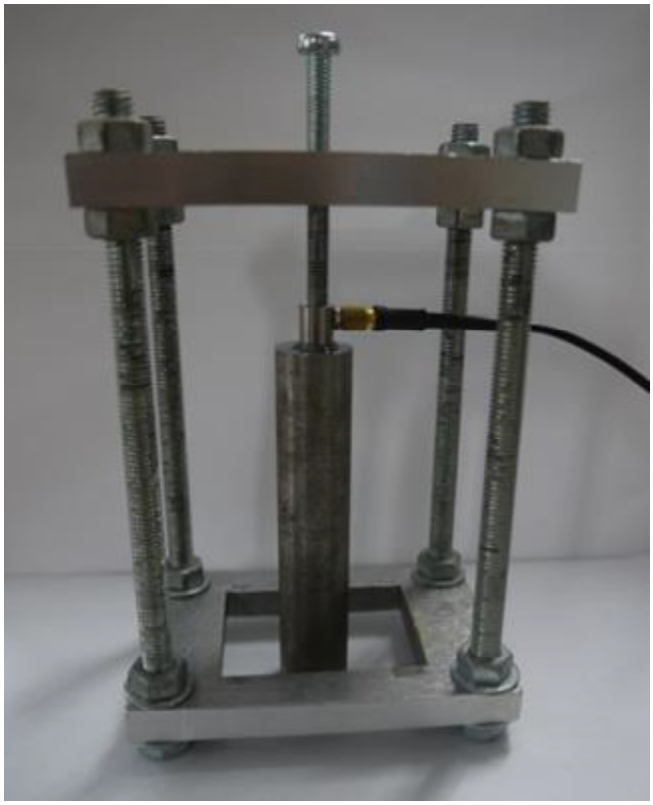

Figure 2-10: Buffer rod is attached on a jig

Figure 2-11: Pulser-receiver

2.3.2 Experiment results and discussion

The measured signal of a 100 mm length cylindrical buffer rod is shown in Figure 2-12. It can be seen that the wave shows a similar behavior in terms of main echoes and trailing echoes as the simulations result. Although the tendency of wave behavior including trailing echoes for the measured waveform is similar with that of simulated waveform, there are some discrepancies on the amplitude of signals. It has been reported that such difference of amplitude may due to the noise distributions that do not implemented in the simulation condition, misalignment of the rod geometry during the fabrication process, generation of noise between the piezoelectric element in the UT and buffer rod and some noise error generated in the measuring system [6]. However, these factors did not give a significant effect on the measured waveform since the measured signal is clearer than that of simulated signal. Therefore, it is believed that the discrepancies of amplitude between the measured and simulated waveforms may be influenced by the voxels of the simulation model. It is noted that a simulation model has even and inclined surfaces, depending on the cross-sectional shape. In order to create a three-dimensional model, the voxels are meshed in rows and columns based on the three-dimensional Cartesian coordinate system (x-axis, y-axis and z-axis). Since the shape of a voxel is a cube, the inclined surfaces of a simulation model are not smooth and may result to diffuse reflection, as shown by Figure 2-13. Such reflection may affect the amplitudes of the reflected waves since specular reflection does not occur on such rough surfaces. However, the tendency of the wave propagations including trailing echoes is similar for both simulation and experimental works; therefore, it is noteworthy to say that the simulation works was carried out appropriately.

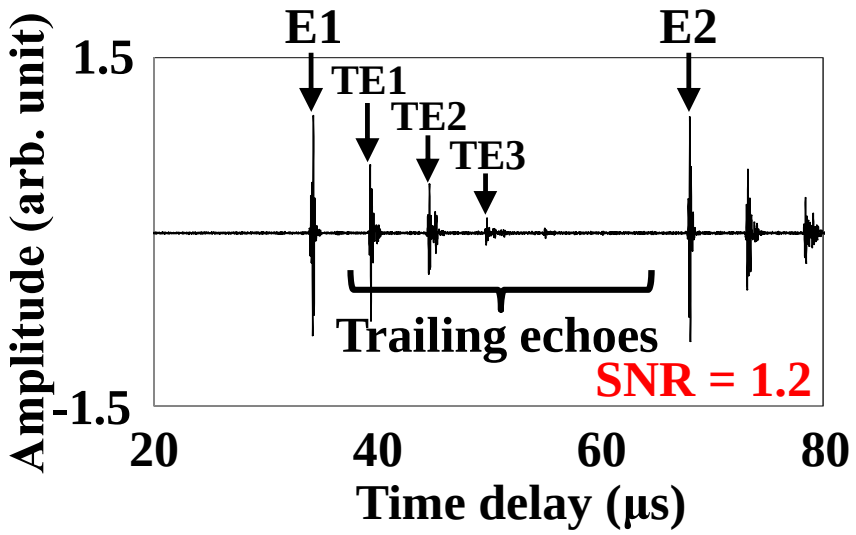

Figure 2-12: Measured waveform for the 100 mm length cylindrical buffer rod

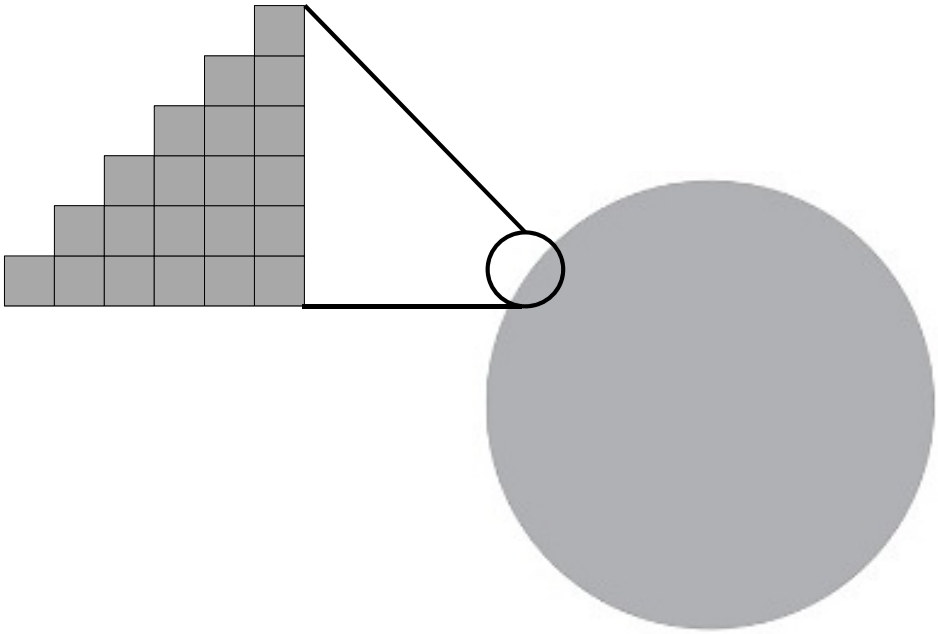

Figure 2-13: Meshed voxels on the boundary of a circle

2.4 Conclusions

The influence of cylindrical buffer rod in generating trailing echoes has been investigated numerically and experimentally.

1) The mechanism to generate trailing echoes is presented. The mechanism for such generation is numerically and experimentally investigated. Therefore, the mechanism to generate trailing echoes for a cylindrical buffer rod is verified.

2) Based on the wave propagation studies, the generation of trailing echoes can be depicted from the cross-sectional shape. From the cross-sectional shape, a trailing echo is generated when the parallel mode converted shear waves propagate to the side wall of the rod perpendicularly, as shown by Figure 2-14.

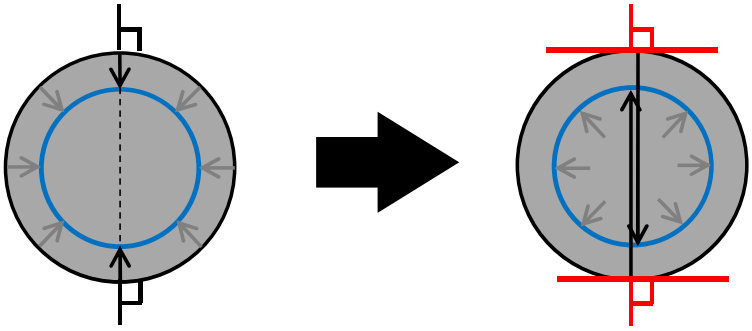

Figure 2-14: Propagation of a pair of parallel mode converted shear waves to the side wall of the rod perpendicularly

3) The trailing echoes are significantly generated in the cylindrical buffer rods due to the cross-sectional shapes which is a circle. Since a circle has infinite symmetry axis, trailing echo is possible to be generated at any point of the cross-sectional shape (circle).

4) In order to overcome or reduce such generation, the cross-sectional shape of a buffer rod having no parallel sides should be used. Therefore, the idea of using polygonal buffer rods in reducing the trailing echoes will be implemented. The effect of such polygonal buffer rods will be numerically and experimentally investigated in the next chapter.

2.5 References

[1] CK Jen and JG Legoux: High performance clad metallic buffer rods, Proc. IEEE Ultrasonic Symposium 1 (1996) pp. 771 – 776

[2] M Redwood: Mechanical waveguides, Pergamon, New York, 1996, pp. 191 – 207.

[3] CK Jen, C Neron, EL Adler, GW Farnell, J Kushibiki, K Abe: Long acoustic imaging probes, Proceedings of IEEE Ultrasonics Synposium (1990) pp. 875 – 880

[4] CK Jen, L Piche, JF Bussiere: Long isotropic buffer rods, Journal of acoustic society of America 88 (1990) pp. 23 – 25.

[5] Y Ono, M Kobayashi, JF Moisan and CK Jen: High Temperature and Broadband Immersion Ultrasonic Probes, IEEE Sensors journal 6(3) (2006) pp. 580-587.

[6] J Garcia-Alvarez, Y Yanez, JL Prego, A Turo, JA Chavez, MJ Garcia, J Salazar: Noise level analysis in buffer rod geometries for ultrasonic sensors, Ultrasonics 44 (2006) pp. 1093 – 1100.

[7] A Puttmer, P Hauptmann, Bernd Henning: Ultrasonic Density Sensor for Liquids, IEEE Transactions on Ultrasonics, Ferroelectrics, and Frequency Control 47(1) (2000) pp. 85 – 92

[8] A Puttmer, R Lucklum, B Henning, P Hauptmann: Improved ultrasonic density sensor with reduced diffraction influence, Sensors and Actuators A67 (1998) pp 8-12

[9] A puttmer, N Hoppe, P Hauptmann: Low Noise Design of Ultrasonic Transducers, IEEE Ultrasonics Symposium 1999 pp 1177 – 1180

[10] CK Jen, C Neron, A Miri, H Soda, A Ohno, A McLean: Fabrication and characterization of continuously cast clad metallic buffer rods, Journal of Acoustic Society of America 91 (1992) pp. 3565 – 3570

[11] CK Jen, JG Legoux and L Parent: Experimental evaluation of clad metallic buffer rods for high temperature ultrasonic measurements, NDT & E International 33 (2000) pp. 145 – 153

[12] Y Ono, CK Jen, CC Cheng, M Kobayashi: Real-time monitoring of injection molding for microfluidic devices using ultrasound, Polymer Engineering and Science 45(4) (2005) pp. 606 – 612.

[13] I Ihara, CK Jen, DR Franca: Detection of inclusion in molten metal by focused ultrasonic wave, Jpn. J. Appl. Phys. 39 (2000) pp. 3152 – 3153

[14] I Ihara, H Aso and D Burhan: In-situ observation of alumina particles in molten aluminum using a focused ultrasonic sensor, JSME International Journal Series A 47(3) (2004) pp. 280 – 287.

[15] I Ihara, CK Jen, DR Franca: Materials evaluation in molten metal using focused ultrasonic sensor: Application to molten zinc, Advances in Technology of Materials and Materials Processing Journal, 3 (2001 pp. 45 – 50

[16] Y Ono, CK Jen and CY Su: Aluminum buffer rods for ultrasonic monitoring at elevated temperatures, IEEE Transactions on Ultrasonics, Ferroelectrics and Frequency Control 52(6) (2005) pp. 1042 – 1047.

[17] Y Ono, CK Jen, CC Cheng and M Kobayashi: Real-time monitoring of injection molding for microfluidic devices using ultrasound, Polymer Engineering and Science 45(4) (2005) pp. 606 – 612.

[18] CK Jen, B Cao, KT Nguyen, CA Loong, JG Legoux: On-line ultrasonic monitoring of a die-casting process using buffer rods, Ultrasonics 35 (1997) pp. 335 – 344.

[19] H Wang, B Cao, CK Jen, KT Nguyen, M Viens: On-line ultrasonic monitoring of the injection molding process, Polymer Engineering & Science 37(2) (1997) pp. 363 – 376

[20] About Wave3000TM (2015). Retrieved from: https://www.cyberlogic.org/about3000.html

[21] BA Auld: *Acoustic Fields and Waves in Solids*, *Vols. 1*, Krieger, 1973, pp. 131 - 157.

Chapter 3

Cladding Effect on Cylindrical Buffer Rods

In this chapter, the influence of cladding effect on cylindrical buffer rods is presented. Cladding is well known for its effectiveness in reducing trailing echoes and improves the signal-to-noise ratio (SNR). However, the effectiveness of cladding effect is mostly presented in experimental works. In this chapter, the influence of a cladding layer on a cylindrical buffer rod is numerically investigated. It is important to obtain an appropriate condition for a cladding layer that can prevent the generation of trailing echoes completely. It is also believed that the presented work in this chapter is beneficial for others to design the optimum clad buffer rod.

3.1 Cladding effect

A clad buffer rod which commonly consists of a core and a cladding layer has been experimentally demonstrated that it is capable to reduce the trailing echoes significantly [1, 2]. Such clad buffer rod has been applied in many materials and process monitoring at high temperature such as die casting process [3], curing process of molten polymer [4], material characterization in molten zinc [5], injection molding process [6], online monitoring of liquid magnesium [7], particle detection in liquid aluminum [8], molten glass measurement [9], plastic forming process monitoring [10], and cleanliness evaluation of molten light metals [11]. Therefore, clad buffer rods are proven to be capable in providing a desirable pulse-echo measurement at high temperature with high SNR. Such high performance of clad buffer rods depends on the core and clad materials where trailing echoes are generated due to the difference of the acoustic impedances at the interface between the cladding layer and the core of buffer rod [12]. Therefore, in this chapter, such combination of core and cladding layer is investigated using numerical simulation. It is expected that the new finding on such optimum cladding layer could be beneficial for others to fabricate and fabricate the desired clad buffer rods.

3.2 Investigate the appropriate cladding layer

In the beginning stage of this study, a 25 mm cylindrical buffer rod is numerically simulated using two-dimensional numerical simulation software that based on a finite difference analysis from CyberLogic, Inc. called Wave2000 Pro. Such 2D simulation is good enough to simulate the influence of a cladding layer on a cylindrical buffer where the result is almost agree with the experimental results [13]. The simulated waveform for a 25 mm length cylindrical buffer rod is shown in Figure 3-1 where the SNR is clearly deteriorated. Since acoustic impedance is known as the product of density and velocity, in this work, such density and velocity of the cladding are changed from 50% to 150% of those of the core which is assumed as mild steel. Figure 3-2 shows the 2D simulation model of a clad cylindrical buffer rod where the rod length, rod diameter, cladding thickness are 25 mm, 5 mm and 2 mm, respectively. Although the size is small which a quarter from the previous 100 mm cylindrical buffer rod presented in Chapter 3,

it is still possible to examine the influence of acoustic impedances at the interface. The ultrasonic transducer (UT) diameter is 1.6 mm and a Gaussian-type longitudinal pulse of 5MHz is employed at the center of the cross-sectional shape. The longitudinal wave velocity, shear wave velocity and density of the steel core used in the analysis are 5900 m/s, 3200 m/s, and 7800 kg/m3, respectively.

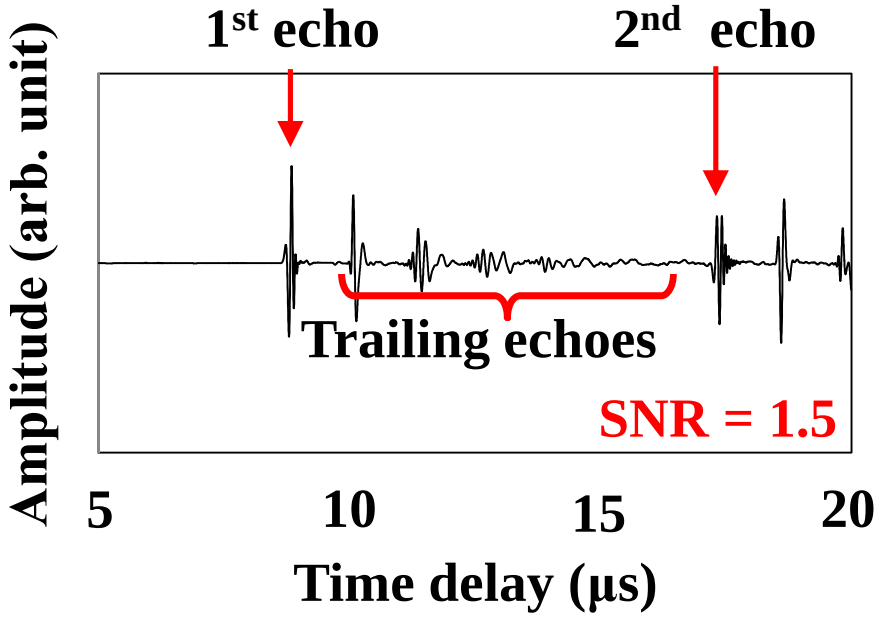

Figure 3-1: Simulated waveform for a 25 mm length cylindrical buffer rod

3.3 The influence of velocity of the cladding layer on trailing echoes

In order to investigate the influence of velocity of the cladding layer on trailing echoes, the density for both core and clad are kept constant. That means the density for core and clad are 7800 kg/m^3, while the velocity of clad is changed from 50% to 150% of the core. Figure 3-3 shows the simulation results in captured images of the pulse wave propagating through seven kinds of clad buffer rods (left) and the corresponding waveforms (right). From the wave propagation images, the bright lines nearest and parallel to the UT are the first echo. Due to the difference of acoustic impedance, it is observed that the waves are reflected at the interface between core and clad. However,

such reflection is not observed for the clad layer of V_{clad} = 100% V_{core} since the acoustic impedance for both core and cladding are the same, as shown by the fourth captured image from top in Figure 3-3. Similar trailing echoes as generated in Fig. 3-2 are observed when the velocity of clad is less than that of core. However, when the velocity of clad is more than that of core (110% to 150%), almost no significant trailing echoes are observed. Such significant reduction is due to the partial conversion of longitudinal waves to shear waves at the interface between the core and cladding is restrained so that less shear waves causing trailing echoes are generated at the interface [12]. In addition, as shown by the simulated waveforms in Figure 3-3, the amplitude, location and number of trailing echoes depend on the velocity of waves. Such velocity dependent phenomenon of the trailing echoes is related to wave reflection and refraction at the interface. The velocity of cladding basically influences the refraction angle in the cladding and the amplitude of reflection and refraction waves. Based on previous studies regarding the influence of velocity of the cladding layer, faster velocities of clad provide better wave guidance for the longitudinal elastic waves in the clad buffer rods [12, 14]. The generation of trailing echoes is based on the fundamental of geometrical optics and the mode conversion from longitudinal to shear waves at the interface between the core and clad. This means that not only the reflected shear wave which is mode-converted at the interface but also refracted waves which are transmitted into the cladding from the core play an important role in generating the trailing echoes although such partial conversion of the waves depends on the incident angle to the interface. In general, the refraction angle increases with the velocity of cladding and can be almost parallel to the interface when the velocity has a particular value with which the incident angle is near a critical angle. In such situation, it is considered that the generation of spurious noises is partially restrained owing to a kind of confinement effect of the refracted waves to the cladding. Therefore, faster velocities of the cladding layer are effective to reduce the trailing echoes. However, faster velocity of clad gives larger difference in acoustic impedance between the core and clad. Such large difference may leads to bigger amplitude of trailing echoes, as shown by the last captured image in the left side of Figure 3-3 where the velocity of clad is more than core by 150%. Thus, faster velocity of cladding may not always effective to reduce trailing echoes and

optimum value of velocity may exist depending on the material combination of the core and clad.

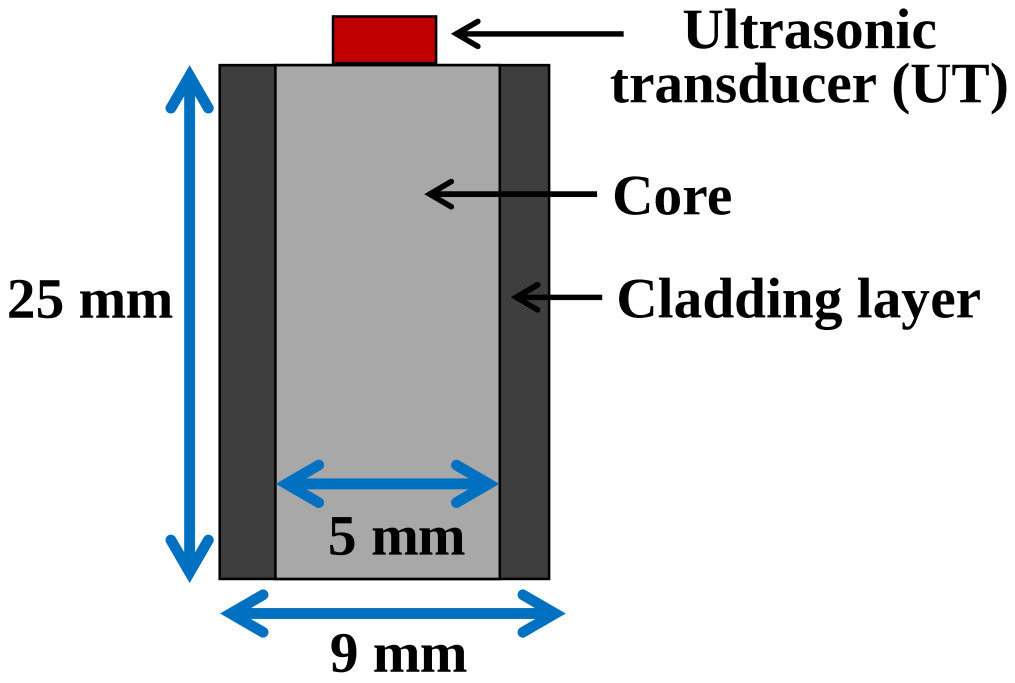

Figure 3-2: Schematic diagram of the two-dimensional simulation model for a clad cylindrical buffer rod.

3.4 Finding the optimum property for the cladding layer

In previous subsection, the influence of velocity of clad on trailing echoes has been investigated where the density for core and clad are constant. In order to find the optimum property for the cladding layer, the influence of acoustic impedance of a cladding layer on SNR is examined for different clad buffer rods. In this work, both the density and clad velocity are systematically changed within the range from 50% to 150% of those of a core. The material for the core is mild steel. Figure 3-4 shows the variations of SNR with the clad velocity for various densities. As expected, high SNR is obtained when the velocity of clad is faster than that of core. Based on this figure, the maximum SNR is obtained when the velocity of clad is 120% and the density of clad is 70%. In addition, it is observed that the SNR seems to be constant when the velocity of clad is 110% that that of the core. In order to investigate such constant values of SNR, another graph is plotted where the x-axis and y-axis are density and velocity of clad, respectively. Figure 3-5 shows the influence of density of the cladding layer on the SNR with various velocities of the cladding layer. Again, as expected, high SNR is obtained when the velocity of clad is higher than that of core. In addition, it is interesting to note here that a constant value of SNR of 25 is obtained when the velocity of clad is 110% of the core. Such plateau is depicted in an oval shape. Such finding is very important and beneficial for designing the optimum clad buffer rods because the density is flexible as long as the velocity of clad is 110% than that of the core.

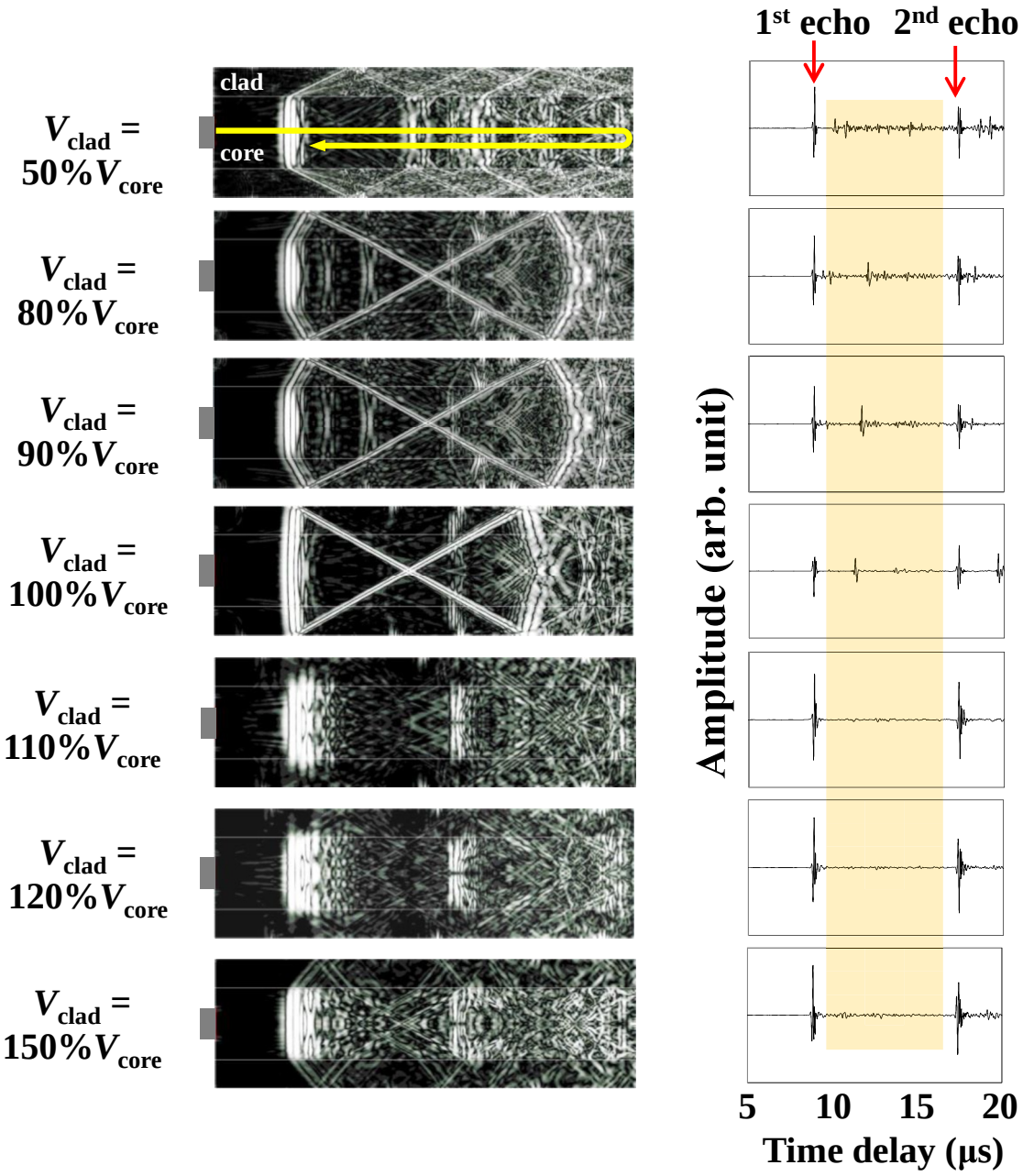

Figure 3-3: Simulation results showing captured images of pulse wave propagations for seven kinds of clad buffer rods (left) and the corresponding final waveforms (right)

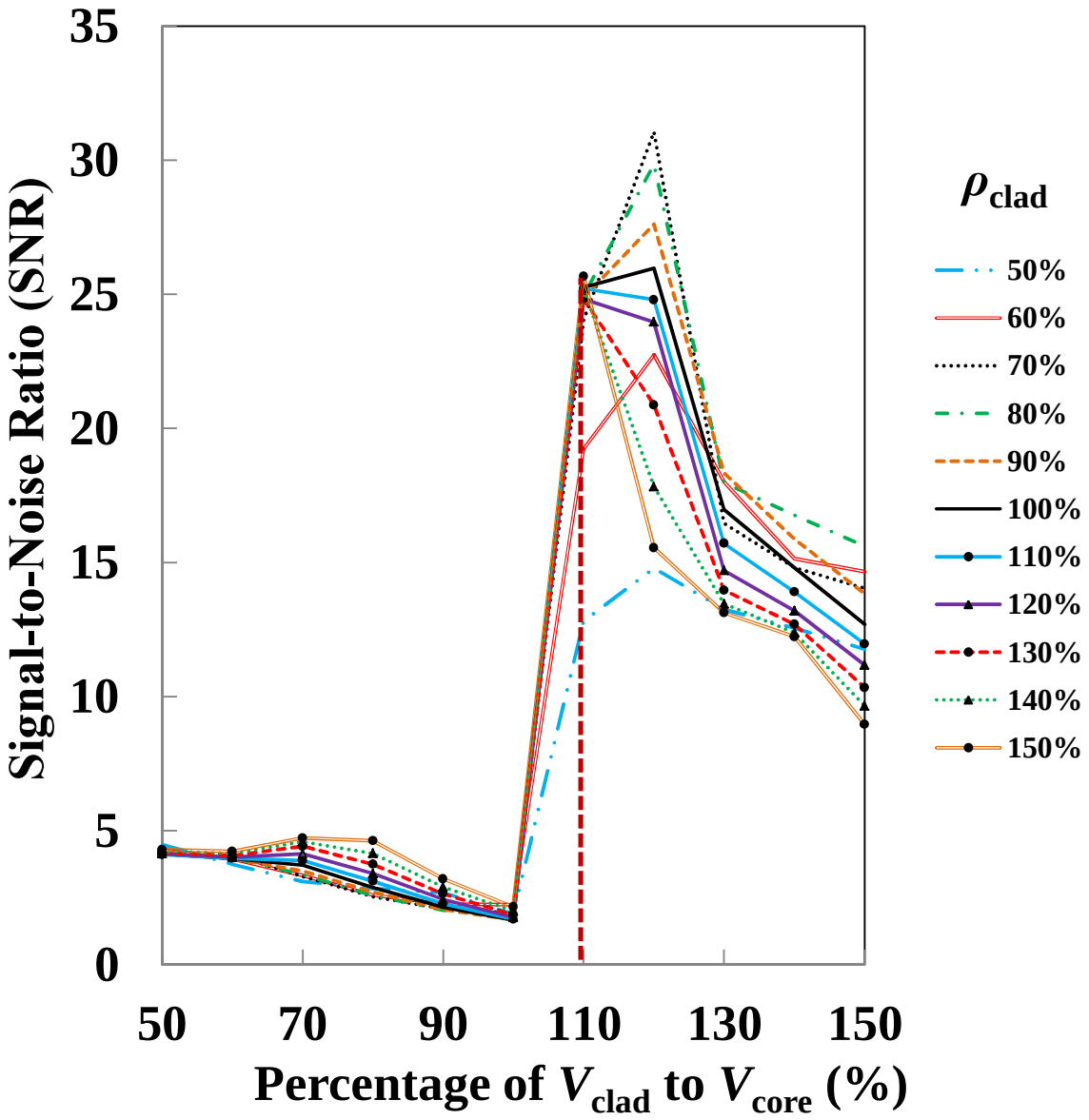

Figure 3-4: Variations of SNR with the velocity of clad for various densities of cladding

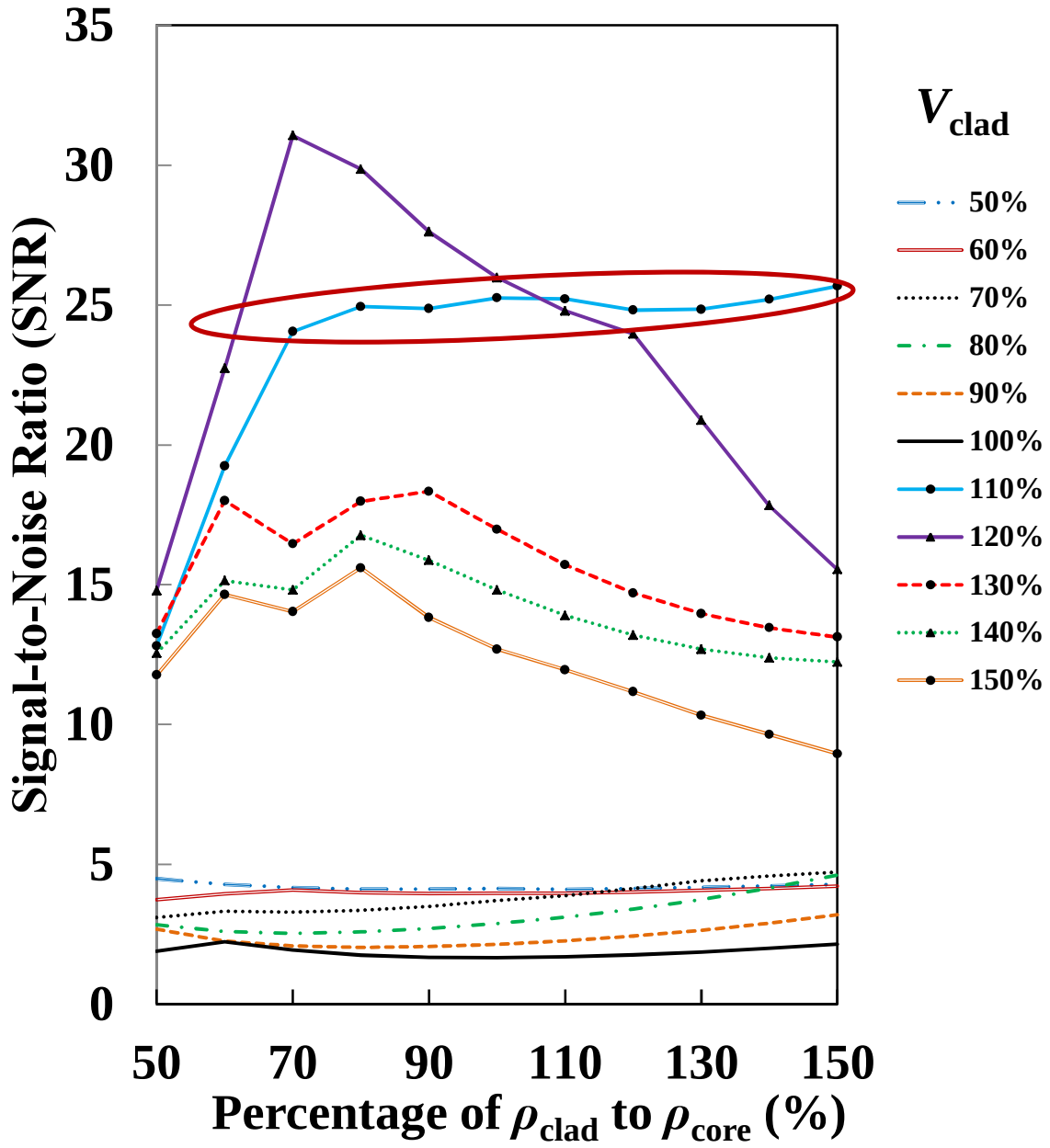

Figure 3-5: Variations of SNR with the density of clad for various velocities of cladding

3.5 Verifying the validity of the optimum condition for a cladding layer

Based on Figure 3-4 and Figure 3-5, it is known that the highest SNR is obtained when the velocity and density of clad are 120% and 70% than that of the core. In addition, it is known that the SNR is improved as long as the clad velocity is higher than that of the core. In order to verify the validity of the results obtained in Figure 3-4 and Figure 3-5, three cladding materials are chosen where the velocity of each material is higher than steel (core). The cladding materials are zirconium oxide, ZrO_2, Molybdenum, Mo and Titanium, Ti, respectively. The velocity for ZrO_2, Mo and Ti are 119%, 107% and 103% of core, respectively while the density for ZrO_2, Mo and Ti are 73%, 128% and 55% of core, respectively. Based on these materials, it is expected that the highest SNR will be given by ZrO_2 since the material properties (velocity and density) are almost similar with the condition that gives the highest SNR in Figure 3-4 where V_{clad} = 120% V_{core} and ρ_{clad} = 70% ρ_{core}. Once again, the rod length and cladding thickness are 25 mm and 2 mm, respectively. The simulated waveforms for such clad buffer rods are shown in Figure 3-6. As expected, excellent waveforms with almost no trailing echoes are successfully obtained for each cladding material. The SNR is also improved tremendously. Therefore, the conditions for a cladding layer presented in Figure 3-4 and Figure 3-5 are verified. The SNR for all the simulated waveforms in Figure 3-6 can be predicted using Figure 3-4. Figure 3-7 shows the SNR for all the cladding materials such as ZrO_2, Mo and Ti, respectively. The highest SNR is given by ZrO2, followed by Mo and lastly, Ti. Although an optimum condition for a cladding layer is achieved, however, the fabrication of a clad buffer rod is sometimes difficult. The common methods to fabricate clad cylindrical buffer rods are thermal spray and electroplating. However, it is difficult to control the density of the cladding layer since these methods will produce a porous layer [1]. However, since a plateau is achieved where high SNR is obtained when the density is clad in the range of 70% ~ 150%, the fabrication process of a clad buffer rod may be less difficult. However, take note some materials may not in such range of density, therefore, the new idea of using polygonal buffer rod is proposed. Such idea eliminates the use of taper and cladding since the cross-sectional shape of a conventional buffer rod is changed from circle to regular polygons.

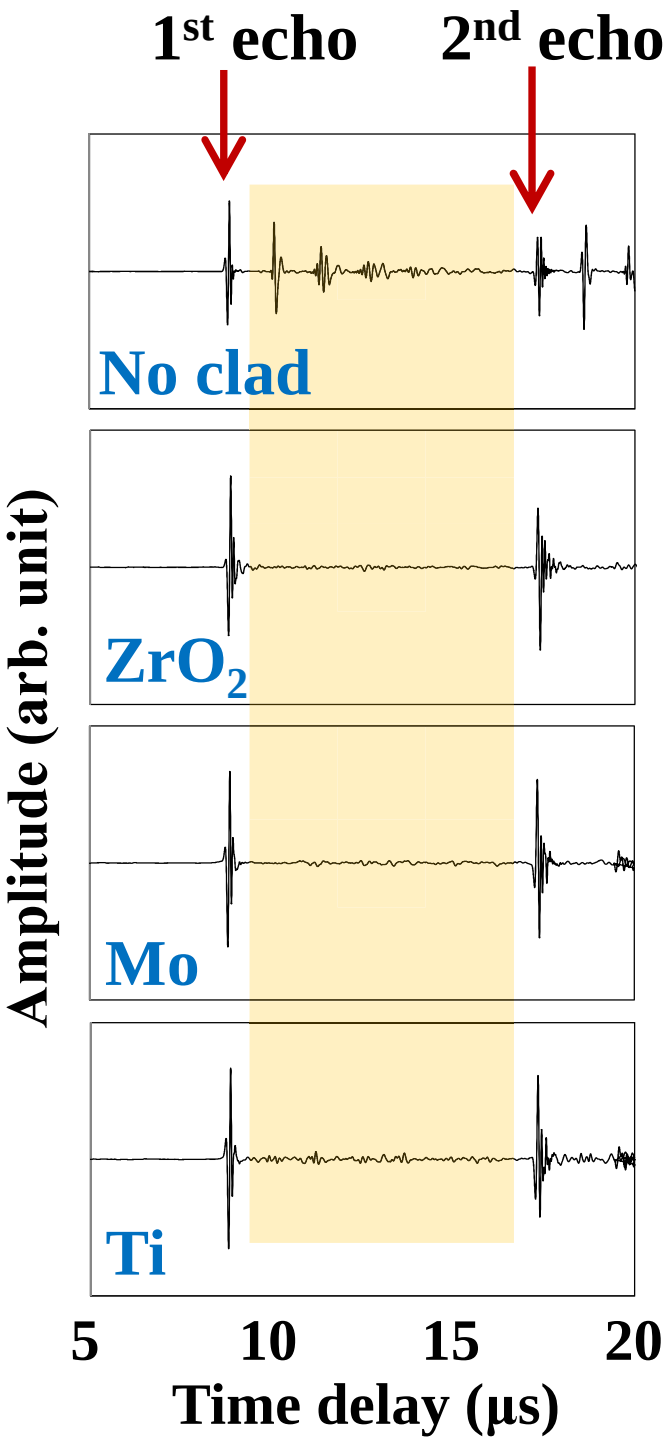

Figure 3-6: Simulated waveform for a clad cylindrical buffer rod where the core is steel while the clad materials are zirconium oxide, ZrO_2, Molybdenum, Mo and Titanium, Ti, respectively.

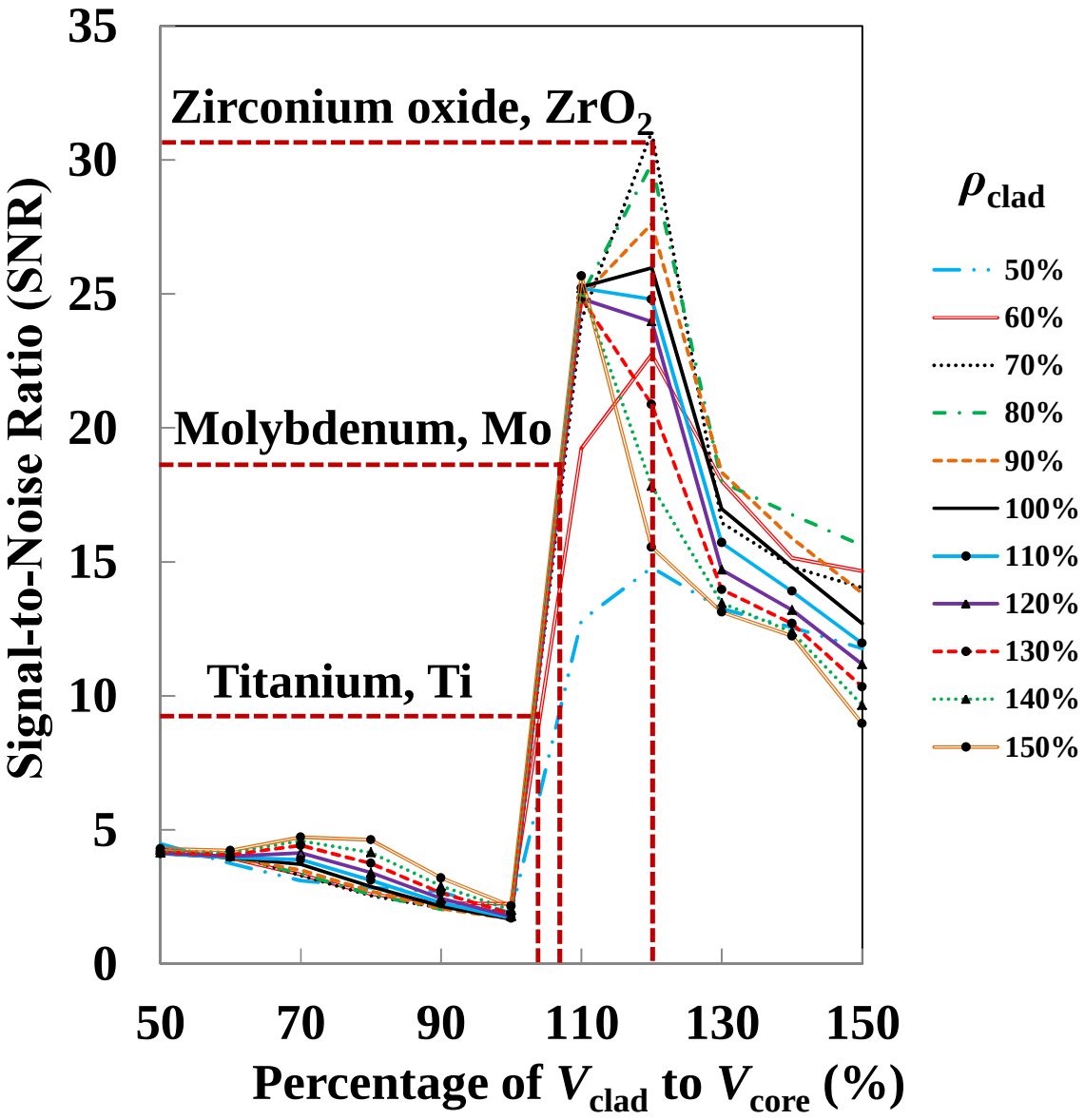

Figure 3-7: Expected value of SNR for each of the cladding materials such as zirconium oxide, ZrO_2, Molybdenum, Mo and Titanium, Ti, respectively.

3.6 Conclusions

The appropriate condition for a cladding layer has been investigated. The results obtained in this Chapter are summarized as follows:

1) Based on the simulation results, trailing echoes are reduced when the velocity of clad is faster than that of core. It is found that at such velocity, the mode converted waves propagate at the interface between the core and cladding layer. Since it is known that trailing echoes are generated due to such mode converted waves in the core, such faster velocity of clad refrain the mode converted waves to reflect in the core. Therefore, the generation of trailing echoes is restrained and the SNR is significantly improved.

2) A plateau of high SNR (approximately 25) when Vclad = 110% Vcore and ρclad = 70% ~ 150% of the core. Such finding is beneficial in designing and fabricating an optimum clad buffer rod since the density of clad is flexible.

3) Highest SNR is obtained when the cladding condition is Vclad = 120% Vcore and ρclad = 70% ρcore. Take note that faster cladding does not always improve the SNR due to huge difference of acoustic impedances between the core and clad.

4) The validity of this investigated is verified with a clad cylindrical buffer rod. Since the highest SNR is obtained when Vclad = 120% Vcore and ρclad = 70% ρcore, zirconium oxide (ZrO2) is chosen as the clad material. The velocity and density for ZrO2 are 122% and 73% than those of steel. As expected, high SNR is obtained where the trailing echoes are almost eliminated. Similar result is expected for other clad materials such as Titanium and Molybdenum since their velocities are faster than steel.

5) Although a plateau is achieved when the density of clad is 70% ~ 150% of core, the fabrication of clad cylindrical buffer rods that uses thermal spray or electroplating can be difficult if the density of clad is less than 70% than that of the core. Such difficulty arises due to the porous state of the cladding layer due to such fabrication processes. Therefore, the idea of using polygonal buffer rod is proposed where such idea eliminates the use of taper and cladding.

3.7 References

[1] CK Jen and JG Legoux: High performance clad metallic buffer rods, Proc. IEEE Ultrasonic Symposium 1 (1996) pp. 771 – 776

[2] CK Jen, JG Legoux and L Parent: Experimental evaluation of clad metallic buffer rods for high temperature ultrasonic measurements, NDT & E International 33(3) (2000) pp. 145 – 153.

[3] JF Moisan, CK Jen, JW Liaw, CQ Zheng, TF Chen, Z Sun and CA Loong, Ultrasonic sensor and technique for in-line monitoring of die casting process, Measurement Science and Technology 12(11) (2001) pp. 1956.

[4] N Legros, CK Jen and I Ihara, Ultrasonic evaluation and application of oriented polymer rods, Ultrasonics 37(4) (1999) pp. 291 – 297.

[5] I Ihara, CK Jen and DR Franca, Ultrasonic imaging, particle detection and V(z) measurements in molten zinc using focused clad buffer rods, Review of Scientific Instruments 71(9) (2000) pp. 3579 – 3586.

[6] H Wang, B Cao, CK Jen, KT Nguyen and M Viens, On-line ultrasonic monitoring of the injection molding process, Polymer Engineering & Science 37(2) (1997) pp. 363 – 376.

[7] D Burhan, I Ihara, S Kamado, H Aso and Y Kojima, On-line monitoring of liquid magnesium using a high temperature ultrasonic probe, Materials Science Forum 419 – 422 (2003) pp. 665 – 670.

[8] I Ihara, H Aso and D Burhan, In-situ observation of alumina particles in molten aluminum using a focused ultrasonic sensor, JSME International Journal 47(3) (2004) pp. 280 – 286.

[9] T Ihara, N Tsuzuki and H Kikura, Development of the ultrasonic buffer rod for the molten glass measurement, Progress in Nuclear Energy 82 (2015) pp. 176 – 183.

[10] L Piche, R Gendron, A Hamel, A Sahnoune and J Tatibouet, Ultrasonic probe for on-line process monitoring, Plastic Engineering 55(10) (1999) pp. 39 – 42.

[11] Y Ono, JF Moisan, Y Zhang, CK Jen, CY Su, An on-line ultrasonic cleanliness analyzer for molten light metals, JOM 56(2) (2004) pp. 59 – 64.

[12] RN Thurston, Elastic waves in rods and clad rods, Journal of Acoustical Society of America 64(1) (1978) pp. 1 – 37.

[13] I Ihara, CK Jen and DR Franca, Materials evaluation in molten metal using a focused ultrasonic sensors: application to molten zinc, Advances in Technology of Materials and Materials Processing Journal 13(1/2) (2001) pp. 45 – 50.

[14] CK Jen, Similarities and differences between fiber acoustic and fiber optics, Proceedings of the 1985 IEEE Ultrasonic Symposium (1985) pp. 1128 – 1133.

Chapter 4

Reducing Trailing Echoes with Regular Polygonal Buffer Rods

Previously, the generation of trailing echoes in cylindrical buffer rods has been numerically and experimentally investigated. It was found that due to the infinite symmetry axis in a circle, infinite interferences will occur among the infinite pairs of the parallel mode converted waves and generate trailing echoes. Such generation can be restrained if the cross-sectional shapes have no parallel sides. In this chapter, several polygon shapes consists of even and odd polygons are proposed. Although the generation of trailing echoes is expected for the even polygons, but for the comparison and verification purposes, the even polygons are also considered in this study. The effectiveness of buffer rods having the cross-sectional shapes of polygons is numerically and experimentally investigated. For a fair comparison with the previous cylindrical buffer rod, the cross-section area and length for the polygonal buffer rods are constant.

4.1 The proposed regular polygons

In this study, the proposed polygons are triangle, square, pentagon, hexagon and heptagon, as shown in Figure 4-1. These shapes are divided into two categories which are even polygons and odd polygons, respectively. The even polygons are square and hexagon while the odd polygons are triangle, pentagon and heptagon, respectively. For a fair comparison with the previous 100 mm length cylindrical buffer rod, the average area for all polygons is 300mm^2 ± 5%. Since all the proposed polygons are regular type, therefore they are equiangular, equilateral and symmetry in shape.

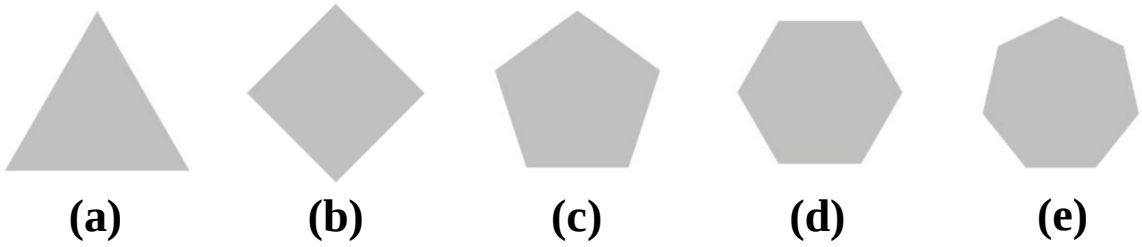

Figure 4-1: The proposed regular polygons for the cross-sectional shapes of buffer rods such (a) triangle, (b) square, (c) pentagon, (d) hexagon and (e) heptagon, respectively.

4.2 Even polygons

The proposed even polygons are square and hexagon. Based on the previous investigation on cylindrical buffer rod, the generation of trailing echoes is possible when the cross-sectional shapes have parallel sides. Therefore, it is highly expected that buffer rods having the cross-sectional shapes of square or hexagon will also generate trailing echoes and deteriorate the SNR.

4.2.1 Mechanism to generate trailing echoes in even polygonal buffer rods

By using the similar approach in investigating the mechanism to generate trailing echoes in cylindrical buffer rods as discussed in the previous chapter, the propagation direction of longitudinal waves is also assumed to be along the axial direction of the rod and normal to the ultrasonic transducer (UT). Therefore, from the cross-sectional view, only

shear waves can be observed. From the previous chapter, it is also found that the generation of trailing echoes can be depicted from the cross-sectional shape itself. Therefore, the mechanism to generate trailing echoes for regular polygonal buffer rods is presented from the cross-sectional view of regular polygonal buffer rods. Figure 4-2 shows the mechanism to generate the first trailing echo for a square polygonal buffer rod where shear wave is depicted as *S* and the subscript number for the shear wave means that it has been reflected once from the side wall of the rod. From each side of the regular square, the first reflected shear waves (S_1) propagate to their opposite boundary separately. Such propagation is also similar with the cylindrical buffer rod where S_1 is parallel with each other. Such parallelism is due to the parallel sides in the regular square. Thus, all S_1 arrived at the side wall of the rod perpendicularly and generate the first trailing echo. Similar mechanism is also depicted for the regular hexagon, as shown in Figure 4-3. Therefore, even polygonal buffer rods having the cross-sectional shapes of square and hexagon are able to generate trailing echoes. Therefore, no improvement of SNR is expected for even polygonal buffer rods.

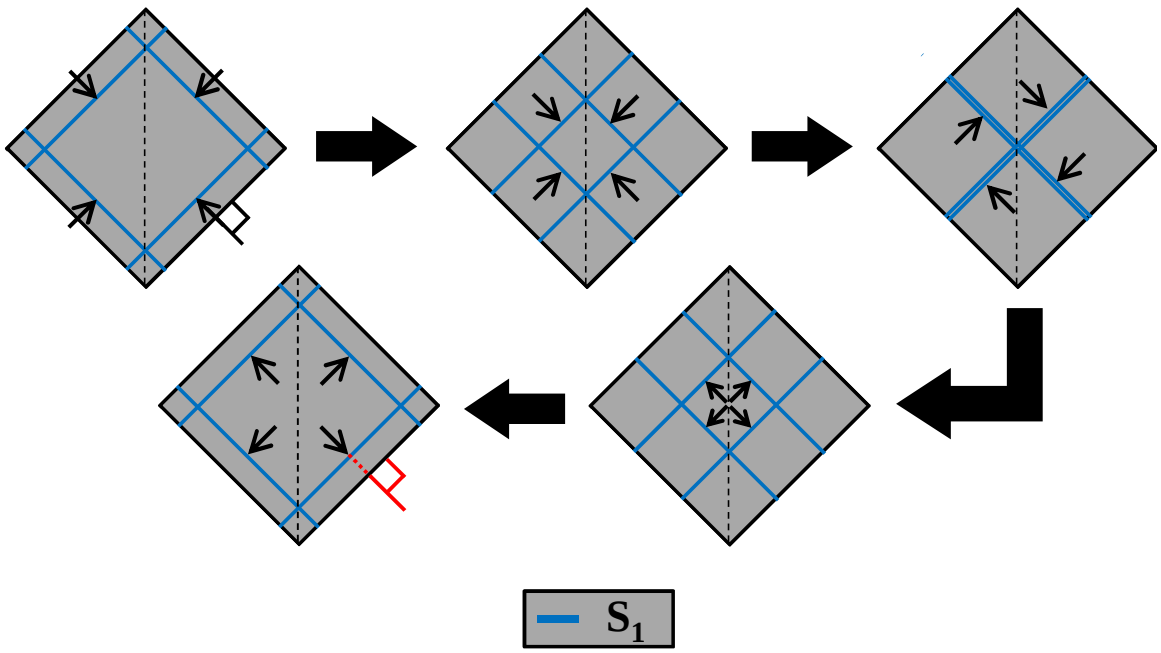

Figure 4-2: Mechanism to generate the first trailing echo for a regular square

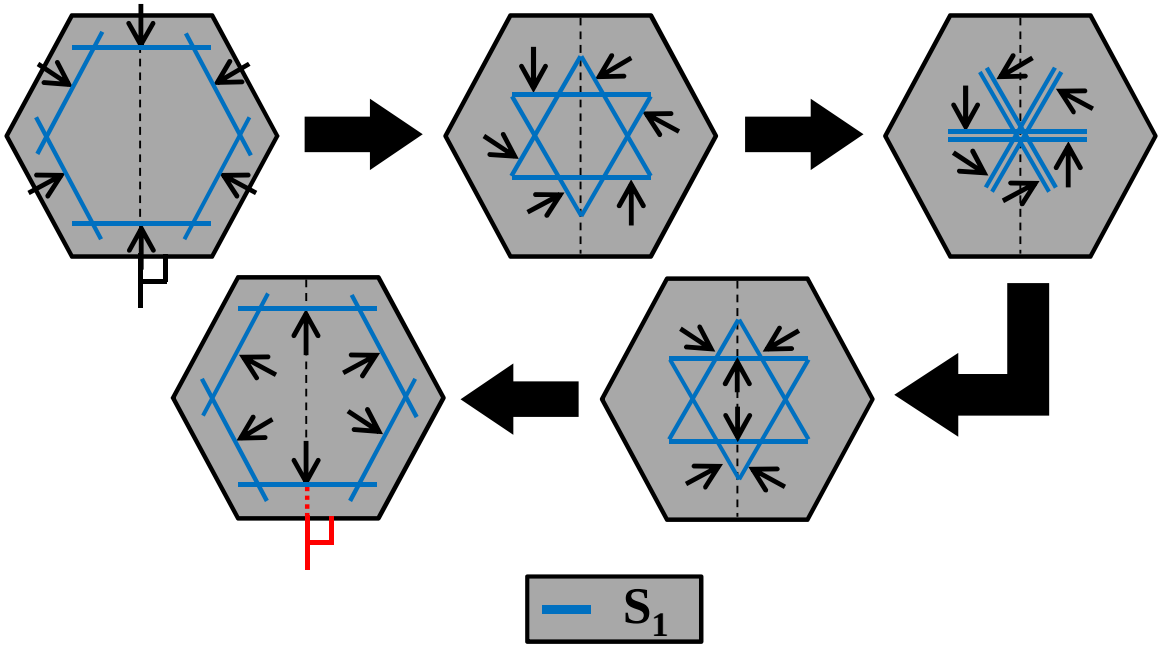

Figure 4-3: Mechanism to generate the first trailing echo for a regular hexagon

4.3 Odd polygons

The proposed odd polygons are triangle, pentagon and heptagon. Since none of the odd polygons have parallel sides, the generation of trailing echoes is expected to be restrained and improve the SNR.

4.3.1 Mechanism to reduce trailing echoes in odd polygonal buffer rods

Figure 4-4 shows the mechanism to reduce trailing echoes for a regular triangle. From each side of the regular triangle, the first reflected shear waves (S_1) propagate to their opposite rod boundary separately. It is observed that none of the S_1 arrived at the side wall of the rod perpendicularly; therefore, no trailing echo is generated. Each of S_1 is then reflected to S_2 where unfortunately, the second reflected shear waves (S_2) propagate to the side wall of the rod perpendicularly and generate the first trailing echo. Take note that

the reflected angle for S_2 is the same as the incident angle for S_1. Such arrival is due to bilateral symmetry shape of the odd polygons where the wave propagation behaviors separated by the symmetry are like a mirror-image. Therefore, it is found that symmetry influences the generation of trailing echoes. Similar mechanism is also observed for other odd polygons such as pentagon and heptagon, as shown in Figure 4-5 and Figure 4-6, respectively. It is also found that the second reflected shear waves (S_2) will generate the first trailing echoes because the propagation directions of such waves are perpendicular to the side wall of the rod. The presented mechanism for all regular polygonal buffer rods is then verified using the three-dimensional numerical simulations.

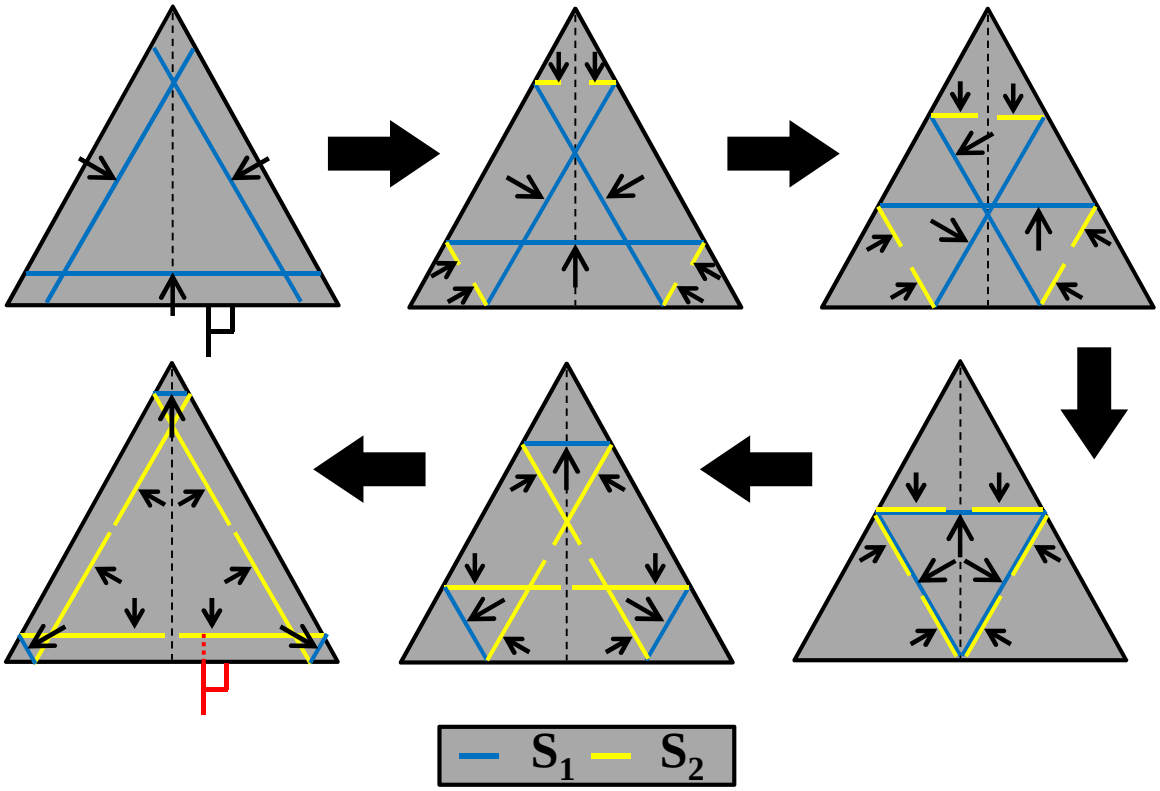

Figure 4-4: Mechanism to generate the first trailing echo for a regular triangle

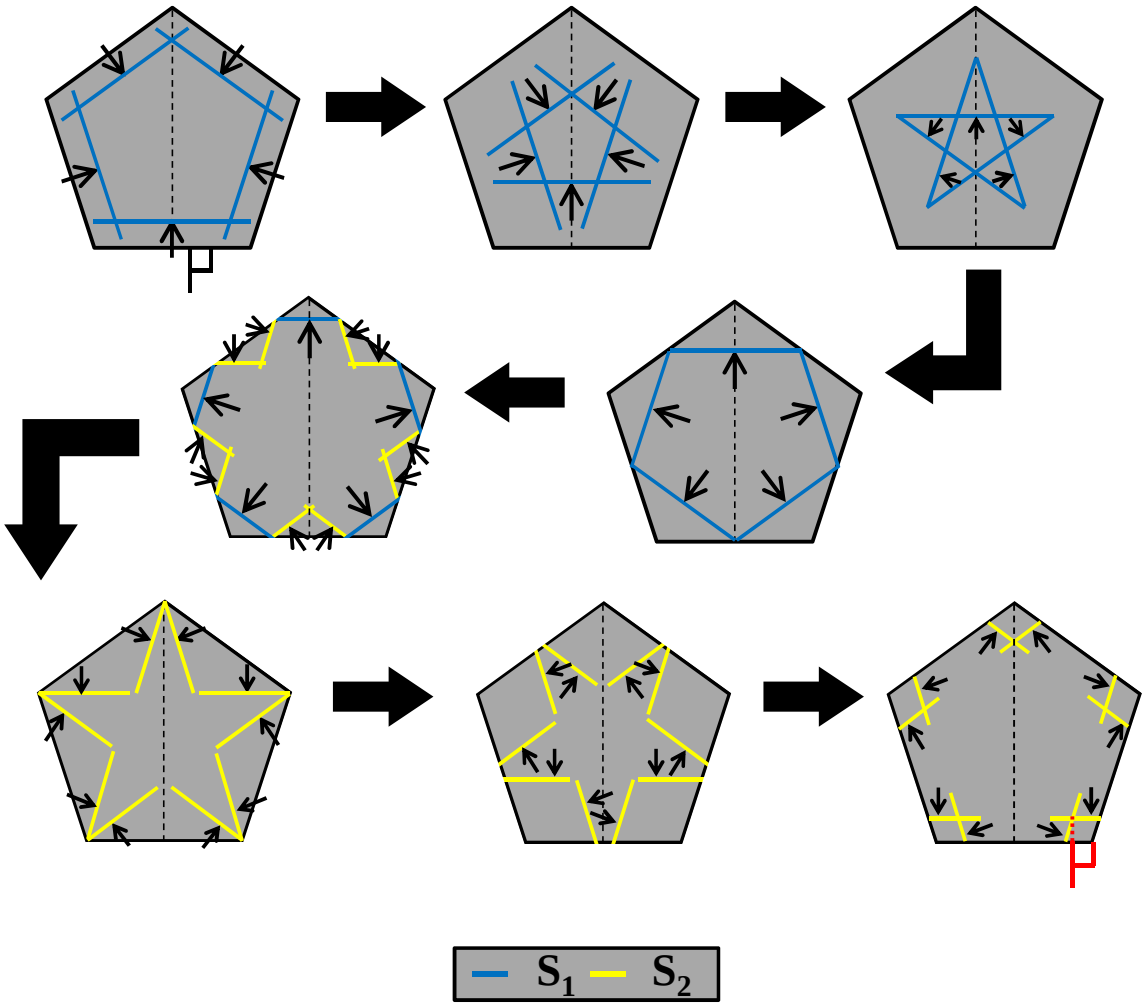

Figure 4-5: Mechanism to generate the first trailing echo for a regular pentagon

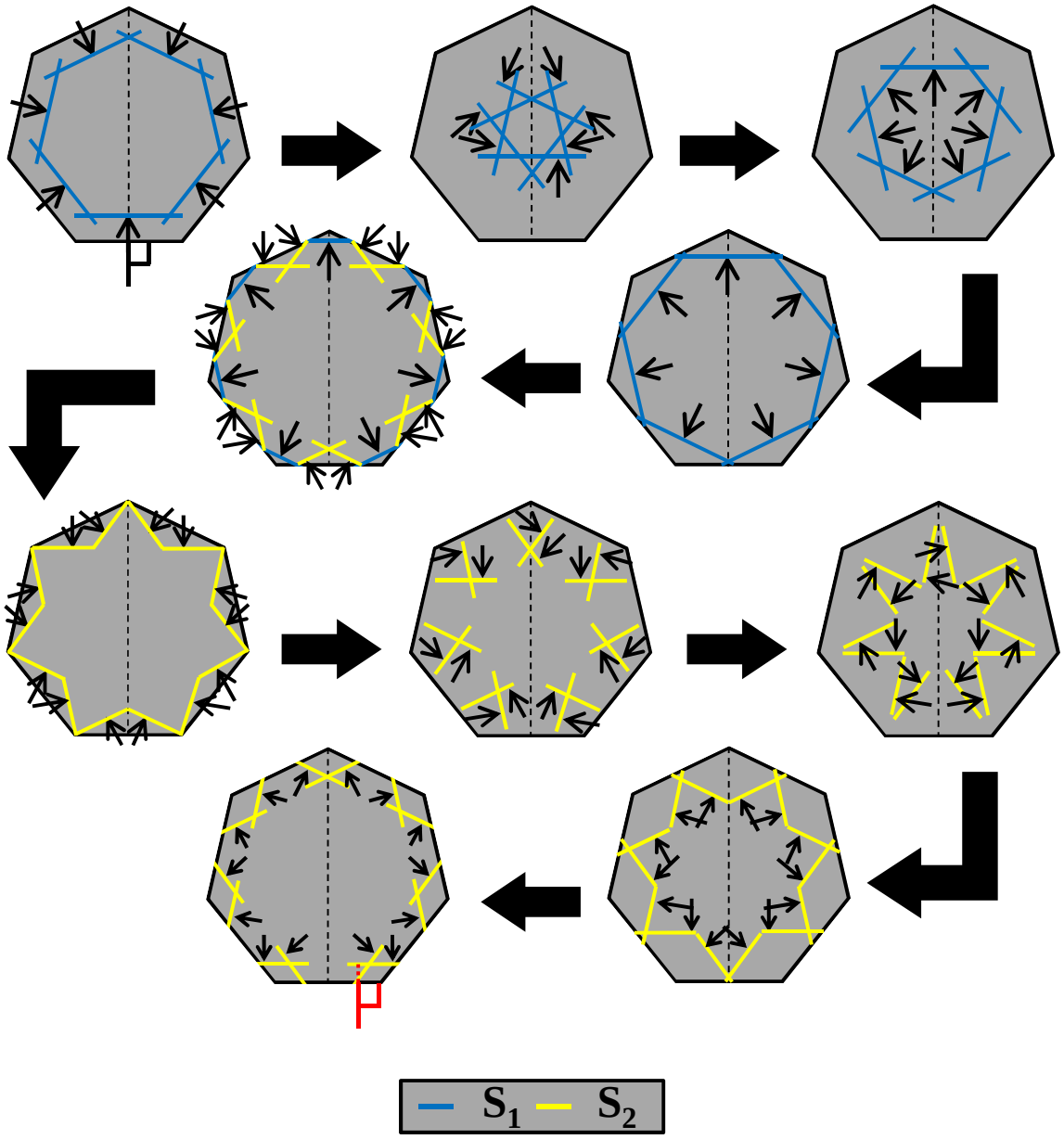

Figure 4-6: Mechanism to generate the first trailing echo for a regular heptagon

4.4 Three-dimensional simulation on the regular polygonal buffer rods

The influence of polygons as the cross-sectional shapes of buffer rod is numerically investigated using the same simulation conditions used on the 100 mm length steel cylindrical buffer rod. The three-dimensional simulation models for all the regular polygonal buffer rods are also created by using the slices command presented in Chapter 2. Figure 4-7 shows the three-dimensional simulation models for all polygonal buffer rods. A 5 MHz longitudinal UT with diameter of 6.35 mm is employed at the center of mass for each cross-sectional shape.

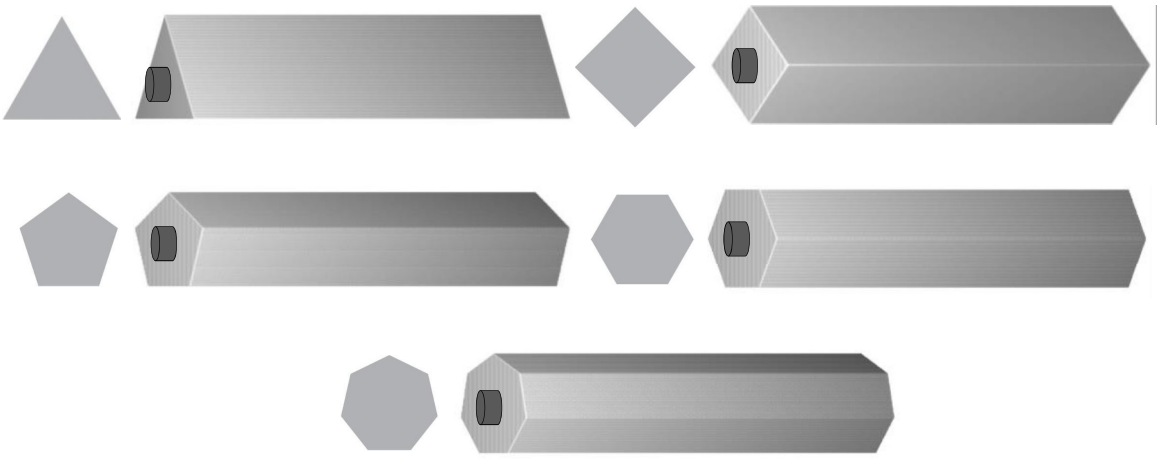

Figure 4-7: Three-dimensional simulation model for all polygonal buffer rods

4.4.1 Simulation results

The simulated waveforms and the SNR for all polygonal buffer rods are shown in Figure 4-8(a) and (b), respectively. As expected, the trailing echoes are significantly generated in even polygonal buffer rods (square and hexagon) due to the parallel sides. It is found that the SNR for the odd polygonal buffer rod is gradually increased from triangle, pentagon and heptagon, where such improvement will be discussed in the next section. In addition, it is believed that the low amplitudes of trailing echoes generated in odd polygonal buffer rods are due to wave attenuation. Since the trailing echoes are generated by the second reflected shear waves (S_2), the wave propagation path is longer than that of the first reflected shear waves (S_1).

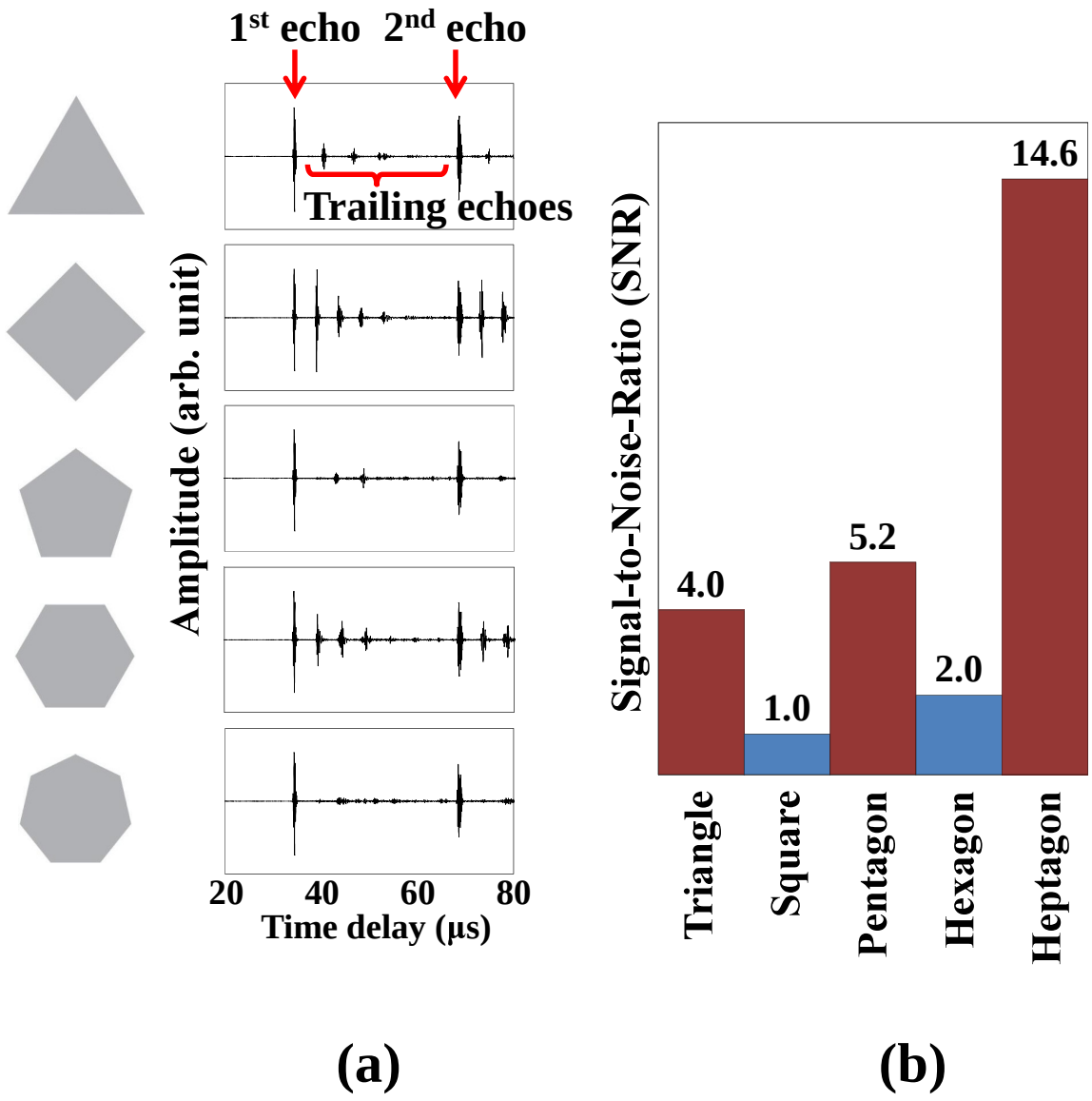

Figure 4-8: (a) Simulated waveform and (b) the SNR for all polygonal buffer rods.

4.5 Wave propagation studies after the generation of the first echo

Since three-dimensional numerical simulation is used to investigate the wave propagation behavior including trailing echoes in all polygonal buffer rods, the wave propagation studies from side view and cross-sectional view are possible. Such wave propagation studies are important to verify the mechanism that has been discussed for all the regular polygonal buffer rods. Since the mechanism is discussed from the cross-sectional view,

the wave propagation studies will also be presented from such view. Take note that the wave propagation studies are carried out after the generation of the first echo.

4.5.1 Even polygon

The wave propagation after the generation of first echo for the regular square and regular hexagon are presented in Figure 4-9 and Figure 4-10, respectively. The generation of the first echo is given by the bright cross section as shown by the first captured image from left in Figure 4-9 and Figure 4-10, respectively. After the generation of the first echo, it is observed that the shear waves (depicted by the bright lines) propagate to the center of the cross-sectional shapes. The direction of such waves is found to be perpendicular to the rod boundary. Such finding is similar with the mechanism depicted in Figure 4-2 and Figure 4-3 for even polygonal buffer rods. Due to such behavior, the wavefronts of the waves are parallel to the side wall of the rod. Due to such parallelism, as expected, shear waves arrived at their opposite rod boundary perpendicularly, as depicted by the last captured image. Such arrival will then generate the first trailing echo. Similar wave propagation behavior is also observed for the regular hexagon, as presented by the captured images in Figure 4-10. Therefore, the mechanism depicted in the previous section is verified.

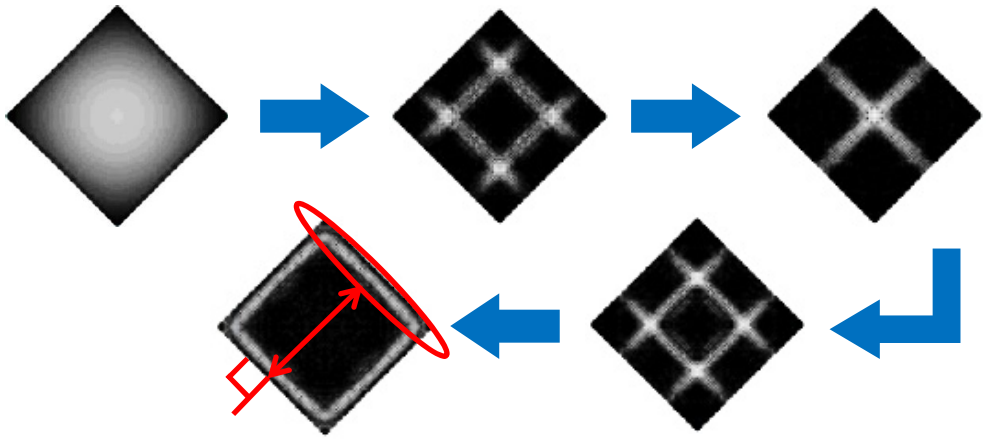

Figure 4-9: Captured images of shear waves starting from the generation of the first echo (bright cross-section) until the generation of the first trailing echo, from the cross-sectional view of a regular square.

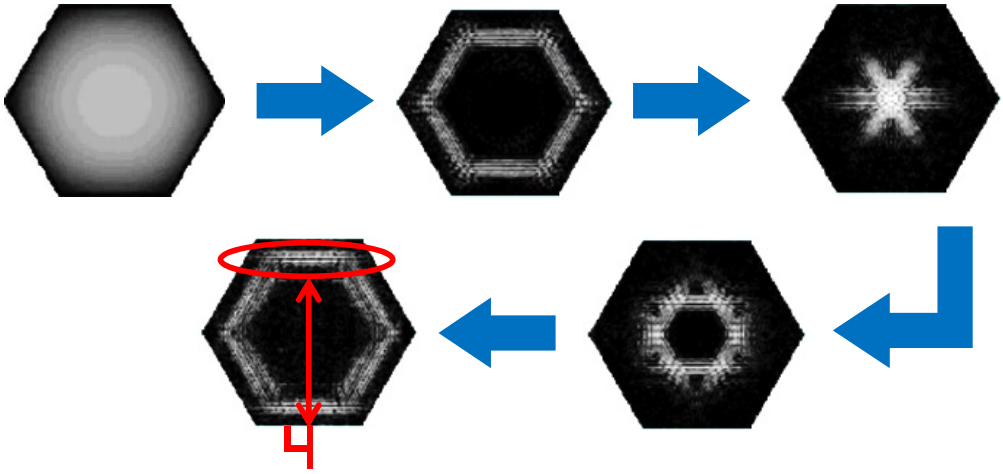

Figure 4-10: Captured images of shear waves starting from the generation of the first echo (bright cross-section) until the generation of the first trailing echo, from the cross-sectional view of a regular hexagon.

4.5.2 Odd polygons

Since the mechanism to generate the first trailing echoes for square and hexagon have been verified, it is also expected that the mechanism depicted for the odd polygons as shown in Figure 4.4, 4.5 and 4.6 are also true. Figure 4-11 shows the captured images during the propagation of shear waves in the regular triangle after the generation of the first echo. As expected, none of the first reflected shear waves arrived at the side wall of the rod perpendicularly. However, since the first reflected shear waves arrived at the side wall of the rod not perpendicularly, they are reflected at the same angle as the incident angle. Such reflected waves, known as the second reflected shear waves are perpendicular to the side wall of the rod, therefore, the first trailing echo is generated. Similar wave propagation behaviors are also observed for the regular pentagon (Figure 4-12) and the regular heptagon (Figure 4-13) where the second reflected shear waves will arrive at the side wall of the rod perpendicularly. The parallelism between the second reflection shear waves and the rod boundary for each odd polygon are depicted in oval. Therefore, the mechanism depicted for each odd polygonal buffer rod is verified. Noted that the shear waves propagate from the inclined surface of a polygon is less bright that the shear waves that propagate from the straight surface. It is believed that the voxels on the inclined surfaces of a polygon influences such brightness. Since it has been

mentioned in Chapter 2 that these voxels will create an uneven surface on the inclined side of a polygon, therefore, a diffuse reflection occurs. Such reflection influences the wave energy where the energy will be reflected in a different reflected angle. That means although the material is the same, the incident angle is not the same as the reflected angle due to the rough surfaces. Therefore, the brightness of the waves that are reflected from such inclined surface of a polygon is less than that of from the smooth plane/surface.

4.6 Wave propagation studies from the side view and the cross-sectional view

4.6.1 Even polygons

Based on the wave propagation studies that are conducted on all regular polygons, the wave propagations with the desired signals such as first echo and trailing echoes are presented from the side view and the cross-sectional view. Figure 4-14 shows the captured images of one-round trip of ultrasonic pulse echo propagating through (a) square buffer rod and (b) hexagon buffer rod. The desired signals such as the first echo and the trailing echoes are identified by the bright lines that are parallel to the UT. Since the brightness indicates the strength of amplitude, square buffer rod shows a set of brighter lines compared to the hexagon buffer rod.

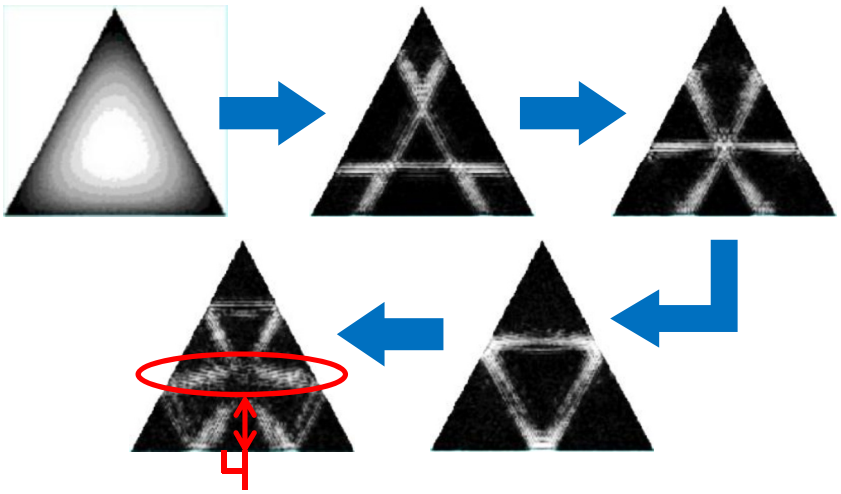

Figure 4-11: Captured images of shear waves starting from the generation of the first echo (bright cross-section) until the generation of the first trailing echo, from the cross-sectional view of a regular triangle.

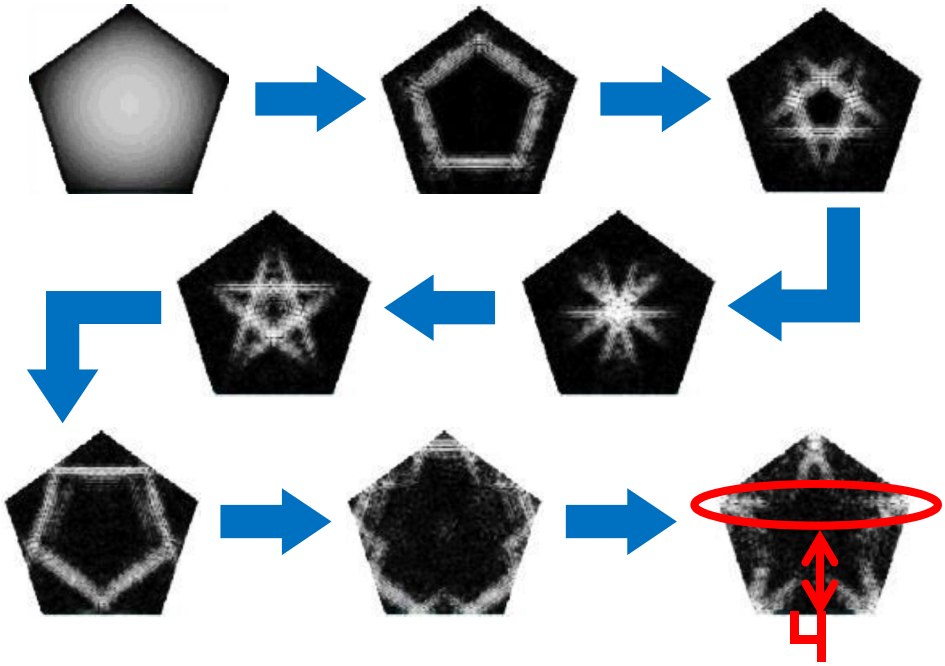

Figure 4-12: Captured images of shear waves starting from the generation of the first echo (bright cross-section) until the generation of the first trailing echo, from the cross-sectional view of a regular pentagon.

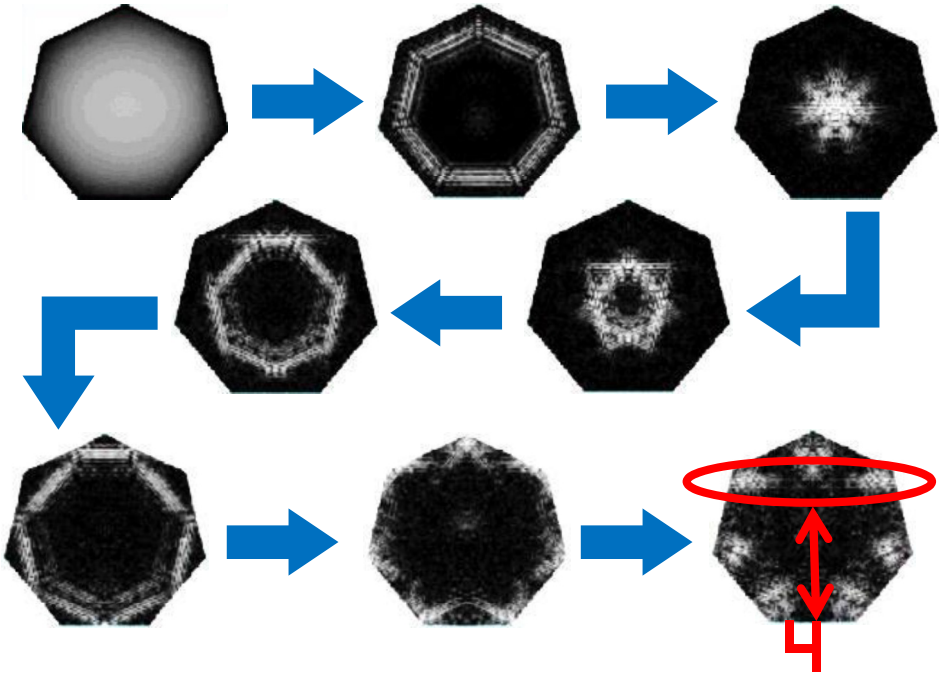

Figure 4-13: Captured images of shear waves starting from the generation of the first echo (bright cross-section) until the generation of the first trailing echo, from the cross-sectional view of a regular heptagon.

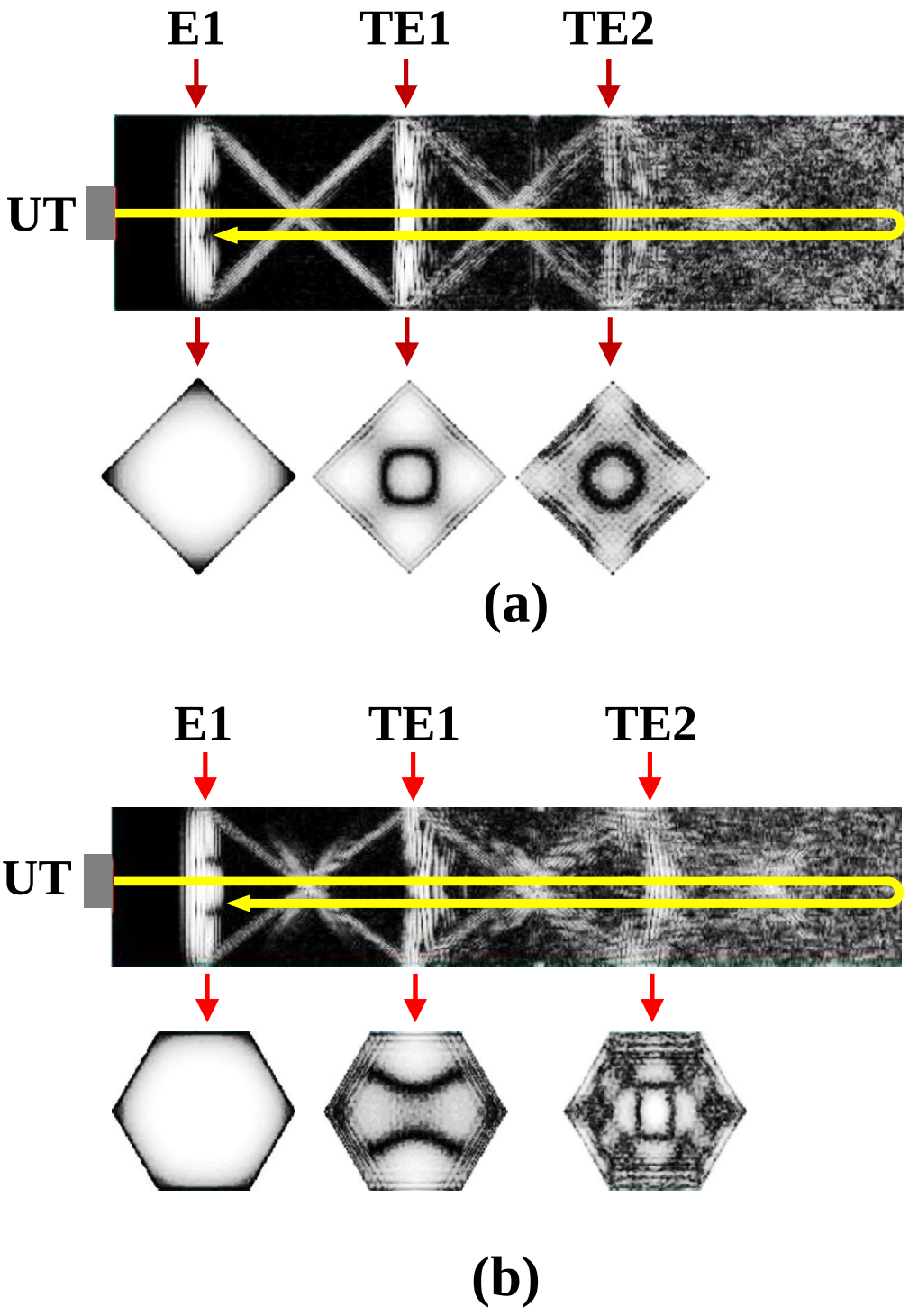

Figure 4-14: Desired signals such as the first echo (E1) and trailing echoes (TE) are identified by the one-round trip propagation of ultrasonic waves from the side view (top image) and cross-sectional view (bottom images) for (a) square buffer rod and (b) hexagon buffer rod, respectively.

4.6.2 Odd polygons

The wave propagation studies from the side view and cross-sectional view for all odd polygonal buffer rods having the cross-sectional shapes of (a) triangle, (b) pentagon and (c) heptagon, are presented in Figure 4-15. Similar behavior is also observed for all the odd polygons where the brightness of the first trailing echo depicted in the side view and cross-sectional view are gradually decreasing, starting from triangle, followed by pentagon and finally, heptagon. Such observations corresponded with the simulated waveforms shown in Figure 4-8(a) where among the odd polygonal buffer rods, the biggest amplitude of the first trailing echo is generated by triangle, followed by pentagon and lastly heptagon. Based on the simulation results and the wave propagation studies on regular polygonal buffer rods, it can be concluded that the symmetry shape of regular polygons influence the generation of trailing echoes. In addition, since the time delay is corresponding to the path of the wave propagation, the time delay for the first trailing echo for all odd polygonal buffer rods are delayed compared to even polygonal buffer rods. This is because the wave propagation of shear waves to generate the first trailing echo is longer for odd polygons compared to even polygons. It is noted that the first trailing echo for odd polygonal buffer rods are generated by the arrival of the second reflection of shear waves. Unlike even polygonal buffer rods, the first trailing echo is generated by the first reflection of shear waves. Therefore, the path of the wave propagation to generate the first trailing echo is shorter for even polygons compared to odd polygons. To verify the simulation results, all regular polygonal buffer rods are fabricated.

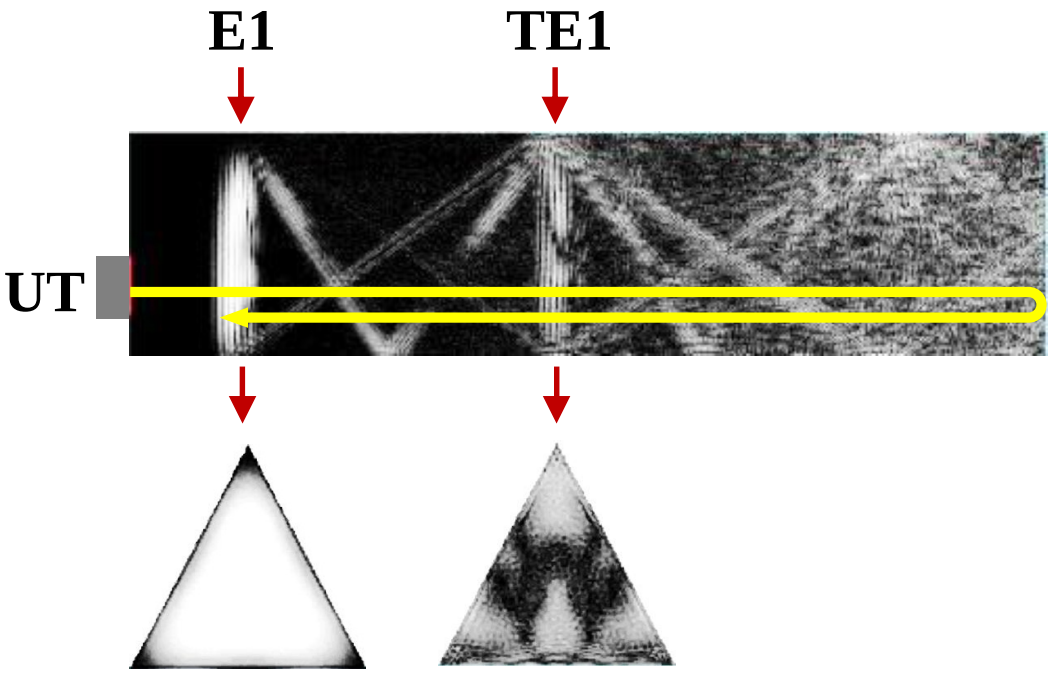

(a)

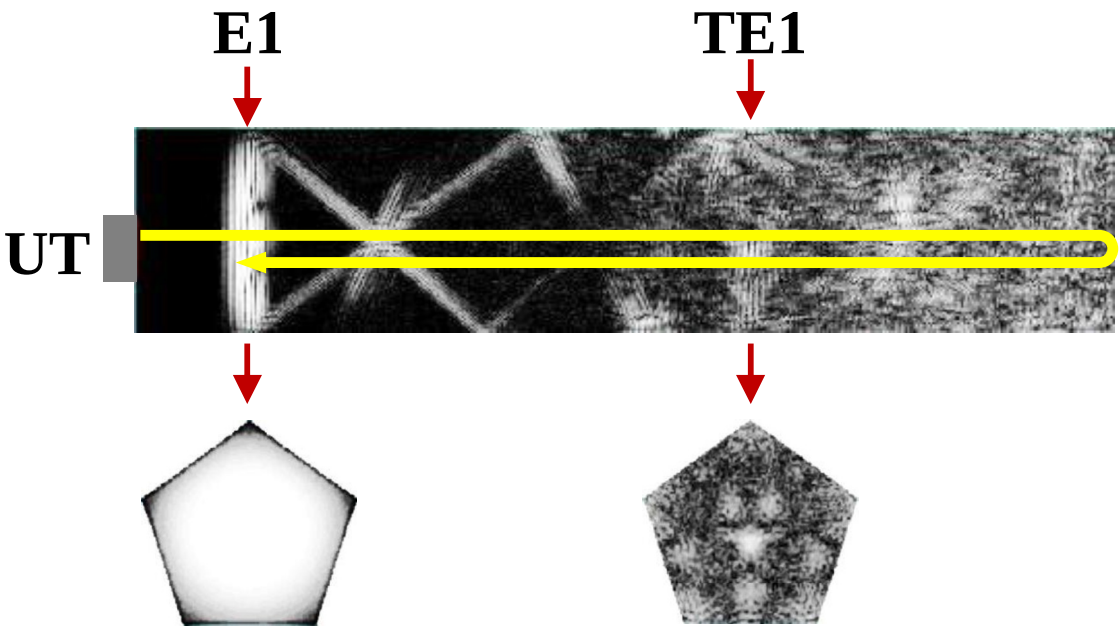

(b)

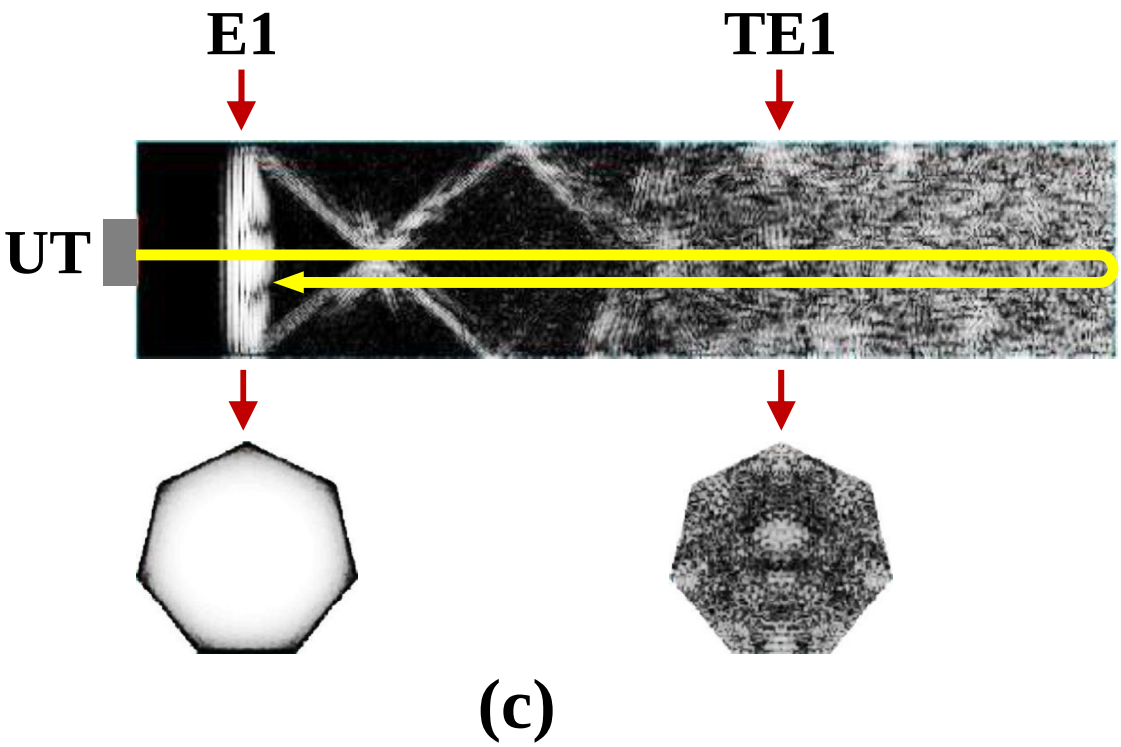

Figure 4-15: Desired signals such as the first echo (E1) and trailing echoes (TE) are identified by the one-round trip propagation of ultrasonic waves from the side view (top image) and cross-sectional view (bottom images) for (a) triangle buffer rod, (b) pentagon buffer rod and (c) heptagon buffer rod, respectively.

4.7 Experiments on the regular polygonal buffer rods

Figure 4-16 shows the fabricated regular polygonal buffer rods having different cross-sectional shapes such as triangle, square, pentagon, hexagon and heptagon. The rod material is steel S45C. For a fair comparison with the simulation results, the rod length and cross-sectional area are kept constant. Figure 4-17 shows the measured waveform for one-round trip of pulse wave propagating through the 100 mm regular polygonal buffer rods. It is found that both waveform and SNR show a similar tendency with the simulation results in Figure 4-8(a). Although there are some discrepancies in the amplitude of trailing echoes, such difference has been explained in Chapter 3. Therefore, the three-dimensional numerical simulation based on a finite difference method has successfully simulated the polygonal buffer rods appropriately.

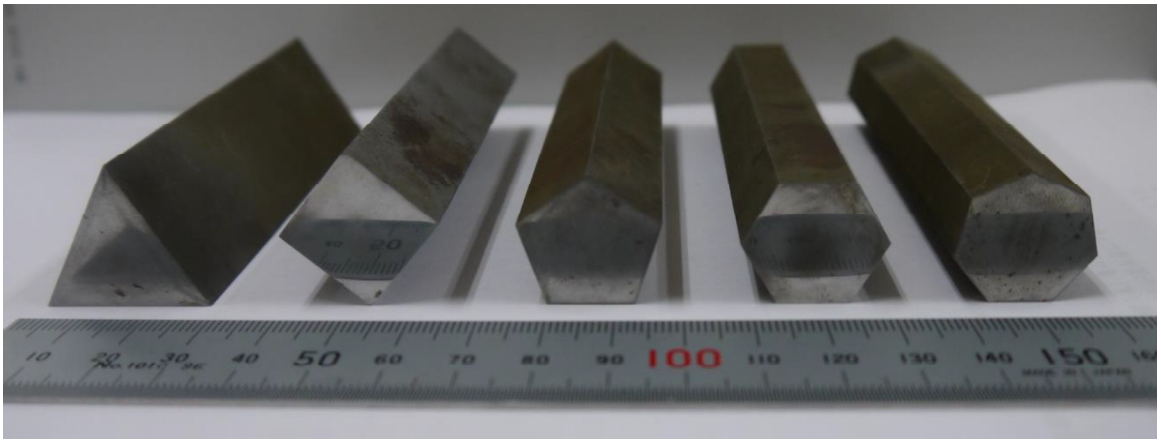

Figure 4-16: The fabricated steel (S45C) polygonal buffer rods having different cross-sectional shapes such as (from left); triangle, square, pentagon, hexagon and heptagon.

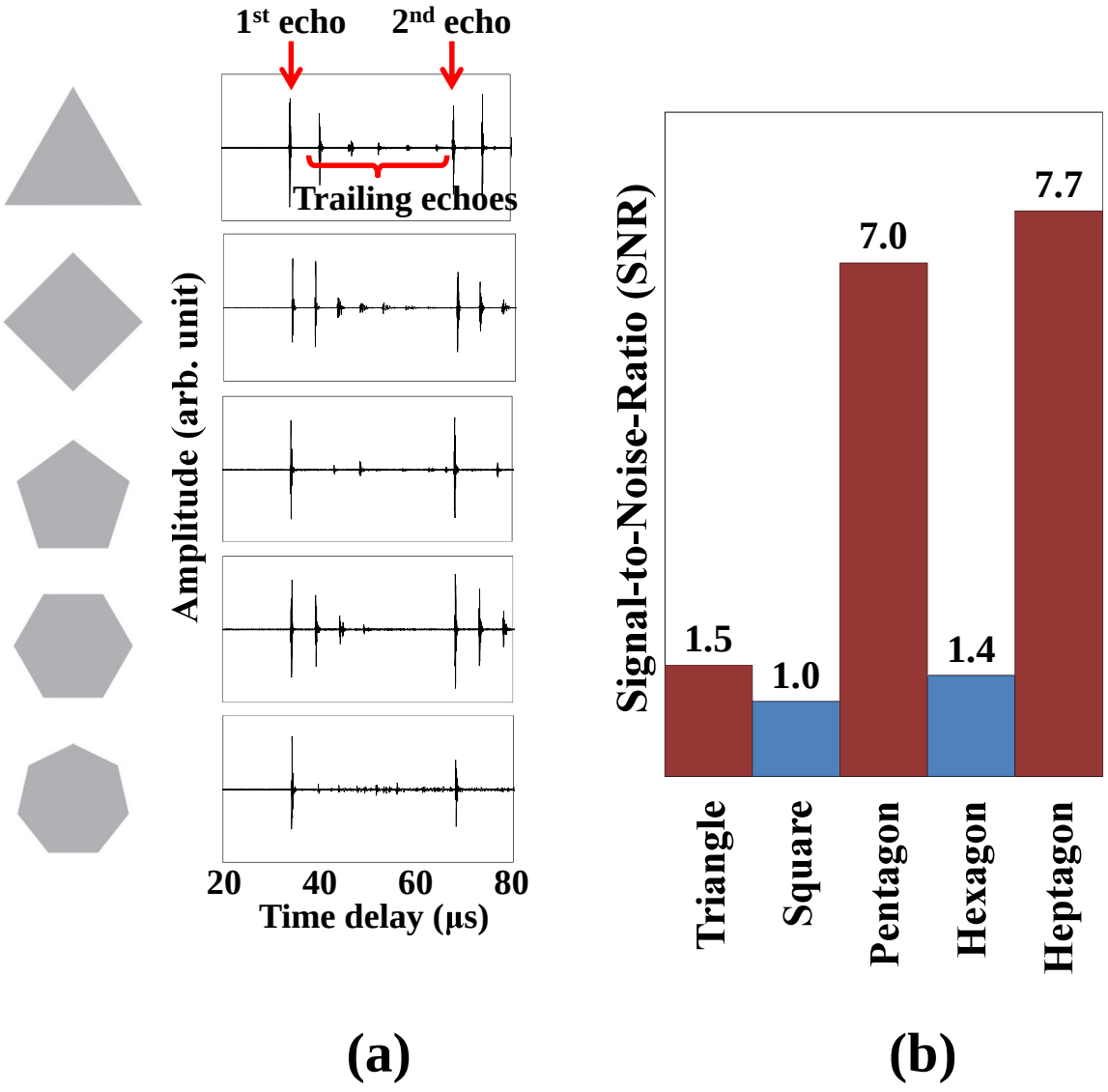

Figure 4-17: (a) Measured waveform and (b) the SNR for all polygonal buffer rods.

4.8 Influence of the polygon shapes on the time arrival of the first trailing echo at the ultrasonic transducer

Based on the simulated waveforms shown in Figure 4.8(s), it is observed that the first trailing echoes are generated at different time for all the polygonal buffer rods. Such arrival time, which depicted by a dash line is shown in Figure 4.18. Take note that the previous cylindrical buffer rod presented in Chapter 2 is also included for the comparison purpose on the arrival time of the first trailing echo. Based on the dash line, it is observed that the first trailing echo to arrive at UT is the regular square. Therefore, the sequence of arrival, from the first to the last to arrive at UT is square, hexagon, circle, triangle, pentagon and heptagon, respectively. The mechanism to generate the first trailing echo has been discussed in the previous section where a trailing echo is generated when the mode converted shear waves arrived at the side wall of the rod perpendicularly. It is believed that such wave propagation also influences the generation time of the trailing echoes. The longer the path it takes to generate a trailing echo, the longer is the time delay (μs). Figure 4.19 shows the comparison of such arrival that is measured in length, *l* (mm), for all the cross-sectional shapes such as circle, triangle, square, pentagon, hexagon and heptagon, respectively. It is observed that the shortest path to generate the first trailing echo is given by square where the path is 17.7 mm. Based on Figure 4.19, the sequence of such path length, from the shortest to the longest, is square, hexagon, circle, triangle, pentagon and heptagon. This sequence is found to be correlated with the arrival time of the first trailing echo as shown in Figure 4.18. Therefore, it can be concluded that the arrival of the first trailing echo can be estimated roughly from the cross-sectional shape. However, such estimation is only possible with a reference. In this work, the estimation is based on the cylindrical buffer rod where the arrival time for the trailing echoes can be calculated since the rod diameter and rod velocity are known [1,2]. Take note that the path shown in Figure 4.19 is only for generating the first trailing echo. Therefore, the path may not be the same for generating the following trailing echoes such as the second trailing echo and the third trailing echo.

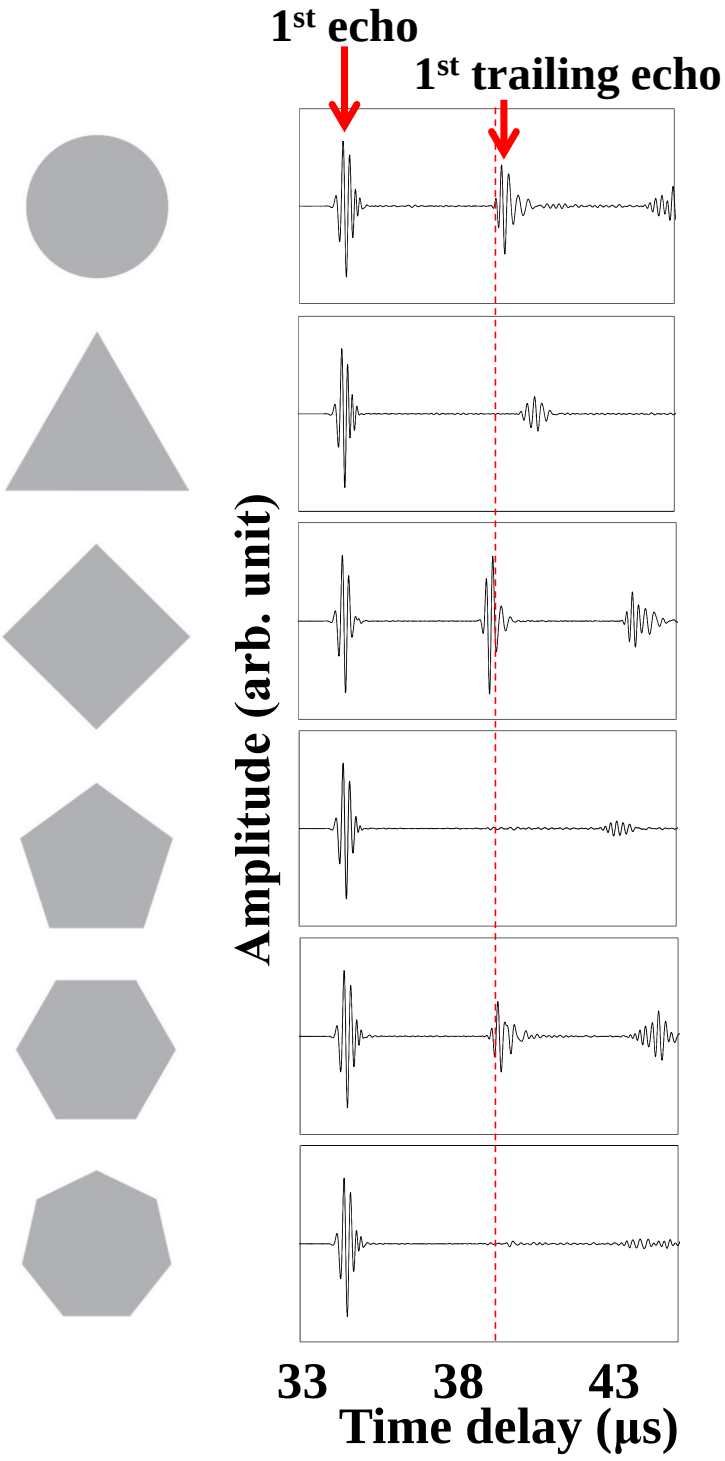

Figure 4-18: Time arrival of the first trailing echo from the simulated waveform for buffer rods the SNR for all polygonal buffer rods.

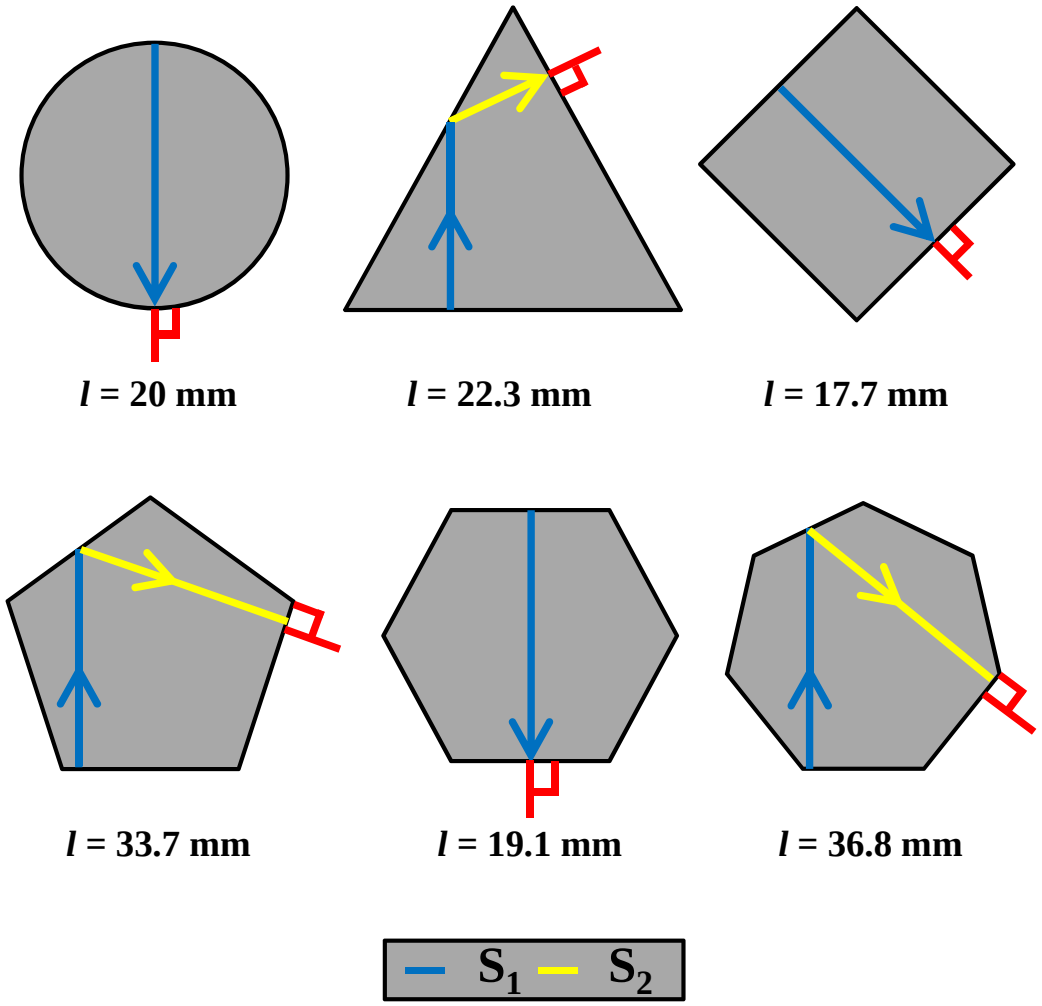

Figure 4-19: The propagation of shear waves for generating the first trailing echoes, measured in length (mm).

4.9 Influence of regular odd polygons on the amplitude of trailing echoes

Based on the simulated and measured waveforms of polygonal buffer rods, it can be seen that the amplitude of trailing echoes are gradually reduced from triangle, pentagon and heptagon. Such reduction improves the SNR where heptagon has the highest SNR compared to other odd polygons. It is believed that such improvement is influenced by the area of a polygon. Previously, it is known that the trailing echo is generated when the mode converted shear waves arrived at the side wall of the rod perpendicularly. Besides

the arrival time for the trailing echoes, the area for such arrival at the side well perpendicularly can also be depicted. Figure 4-20 shows the comparison for such area for triangle, pentagon and heptagon, respectively. Take note that such area is discussed from one side of the polygon since the odd polygons are regular. Therefore, the wave propagation behaviors from any side of a regular polygon are the same. The area which contributes to the generation of trailing echoes is depicted with dash lines. Based on Figure 4-20, it can be concluded that the bigger the area, the greater amplitude of trailing echoes will be generated. Based on the simulation and experimental results, among the odd polygonal buffer rods, the biggest amplitude of trailing echoes is generated by the regular triangle. Such finding corresponds to the largest area depicted in the regular triangle compared to pentagon and heptagon. In addition, such area for both pentagon and heptagon are almost similar, therefore, similar amplitude of trailing echoes are also generated, as shown by the measured waveform in Figure 4-17(a). In addition, it is found that the second trailing echo in the pentagon buffer rod has bigger amplitude than the first trailing echo. Figure 4-21 shows the influence of area for generating the first and second trailing echoes for a regular pentagon. It is found that the second trailing echo is generated by the fourth reflected shear waves (S_4). It is observed that the area for generating the second trailing echo is bigger than that of the first trailing echoes. Based on the measured waveform for the regular pentagon as shown in Figure 4-17(a), the second trailing echo is indeed has a bigger amplitude than that of the first trailing echo. Based on Figure 4-20, the smallest area that influences the generation of trailing echoes is given by heptagon. Therefore, heptagon is capable to generate the smallest amplitude of trailing echoes compared to other regular polygonal buffer rods. Such hypothesis has been verified by the simulated and measured waveform shown in Figure 4-8(a) and Figure 4-17(a), respectively. Therefore, the greater the number of sides of odd polygon, the smaller amplitude of trailing echoes is generated. Such hypothesis is then investigated with a nonagon buffer rod since nonagon has bigger number of sides compared to heptagon.

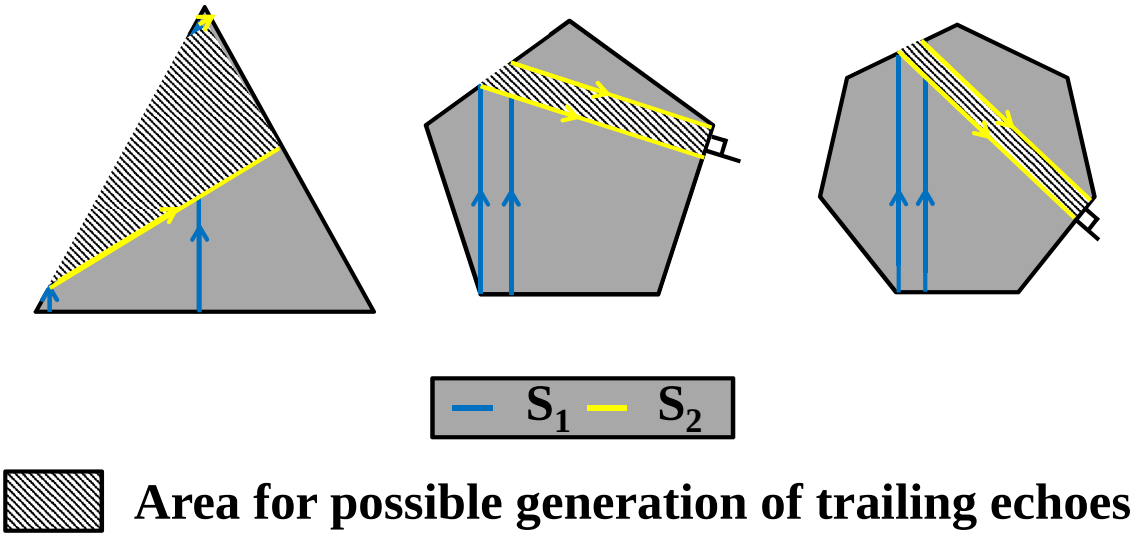

Figure 4-20: Comparison of the area that contributes to the generation of the first trailing echoes between triangle, pentagon and heptagon.

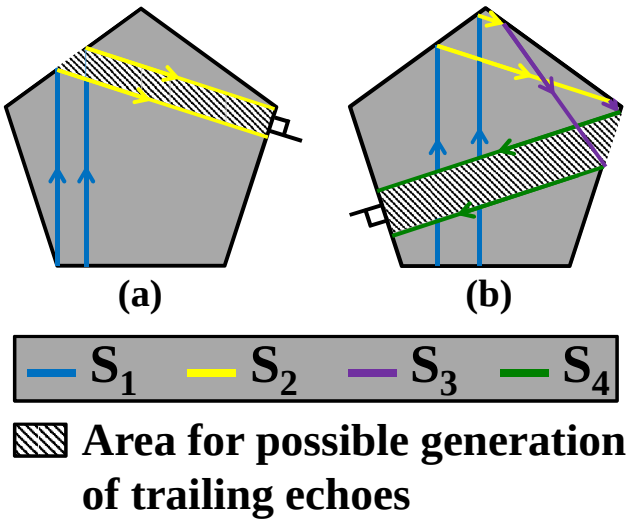

Figure 4-21: Comparison between the area that contributes to the generation of the first and second trailing echoes for a regular pentagon.

4.10 Influence of regular nonagon on the trailing echoes

Figure 4-22 shows the measured waveform of a 100 mm length nonagon buffer rod. Unfortunately, it is found that the amplitude of trailing echoes is bigger than that of heptagon. In addition, the delay time (μs) for generating the first trailing echo is faster than that for the regular odd polygons such as pentagon and heptagon. Such finding is believed to be influenced by the shape of a regular nonagon that is almost similar with a circle, although no parallel sides in the regular nonagon. Figure 4.23 shows that the first (S_1) and second reflected (S_2) shear waves are capable to arrive at the side wall of the rod perpendicularly. Take note that although such propagation is also occurred in the odd polygons such as triangle, pentagon and heptagon, however, due to a smaller number of sides, the interference between the first reflected shear waves (S_1) is not that significant. Therefore, the first trailing echo can be generated by the first reflected shear waves (S_1) in the regular nonagon. Based on such finding, heptagon is still the most suitable shape compared to the other regular polygons for effectively reduce the trailing echoes and improves the SNR

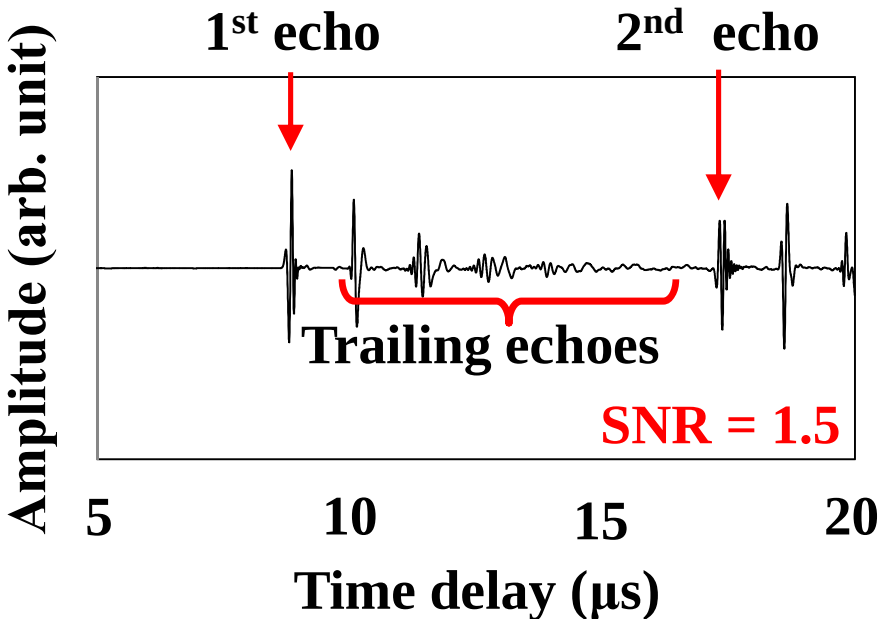

Figure 4-22: Measured waveform for a 100 mm length nonagon buffer rod.

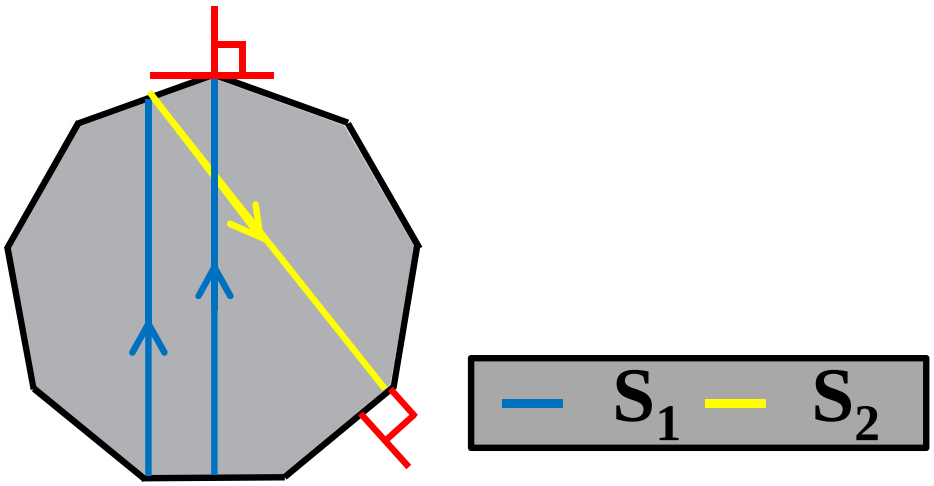

Figure 4-23: Measured waveform for a 100 mm length nonagon buffer rod.

4.11 Clad polygonal buffer rods

Based on the simulation and experimental results, it is found that the trailing echoes can be generated for all regular polygonal buffer rods due to the symmetry shapes. Since an optimum condition of a cladding layer has been obtained, as discussed in the previous chapter, it will be interesting to apply such condition on the regular polygonal buffer rods. Since it has been verified the zirconium oxide (ZrO_2) is effective to reduce the trailing significantly when the core is steel, clad regular polygonal buffer rods are numerically investigated

4.11.1 Simulation results and discussions

By using the same command to create the 3D models for the polygonal buffer rods, clad polygonal buffer rods with rod length of 25 mm and cladding thickness of 2 mm are created. Figure 4-24 shows the 3D models for (a) unclad and (b) clad regular polygonal buffer rods having different cross-sectional shapes such as triangle, square, pentagon, hexagon and heptagon, respectively. Based on Chapter 3, a plateau of high SNR has been obtained when V_{clad} = 110% V_{core} and ρ_{clad} = 70% ~ 150% ρ_{core}. Although such condition has been verified with other materials that have faster velocity than steel, it is necessary to investigate if such cladding layer is applicable on the polygonal buffer rods. Therefore,

the effectiveness of the optimum cladding layer on regular polygonal buffer rod is numerically investigated. The core is defined as steel where the longitudinal velocity, shear velocity and density are 5900 m/s, 3200 m/s and 7800 kg/m^3, respectively. Meanwhile, the cladding layer is defined as zirconium oxide (ZrO_2) since it has been proven that the trailing echoes are significantly reduced and the SNR is tremendously improved. The dimeter of UT is 1.6 mm and the operating frequency is 5 MHz. Figure 4-25 shows the simulated waveforms for unclad and clad regular polygonal buffer rods. As expected, the trailing echoes are significantly reduced and the SNR is greatly improved as shown in Fig. 4-26. Therefore, the condition of a cladding layer presented in Chapter 3 is applicable on other types of rods.

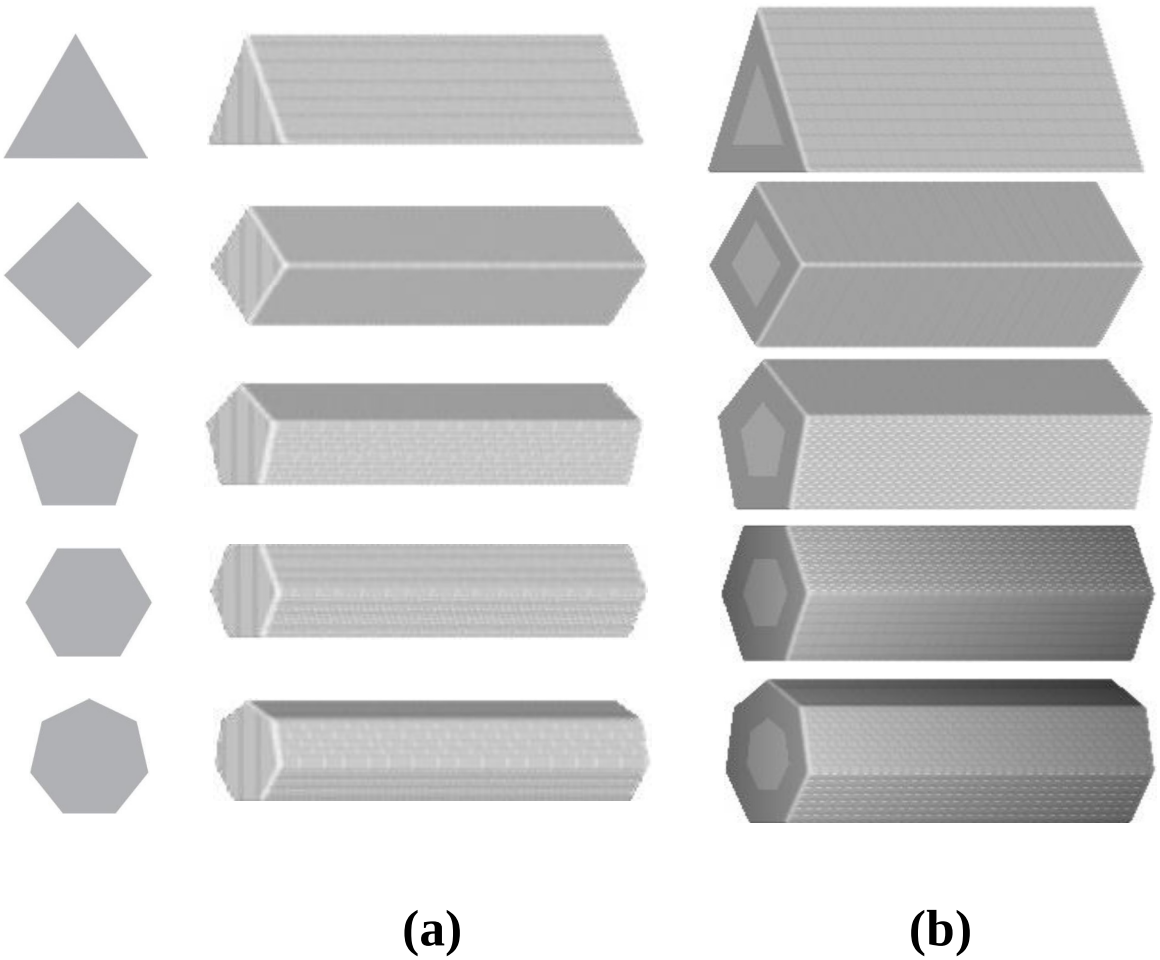

Figure 4-24: Three-dimensional simulation model for (a) unclad and (b) clad regular polygonal buffer rods.

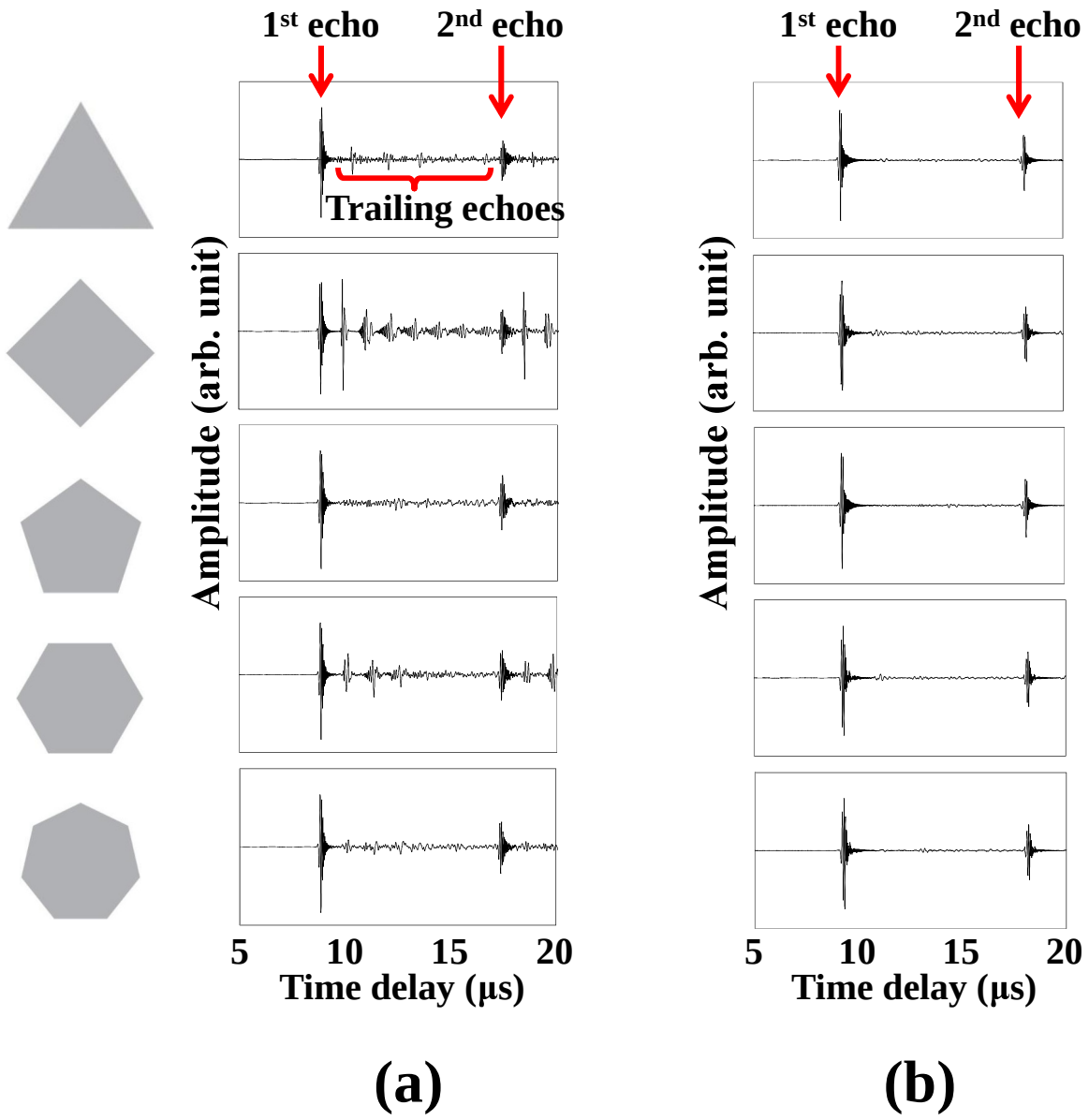

Figure 4-25: Simulated waveforms for (a) unclad and (b) clad regular polygonal buffer rods.

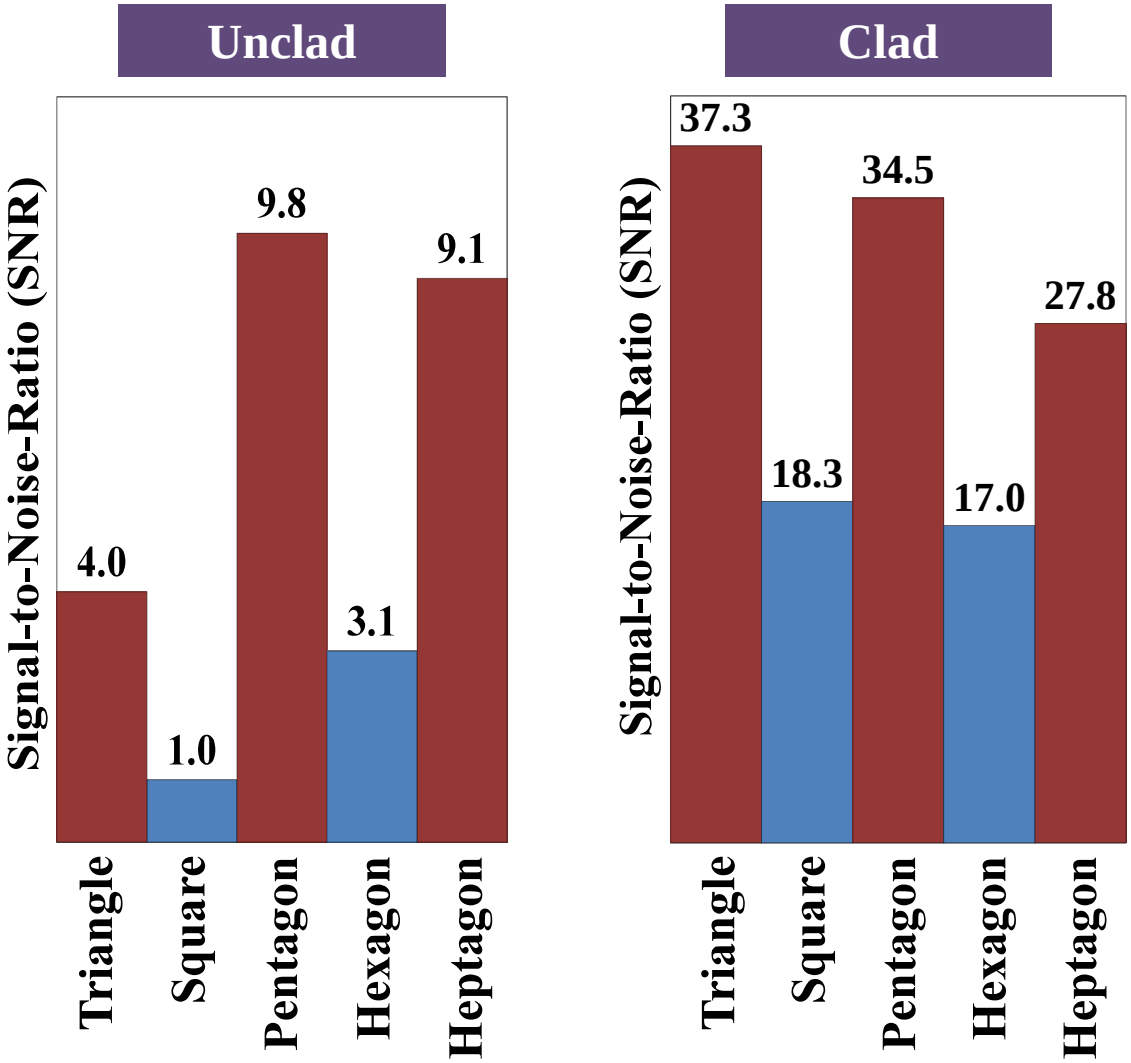

Figure 4-26: Signal-to-noise ratio (SNR) for (a) unclad and (b) clad polygonal buffer rods.

Although the clad polygonal buffer rods are proven to be effective in eliminating the trailing echoes significantly, however, the fabrication of such clad rods may be difficult. Since it known that trailing echoes are possible to be generated in any regular polygons due to their symmetry shapes; therefore, for the novelty purpose of this work, the idea of using irregular polygons as the cross-sectional shapes of buffer rods is proposed.. That means the influence of symmetry is eliminated by the irregular polygons. By eliminating such influence, it is highly expected that the reflected shear waves will not arrive at the side wall of the rod perpendicularly. Therefore, no trailing echoes will be generated and the SNR will be significantly improved.

4.12 Conclusions

1) The idea of using regular polygonal buffer rods is proposed and its effectiveness on reducing trailing echoes and improving the SNR is numerically and experimentally investigated.

2) It is found that odd polygonal buffer rods (triangle, pentagon and heptagon) are better in terms of reducing trailing echoes compared to even polygonal buffer rods (square and hexagon). Such finding is corresponding with the parallel sides in a regular polygon where due to the parallel sides, even polygons such as square and hexagon produce significant amplitude of trailing echoes compared to odd polygons.

3) Trailing echoes are still generated in odd polygons due to the influence of bilateral symmetry of odd polygons. Due to such influence, the wave propagation behavior separated by a symmetry axis is the same at both sides.

3) The path for the wave propagation for generating the first trailing echo for odd polygons is longer than that for even polygons. This is because for odd polygons, the first trailing echo is generated by the second reflection of shear waves. Unlike even polygons, the first trailing echo is generated by the arrival of the first reflection of shear waves at the side wall of the rod perpendicularly. Therefore, the path that is responsible for generating the first trailing echo for odd polygons is longer than that of even polygons. In addition, it is also found that such path influences the arrival time of the trailing echoes where the longest time delay for the first trailing echo to arrive at the UT is given by heptagon since the path for such arrival for heptagon is the longest. Therefore, the longer the path, the longer time it takes to arrive at the UT.

4) The amplitude of the first railing echo for odd polygons is gradually decreased from triangle, followed by pentagon and lastly, heptagon. Such reduction is found to be influenced by the area at which a generation of a trailing echo is possible. It is found that the biggest area for possible generation of trailing echoes is given by triangle, followed

by pentagon and lastly heptagon. The validity of such approach is also proven for a regular pentagon where the area for generating the second trailing echo is bigger than that of the first trailing echo

5) Although the amplitude of trailing echoes are gradually decreases as the number of sides increases, however, such hypothesis is found to be untrue for nonagon. Although nonagon has bigger number of sides compared to heptagon, however, due to its similar shape to circle, bigger amplitude of trailing echoes are generated compared to regular heptagon. In addition, it is possible to generate the first trailing echo by the first reflected shear waves (S_1) to the bigger number of sides in a regular nonagon. Therefore, the SNR for nonagon is smaller than that for heptagon. In addition, due to such finding, heptagon is the most suitable shape for reducing trailing echoes and improving the SNR compared to other regular polygons.

6) In order to reduce the trailing echoes generated in regular polygonal buffer rods, the influence of cladding is numerically investigated. Based on the investigation carried in Chapter 4, the material for both core and clad are defined as steel and zirconium oxide (ZrO_2), respectively. The cladding thickness is also similar, which is 2 mm. As expected, the SNR for all clad polygonal buffer rods is improved. This means that such cladding condition is applicable on any cross-sectional shapes of buffer rods.

7) Since the fabrication of clad regular polygonal buffer rods may be difficult, the idea of using irregular polygons as the cross-sectional shapes of buffer rods is proposed. Such new idea is expected to prevent the generation of trailing echoes completely. The effectiveness of the new idea is presented in the next chapter.

4.13 References

[1] CK Jen, C Neron, EL Adler, GW Farnell, J Kushibiki, K Abe: Long acoustic imaging probes, Proceedings of IEEE Ultrasonics Synposium (1990) pp. 875 – 880

[2] M Redwood: Mechanical waveguides, Pergamon, New York, 1996, pp. 191 – 207.

Chapter 5

Preventing the Generation of Trailing Echoes with Irregular Polygonal Buffer Rods

Based on the investigation on the influence of polygonal buffer rods on the generation of trailing echoes, it was found that the odd polygonal buffer rods (triangle, pentagon and heptagon) are better than the even polygonal buffer rods (square and hexagon) for improving the SNR. Such improvement is due to the generation of trailing echoes that occur during the second reflection of shear waves where the wave propagation path for such waves is longer than that of the first reflection of shear waves. Therefore, the second reflection of shear waves will be attenuated due to a longer path of wave propagation and result to generating a trailing echo having smaller amplitude. Unfortunately, although the odd polygons are better than the even polygons due to no parallel sides, all regular polygons are capable to generate trailing echoes due to their symmetry shape. Therefore, it is believed that the trailing echoes can be eliminated completely if the cross-sectional shapes (polygons) have no parallel sides and not symmetry. In this chapter, the irregular polygons are designed and proposed. The effectiveness of irregular polygonal buffer rods in preventing the generation of trailing echoes is numerically and experimentally investigated.

5.1 Definition of irregular polygons

An irregular polygon is defined as a shape that has no symmetry axis where one or more side lengths of the irregular polygon are different from the side length of a regular polygon having the same number of edges. By referring to this definition, the possible shapes for an irregular polygon are infinite. Therefore, for simpler designs of the irregular polygons, only one vertex of a regular polygon is distorted. Figure 5-1 shows the schematic figure of a regular polygon which is square. The edge that connects two sides of a square is denoted as vertex. A regular square has two symmetry axes and all the side lengths are the same (equilateral).

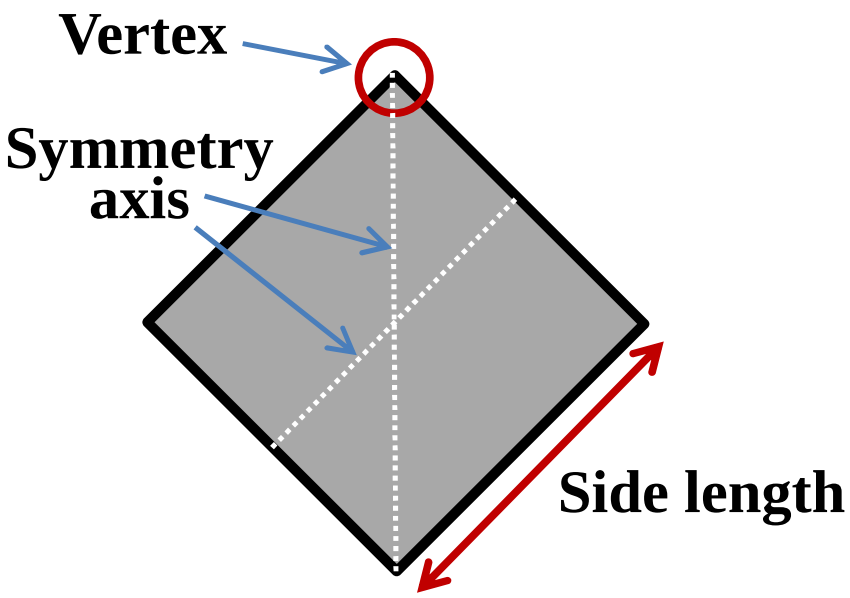

Figure 5-1: Schematic figure for a regular square denoting the parts of a polygon such as vertex, symmetry axis and side length, respectively.

5.1.1 Designing the irregular polygons.

Since it is known that a trailing echo can be generated due to the symmetry of the cross-sectional shapes, the influence of such symmetry needs to be eliminated. Such elimination is possible where one or more vertices of a regular polygon are distorted. However, in order to design simple and less complicated shapes of irregular polygons, in this work, only one vertex of a regular polygon is distorted. Therefore, the value of the

side length at which the distortion takes place will be different from the value of such length where the polygon is regular shape. Such distortion is due to design less complex shapes of irregular polygons where the location of the ultrasonic transducer (UT) at one end of the buffer rod can be easily defined. This is because the UT must be located at the center of mass of each of the cross-sectional shapes. However, it is noted that by distorting only one vertex of a regular polygon, the possible design of an irregular polygon is infinite. Therefore, it is important to choose a distortion point so that it can be used as a guideline to design the irregular polygons. Figure 5-2 shows a regular square with four different points of distortion denoted as I, II, III and IV, respectively. Such different distortions produce the irregular square where the influence of symmetry is eliminated. In addition, such distortion also results to a constant value of area for both regular and irregular squares. Based on Figure 5-2, it is observed that only two sides for each of the irregular square have the same value. Therefore, all the proposed designs of the irregular square are not equilateral neither equiangular. All the proposed shapes of the irregular square (I, II, III and IV) are simulated where the rod length, rod diameter and UT frequency are 25 mm, 5 mm and 20 MHz, respectively.

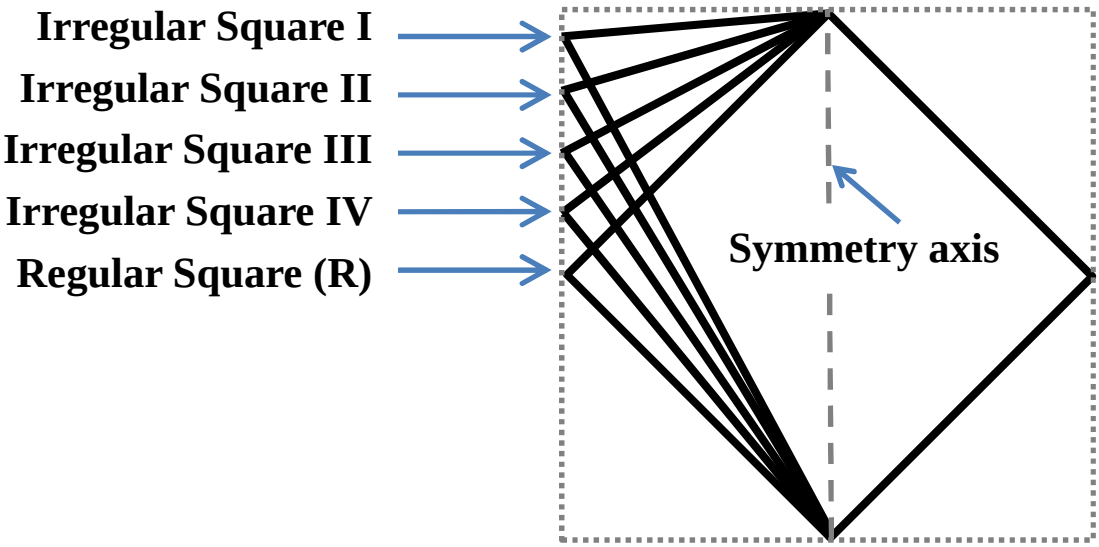

Figure 5-2: Regular square with its irregular designs denoted as I, II, III and IV, respectively.

Figure 5-3 shows the simulated waveforms and the signal-to-noise ratio (SNR) for all the proposed shapes of the Irregular Square such as I, II, III and IV, respectively. As expected, the SNR for all the irregular square are improved since the influence of symmetry has been eliminated by distorting one vertex of a regular square. Based on Figure 5-3, the highest SNR is given by the Irregular Square II where the value is 15.6. Such value is found to be 15 times higher than the SNR for a regular square. Based on Figure 5-3, it can be concluded that a significant improvement of the SNR can be obtained when the distortion is carried out at a point that is far from its initial regular point and close to the peak of a regular shape. It is believed that such significant improvement is due to less number of the reflected shear waves that can arrived at the side wall of the rod perpendicularly compared to the other Irregular Squares such as I, III and IV. In addition, the SNR for the Irregular Square I is smaller than that of the Irregular Square II where such difference may be caused by the possible arrivals of the shear waves to the side wall of the rod perpendicularly during the early stage of reflection of shear waves. Based on the magnified waveform shown in Figure 5-3, it is observed that the amplitude of the trailing echoes generated in Irregular Square I is bigger than that of Irregular Square II. Based on this finding, the irregular shapes for triangle, pentagon, hexagon and heptagon are designed. The guidelines for designing an irregular polygon are:

1) The influence of symmetry is eliminated by distorting only one vertex of a regular polygon. The distorted point must be far from the initial regular point and close to the peak of a regular polygon.
2) No parallel sides are created by such distortion in (1)
3) The area for the irregular polygon is kept constant, for a fair comparison with the regular polygons,

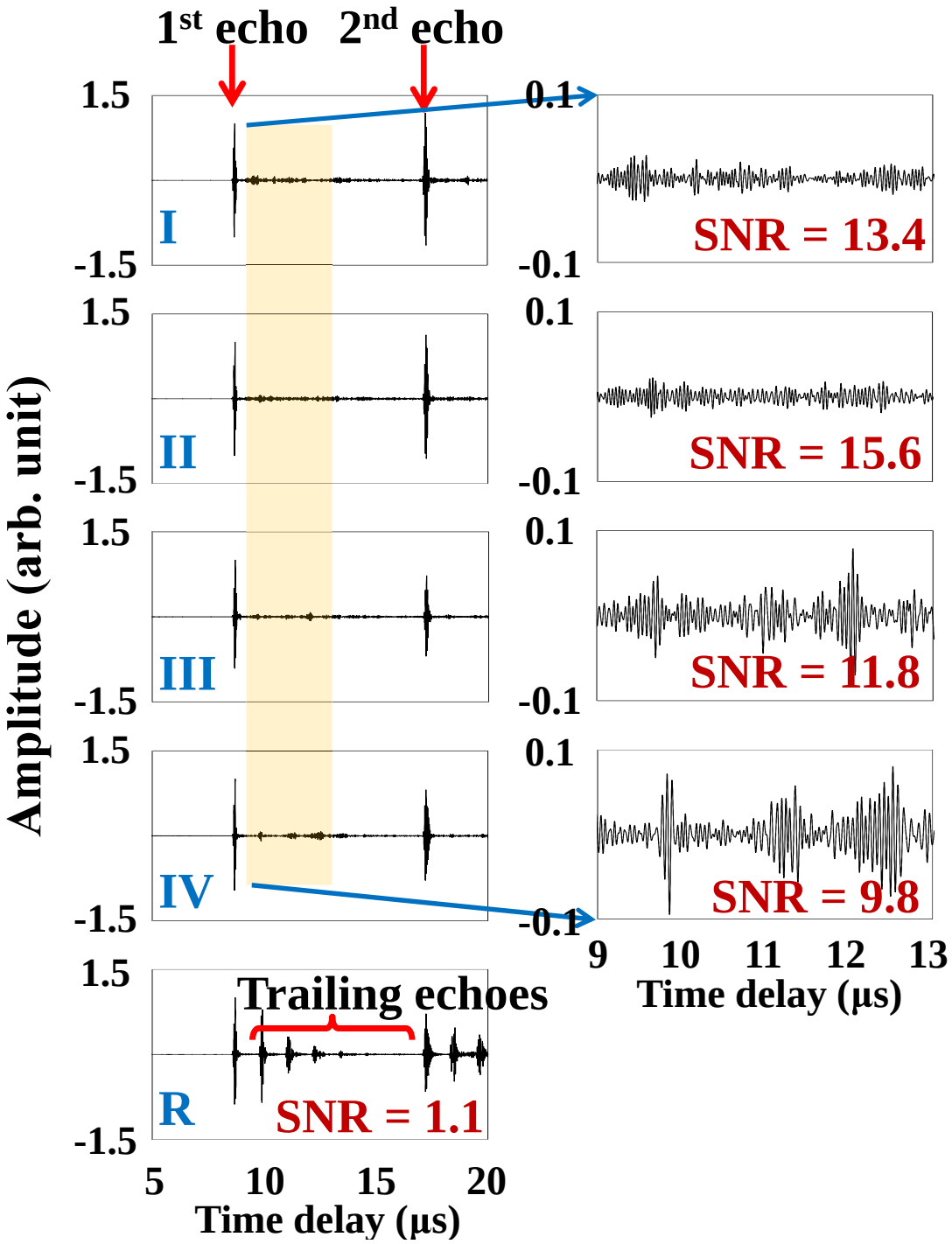

Figure 5-3: Simulated waveforms and the signal-to-noise ratio (SNR) for regular (R) square and its irregular shapes such as I, II. III and IV, respectively.

5.1.2 Proposed irregular polygons

The irregular polygons such as triangle, square, pentagon, hexagon and heptagon are designed using the presented guidelines. Unfortunately, there is an obstacle that occurred due to the current guidelines where the distortion point must be far from the initial regular point. Based on Figure 5-4, it is observed that such guideline is successfully applied on designing the irregular polygons such as square, pentagon, hexagon and heptagon, but not for the irregular triangle where the distortion point is near to its initial regular point. This is due to the limitation of the raw material where the raw material is in the shape of a cylindrical rod having the diameter of 28 mm. Since the side length of a regular triangle is almost 26 mm, it is impossible to machine an irregular triangle where the distortion point is far from its initial regular point. In order to overcome such problem, a vertex of a regular triangle is distorted as far as the machining is possible. Figure 5-5 shows the obstacle during designing and machining the irregular triangle using the raw material which is in the shape of a cylindrical rod.

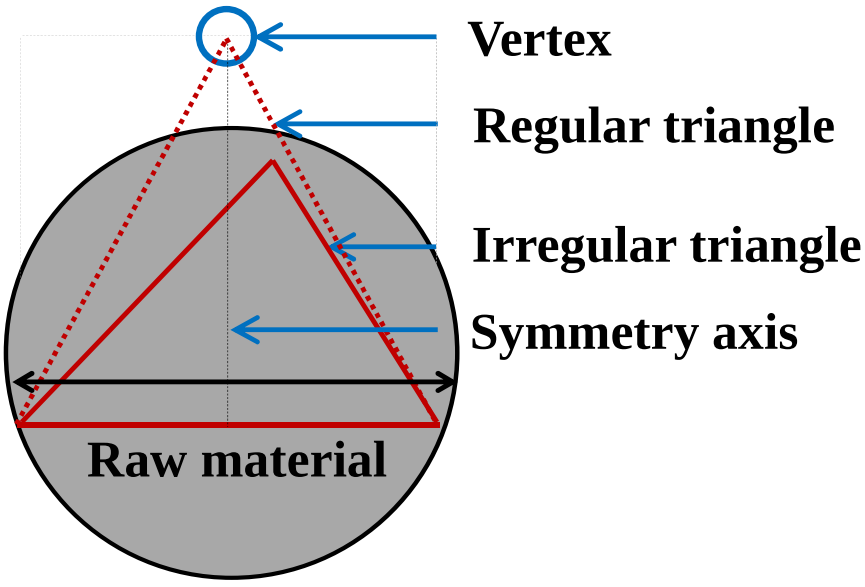

Figure 5-4: Designing and machining limitations of the irregular triangle due to the raw material.

Due to this problem, the area for the irregular triangle is smaller than that of a regular triangle. Although the comparison between the regular and irregular triangle is no longer fair, a significant improvement of SNR for the irregular triangle is expected to be occurred since the influence of symmetry is eliminated. The second obstacle arises during designing the irregular hexagon using the current guidelines. It is found that although the influence of symmetry is eliminated due to the distortion on one vertex of a regular hexagon and no parallel sides are generated due to the distortion, a pair of the original parallel sides in a regular hexagon is still remained, as shown by Figure 5-5. Therefore, trailing echoes can still be generated for the irregular hexagon and the SNR will not be significantly improved.

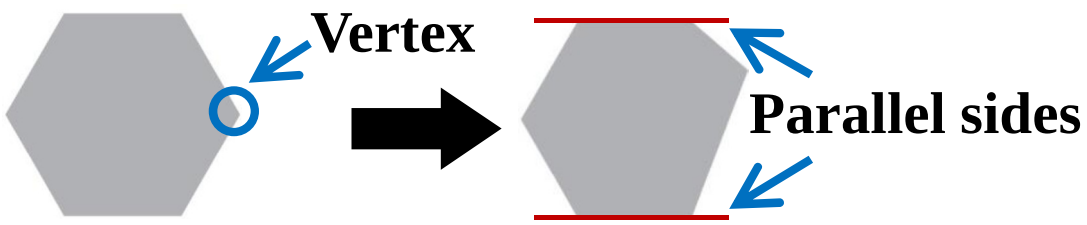

Figure 5-5: A pair of parallel sides is still remained in the irregular hexagon due to only one vertex is distorted.

In order to eliminate the remaining parallel sides in the irregular hexagon as shown in Figure 5-5, two vertices should be distorted. However, by distorting the second vertices, the area for the new irregular hexagon is slightly bigger than the previous irregular hexagon. Figure 5-6 shows how the new irregular hexagon is designed by distorting two vertices instead of one vertex. It is highly believed that the generation of trailing echoes can be completely eliminated by such distortion on two different vertices of a regular hexagon. It is believed that the difference of area may not affect the performance of the ultrasonic pulsed echoes in the irregular polygonal buffer rods as long as no shear waves can arrive at the side wall of the rod perpendicularly.

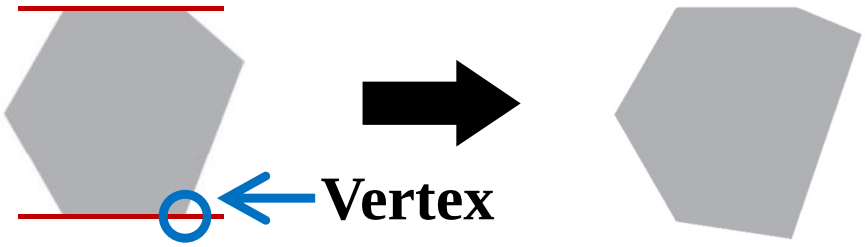

Figure 5-6: Designing a new irregular hexagon where a second vertex (depicted in a circle) is distorted in order to eliminate the parallel sides.

Although the obstacles found in triangle and hexagon are overcome by proposing the new designs of irregular polygons, in this work, the effectiveness of buffer rods having the cross-sectional shapes of irregular polygons with only one distorted vertex on preventing the generation of trailing echoes is numerically investigated. Figure 5-7 shows the proposed designs for all the polygons such as triangle, square, pentagon, hexagon and heptagon, respectively. Take note that the area for all the proposed irregular polygons is kept constant with their corresponding regular polygons, except for triangle.

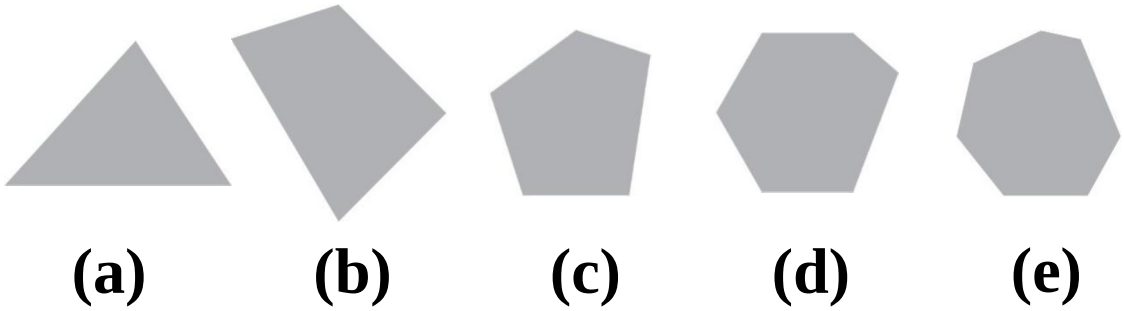

Figure 5-7: The proposed irregular polygons for the cross-sectional shape of buffer rods such (a) triangle, (b) square, (c) pentagon, (d) hexagon and (e) heptagon, respectively.

5.2 Mechanism to prevent the generation of trailing echoes for irregular polygonal buffer rods

5.2.1 Even polygons

Figure 5-8 shows the propagation of shear waves in an irregular square II, as proposed in Figure 5-2 and Figure 5.7(b), respectively. It is found that although the parallel sides have been eliminated, however, the second reflected shear waves (S_2) which are originated from side B and side D, arrived at the side wall of the rod perpendicularly. Therefore, the first trailing echo for the irregular square is generated. Meanwhile, the second reflected shear waves (S_2) which are originated from from side A and side C did not arrive at the side wall of the rod perpendicularly. Therefore, although the parallel sides in the irregular square have been eliminated, the generation of trailing echoes is not completely prevented due to some of the second reflected shear waves (S_2) that can arrive at the side wall of the rod perpendicularly. Since the trailing echo is possible to be generated by the second reflected shear waves (S_2) that arrive at the side wall of the rod perpendicularly, the propagation of the third reflected shear waves (S_3) is then investigated. Figure 5-9 shows the propagation of the third reflected shear waves (S_3) that are originated from side A and side C, respectively. Unfortunately, the third reflected shear wave (S_3) which is originated from side C arrived at the side wall of the rod perpendicularly and generate a trailing echoes. Since the propagation length for S_3 is longer than that of S_2, it can be concluded that the first trailing echo is generated by S_2 while the second trailing echo is generated by S_3. Therefore, the generation of trailing echoes for the irregular square is not completely prevented.

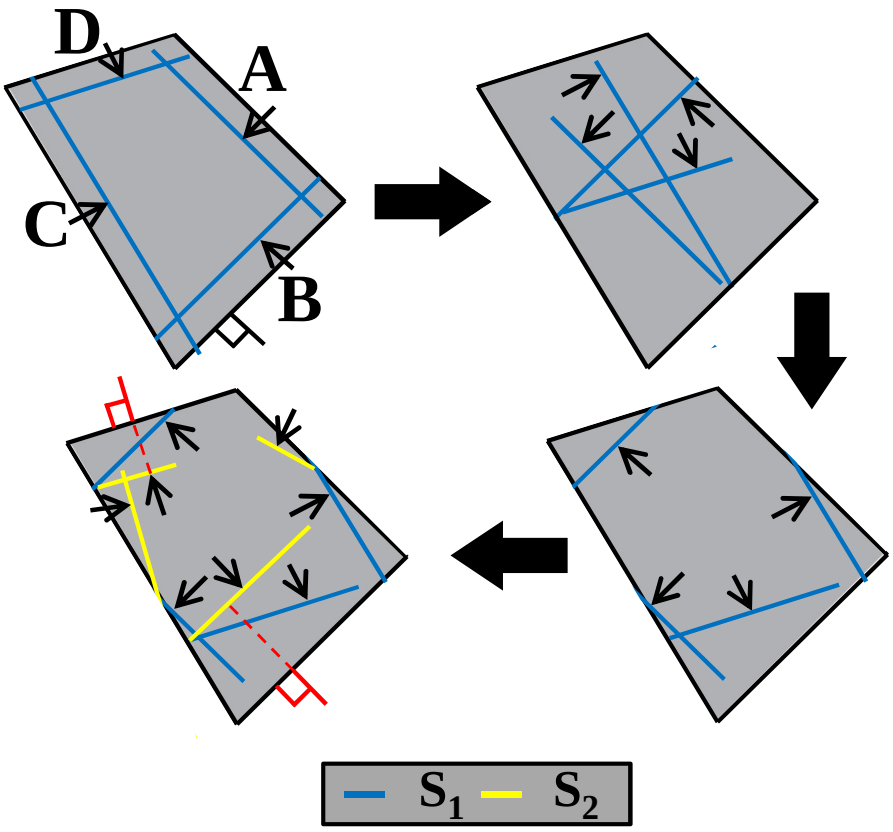

Figure 5-8: Propagation of the first (S_1) and second (S_2) reflected shear waves for the irregular square.

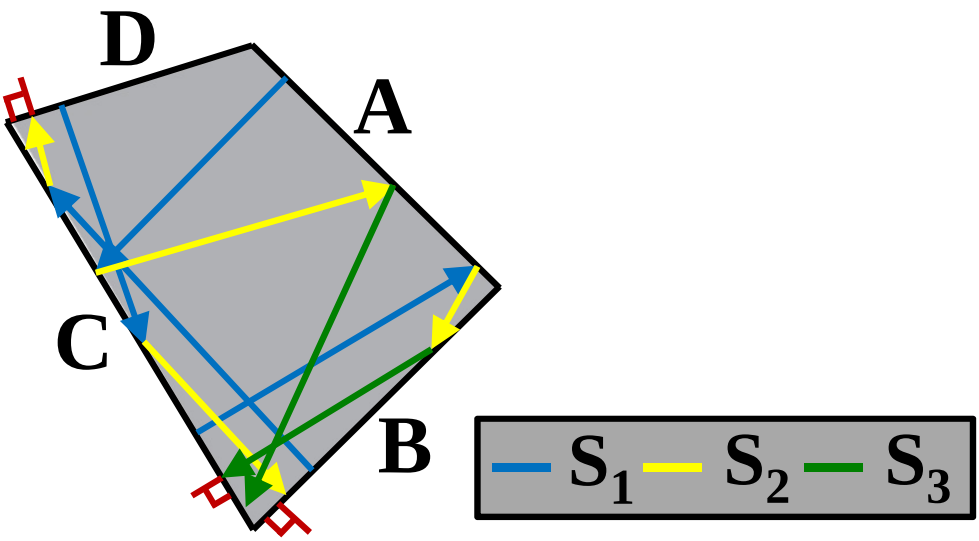

Figure 5-9: Possible generation of trailing echoes for the irregular square where the reflected shear waves arrived at the side wall of the rod perpendicularly.

It has been mentioned that the proposed irregular hexagon will show the least improvement on the SNR due to only one vertex is distorted. Therefore, a pair of parallel sides is still remained and will generate trailing echoes. The reason and solution to overcome such problem has been discussed in the previous subsection. In addition, since the remaining parallel sides are not inclined, strong amplitude of trailing echo is expected to be generated. This is due to the ultrasonic waves that are not reflected diffusely on a straight plane. The mechanism for generating the first trailing echo in the irregular hexagon is shown in Figure 5-10. As expected, due to the parallel sides between the upper and bottom sides of the irregular hexagon, a pair of parallel first reflected shear waves (S1) is generated. Such parallelism leads to the arrival for each of the S1 to the opposite side wall of the rod perpendicularly and generate the first trailing echo.

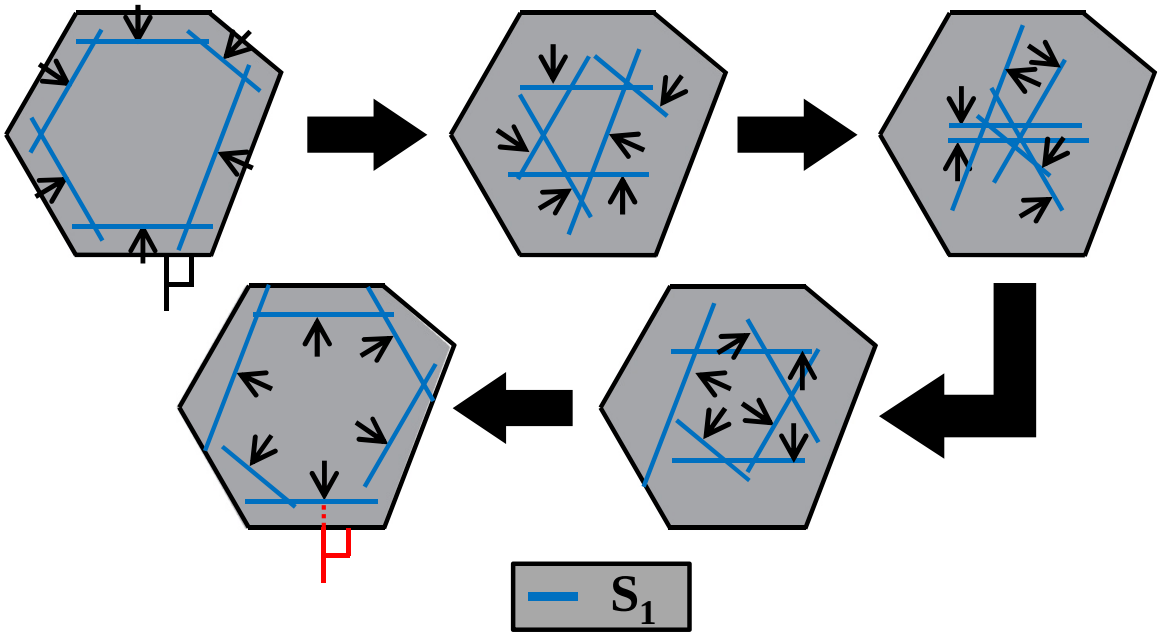

Figure 5-10: Propagation of the first reflected shear waves (S_1) for the irregular hexagon.

Based on the mechanism for generating trailing echoes for the irregular even polygons such as square and hexagon, it can be concluded that the generation of trailing echoes is

still possible where some of the shear waves arrived at the side wall of the rod perpendicularly. Therefore, the generation of trailing echo is not completely prevented. As mentioned previously, such generation is not completely prevented due to the guidelines where only one vertex of a regular even polygon is distorted. Such distortion leads to two obstacles. The first obstacle is that some of the second reflected shear waves (S_2) arrive at the side wall of the rod perpendicularly and generate the first trailing echo. However, the SNR can still be improved since the propagation path for S_2 is longer than that of S_1. Therefore, the generated trailing echoes will have a smaller amplitude. The second obstacle is that some of the parallel sides are still remained although the influence of symmetry has been eliminated. In order to overcome such problem, a new irregular hexagon has been designed and proposed, as shown in Figure 5-6 where two vertices of a regular hexagon are distorted. However, by such approach, the area for the new irregular hexagon is slightly bigger than the previous irregular hexagon. Therefore, for a constant area between the regular hexagon and the new irregular hexagon with two distorted vertices, a different design for such irregular hexagon is shown in Figure 5-11. Take note that each vertices are distorted at a point where it is far from the initial regular point. From this new design, it is observed that all the parallel sides in the regular hexagon are eliminated. In addition, no new pairs of parallel sides are created by these two distorted vertices. Therefore, it is highly expected that the generation of trailing echoes will be completely prevented and the SNR will be significantly improved.

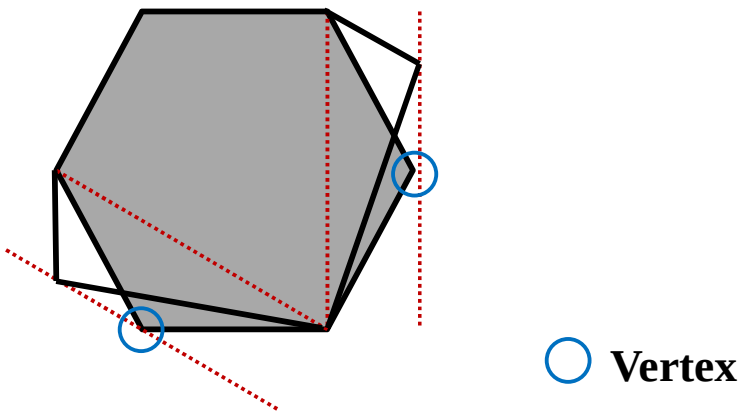

Figure 5-11: New design of the irregular hexagon having two distorted vertices and constant area with the regular hexagon.

5.2.2 Odd polygons

Figure 5-12 shows the propagation of shear waves for the irregular triangle. Unlike the regular triangle, the first trailing echo is generated due to the arrival of the second reflection of shear waves (S_2) to the side wall of the rod perpendicularly. However, based on Figure 5-12, it is observed that none of the second reflection of shear waves (S_2) propagates to the side wall of the rod perpendicularly. Therefore, no trailing echo is generated and the SNR is expected to be improved. A similar mechanism is also observed for the irregular pentagon where none of the second reflected shear waves (S_2) arrived at the side wall of the rod perpendicularly, as shown by Figure 5-13.

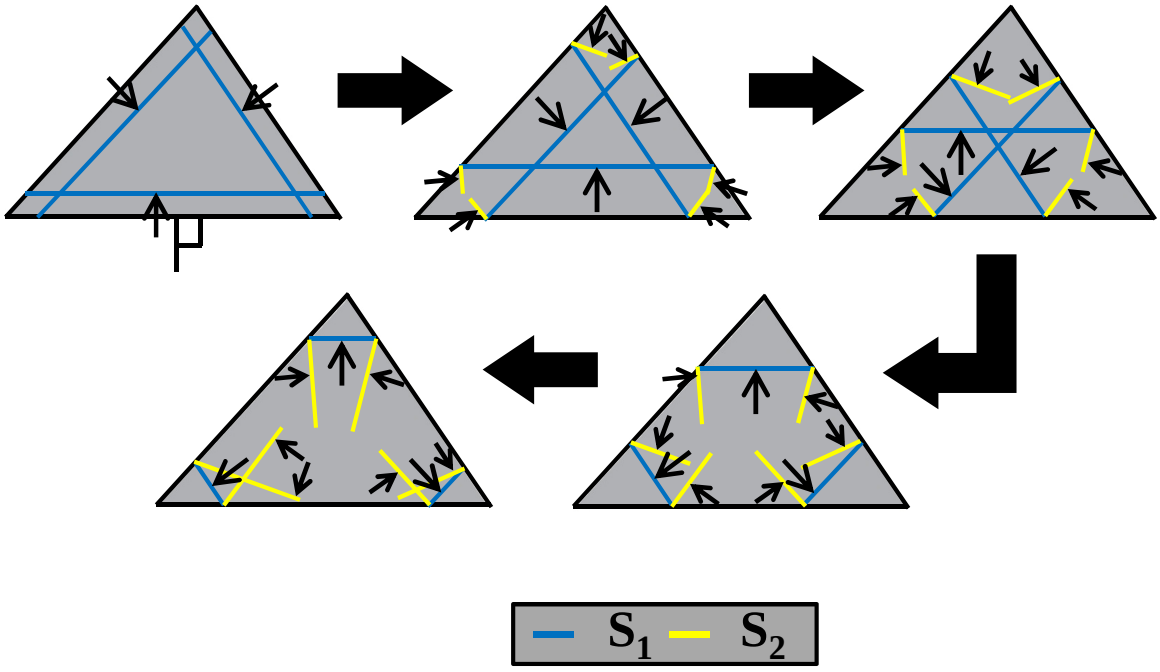

Figure 5-12: Propagation of the first (S_1) and second (S_2) reflected shear waves for the irregular triangle.

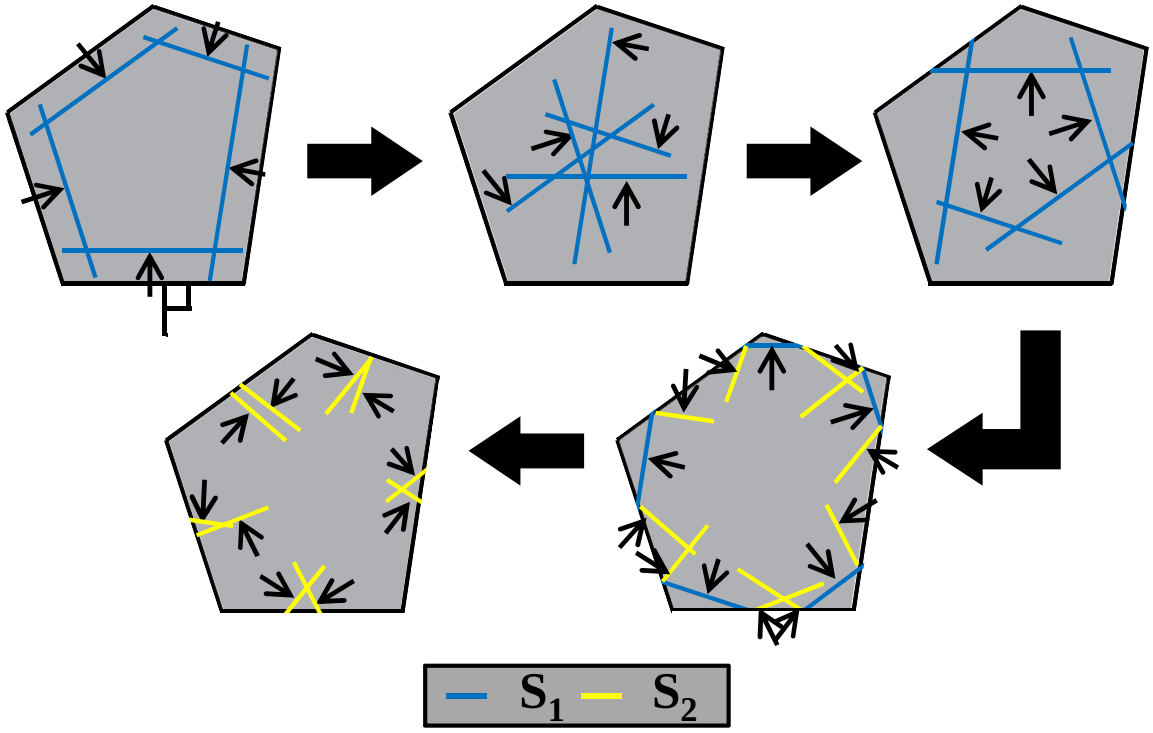

Figure 5-13: Propagation of the first (S_1) and second (S_2) reflected shear waves for the irregular pentagon.

Lastly, the propagation of shear waves for the irregular heptagon is presented in Figure 5-14. However, unfortunately, it is observed that one of the second reflected shear wave (S_2), as depicted in oval, propagates to the side wall of the rod perpendicularly. Such arrival is presented in Figure 5-15. From side A, the first reflected shear wave (S_1) propagates to its opposite boundary which is side B. Since such arrival is not perpendicular to the side wall of the rod, therefore, S_1 is reflected at side B as S_2. It is observed that the propagation direction of S_2 is perpendicular to side C; therefore, a trailing echo is generated. Although the influence of symmetry has been eliminated in the irregular heptagon, some of the reflected shear waves are able to arrive at the side wall of the rod perpendicularly and generate trailing echoes. This phenomena is similar with the irregular square where the first trailing echo is generated by the arrival of the second reflected shear waves (S_2) at the side wall of the rod perpendicularly. Since it shows the same mechanism, it can be concluded that two vertices need to be distorted rather than

one. Since it has been mentioned before, the reason why only one vertex is distorted is that the possible designs of the irregular polygons are less than the irregular polygons having two or more distorted vertices. In order to prevent the arrival of the second reflected shear waves (S_2) to the side wall of the rod for the irregular heptagon, a new design for the irregular heptagon is proposed as shown in Figure 5-16. Take note a same approach used for designing the new irregular hexagon is applied on this new irregular heptagon. Again, take note by this approach, the area for the new irregular heptagon is slightly bigger than the regular heptagon. The second vertex is chosen so that it will prevent the arrival of the second reflected shear waves (S_2) generated from side B to the side C perpendicularly. The propagation of shear waves for the new irregular heptagon is presented in Figure 5-17. From such propagation, it is observed that none of the second reflected shear waves (S_2) arrived at the side wall of the rod perpendicularly. Therefore, the SNR for the new irregular heptagon having two distorted vertices is expected to be better than that of the irregular heptagon having only one distorted vertex.

The mechanism that shows the propagation of shear waves for all the irregular polygons such as triangle, square, pentagon, hexagon and heptagon are numerically simulated. However, take note that only the new irregular heptagon having two distorted vertices is simulated rather than the new irregular hexagon that also has two distorted vertices. Such approach is due to the good performance of the regular heptagon that gives the highest SNR compared to the other regular polygons.

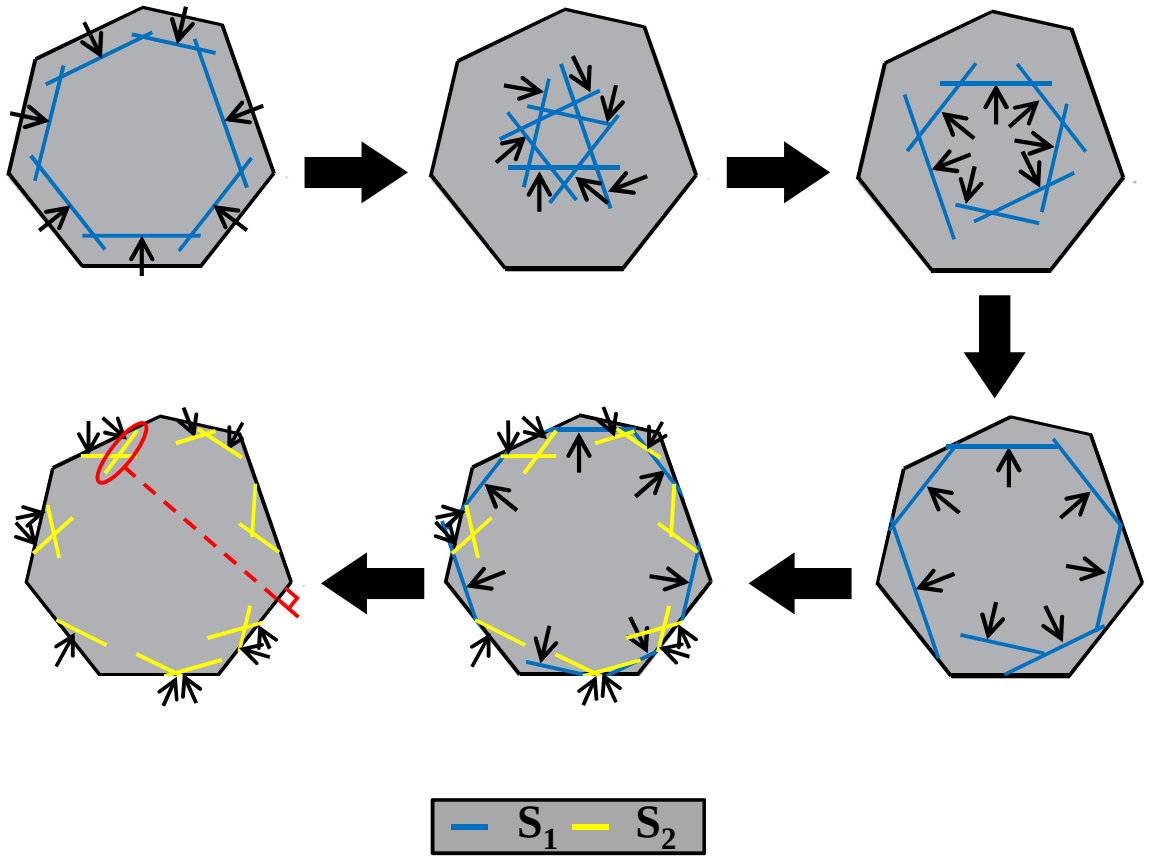

Figure 5-14: Propagation of the first (S_1) and second (S_2) reflected shear waves for the irregular heptagon.

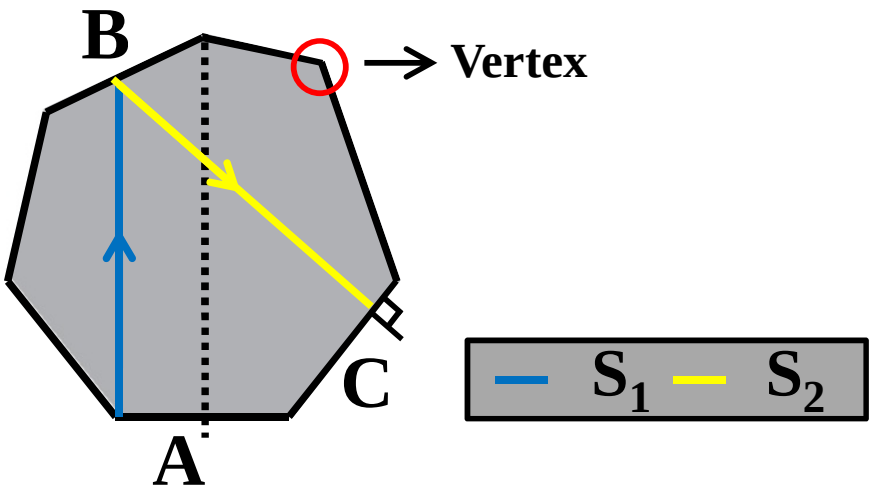

Figure 5-15: Mechanism to generate the first trailing echo for the irregular heptagon.

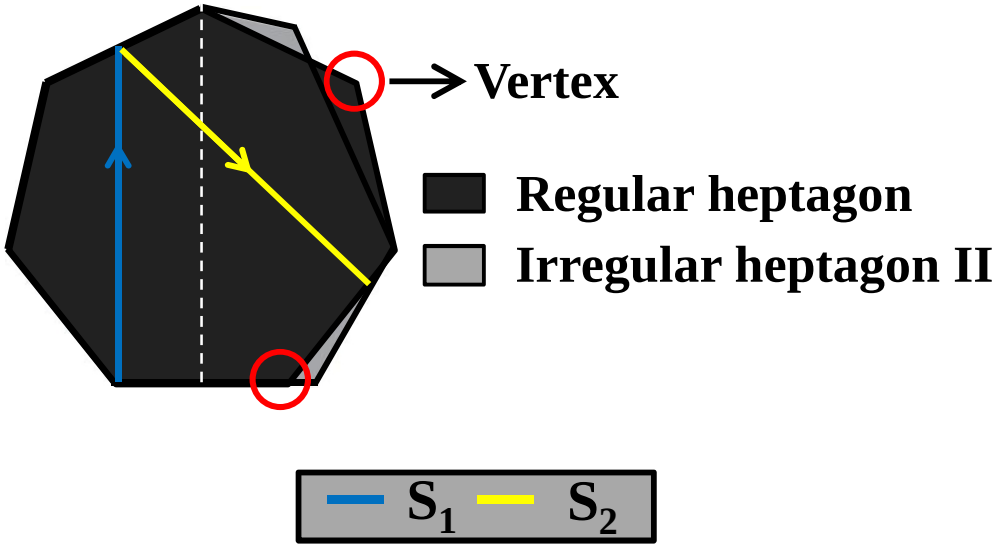

Figure 5-16: New design for an irregular heptagon

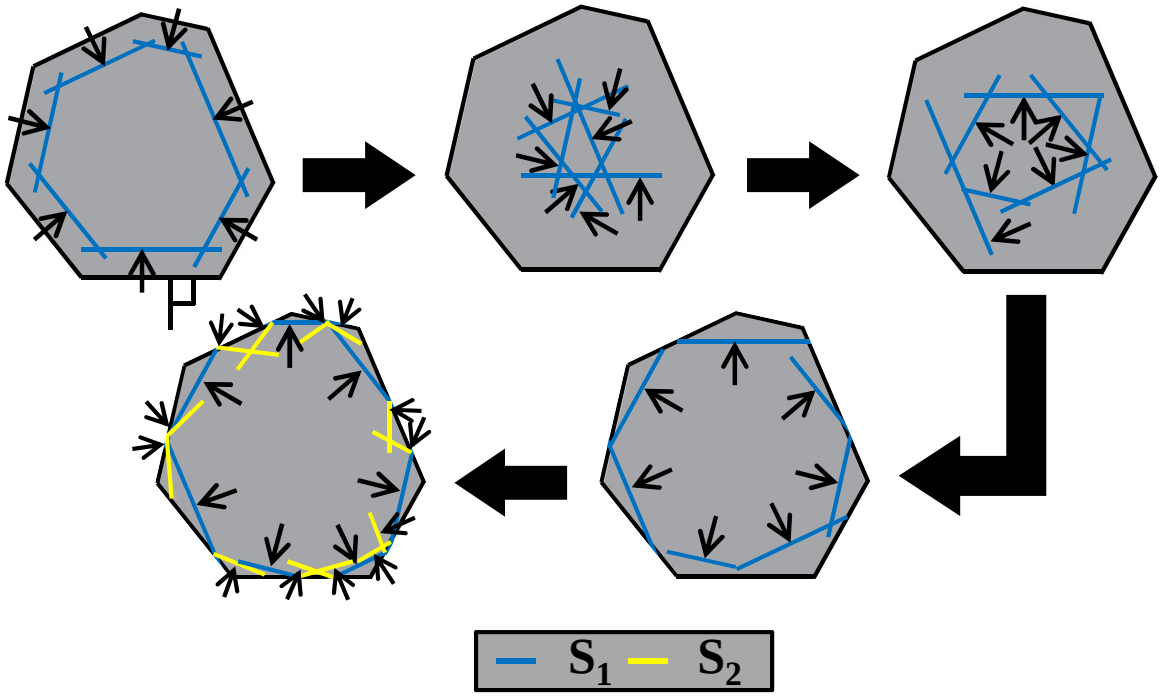

Figure 5-17: Propagation of the first (S_1) and second (S_2) reflected shear waves for the new irregular heptagon.

5.3 Three dimensional simulations on the irregular polygonal buffer rods

In order to verify the mechanism for all the proposed irregular polygons, numerical simulations are conducted on each irregular polygonal buffer rod using the same simulation conditions used on the regular polygonal buffer rods.

5.3.1 Simulation results and discussions

Figure 5-18 shows the simulated waveforms for (a) regular and (b) irregular polygonal buffer rods. As expected, all irregular polygonal buffer rods except for irregular hexagon show a significant reduction of trailing echoes. Therefore, the mechanism to prevent the generation of trailing echoes is verified.

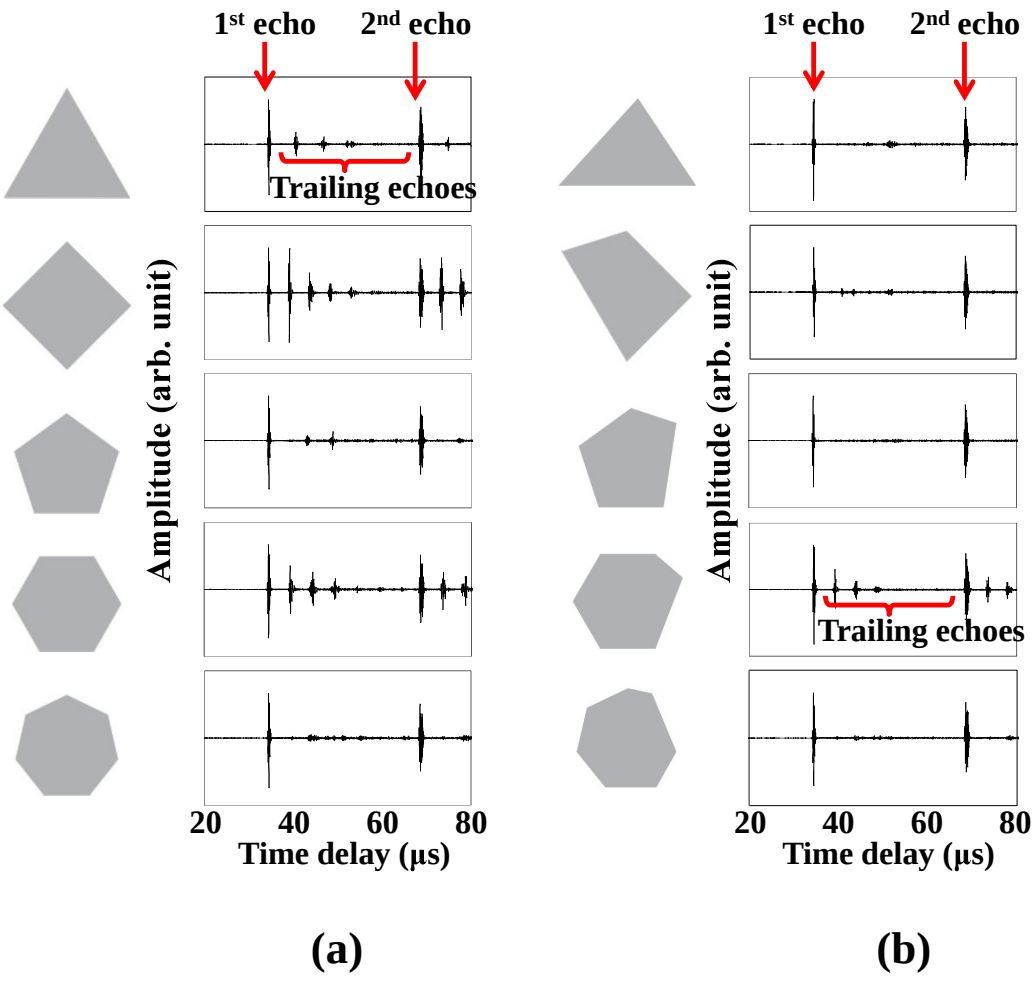

Figure 5-18: Simulated waveforms for (a) regular polygonal buffer rods and (b) irregular polygonal buffer rods.

The SNR for the comparison between the regular and irregular polygonal buffer rods is presented in Figure 5-19. It can be seen that the SNR for pentagon is significantly improved compared to other irregular polygons.

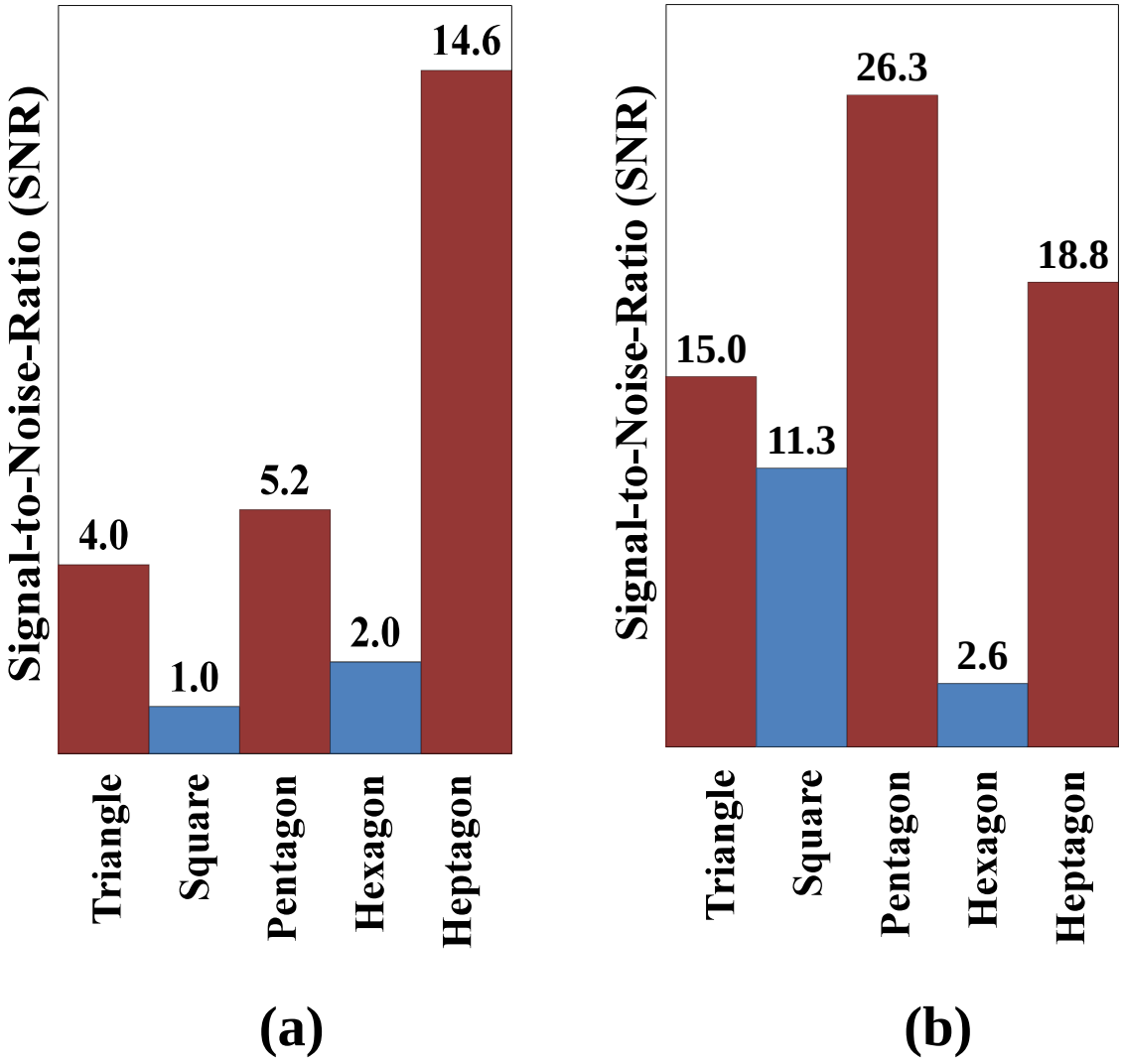

Figure 5-19: Signal-to-noise ratio (SNR) for (a) regular polygonal buffer rods and (b) irregular polygonal buffer rods based on the simulated waveforms.

However, based on the simulated waveforms in Figure 5-18(b), a trailing echo having small amplitude is still generated for the irregular triangle buffer rod. Such trailing echo is also observed from the wave propagation studies of the irregular triangle buffer rod, as shown by the captured images in Figure 5-20 where E1 and TE1 are the first echo and first trailing echo, respectively. An investigation is then carried out to determine the reason for generating such trailing echo. Figure 5-21 shows the mechanism to generate such trailing echo for an irregular triangle buffer rod. It is observed that after several reflections, the mode converted shear waves (S_6) arrived at the side wall of the rod perpendicularly and therefore, generates the first trailing echo. Therefore, it can be concluded that although at first it seems that none of the reflected shear waves are able to arrive at the side wall of the rod perpendicularly, after several times of reflections, some of the reflected shear waves are still possible to arrive at the side wall of the rod perpendicularly and generate trailing echoes. However, take note that the amplitude for such trailing echoes is expected to be small since the shear waves have been reflected for several times.

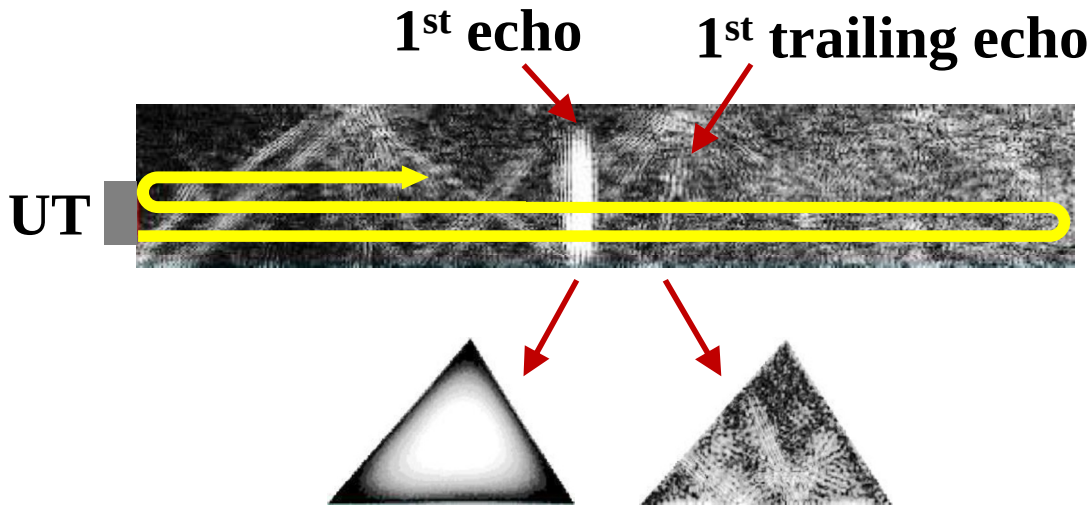

Figure 5-20: Captured images of one round-trip ultrasonic pulsed echo for a 100 mm length irregular triangle buffer rod.

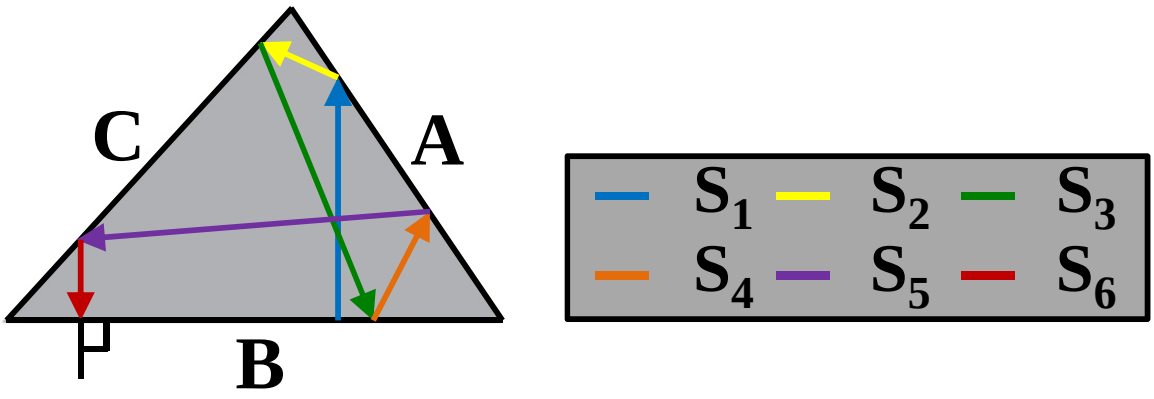

Figure 5-21: Possible generation of a trailing echo for the irregular triangle.

For the irregular square, it is expected that two trailing echoes will be generated based due to the second (S_2) and third (S_3) reflection of shear waves that arrived at the side wall of the rod perpendicularly. Both arrival are shown in Figure 5-8 and Figure 5-9, respectively. Such arrival is verified from the wave propagation studies on the irregular square, as shown in Figure 5-22. It is observed that there are two bright lines that are parallel to the UT after the first echo (E1). These two bright lines are identified as the trailing echoes. The first bright line that arrived at UT is the first trailing echoes (TE1) while the later arrival of the bright line is the second trailing echo (TE2). The propagation of shear waves for generating the first trailing echo by the second reflection of shear waves (S_2) is also shown by the captured images in Figure 5-23. The first image shows the generation of the first echo which gives a bright cross-section while the last image shows the propagation of the second reflected shear waves (S_2) to the side wall of the rod which is in a perpendicular direction.

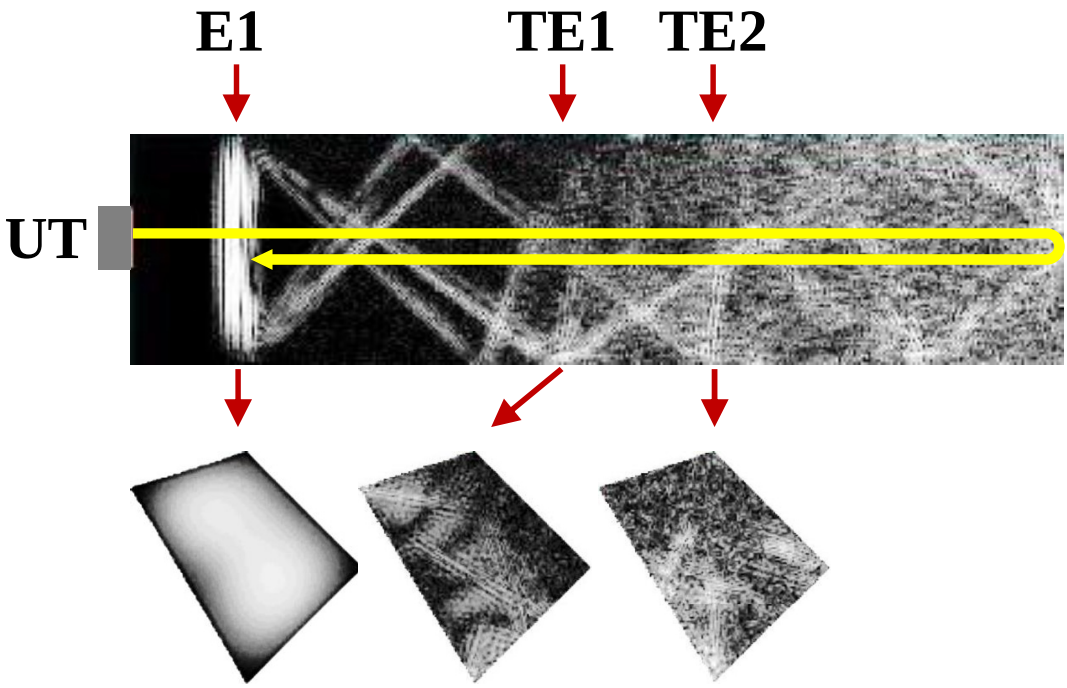

Figure 5-22: Captured images of one round-trip ultrasonic pulsed echo for a 100 mm length irregular square buffer rod.

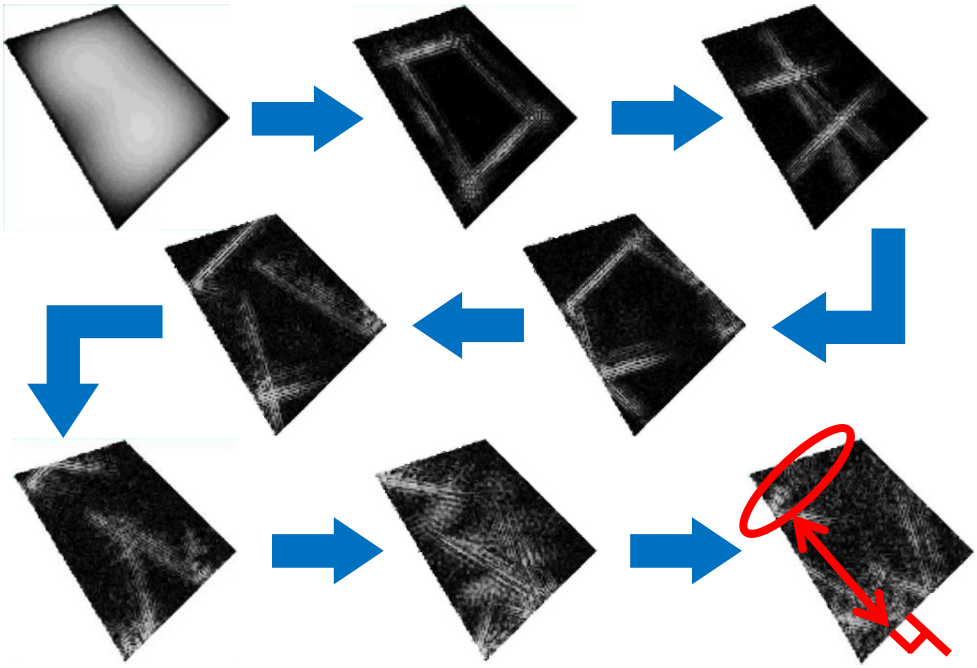

Figure 5-23: Captured images during the wave propagation studies for generating the first trailing echo for an irregular square.

The highest SNR is given by the irregular pentagon where the SNR is improved five times higher compared to the regular pentagon. It is found that such guideline in designing an irregular polygon is good enough for successfully developing an irregular polygonal buffer rod with high SNR. Figure 5-24 shows the captured images during the one round-trip of ultrasonic pulsed echoes propagating through the 100 mm length irregular pentagon buffer rod. Since it is observed in Figure 5-18(b) that no trailing echoes are generated for the irregular pentagon, therefore, no bright lines that indicate the presence of trailing echoes are observed. Therefore, the UT only received the first echo since the direction of such echo is parallel to the UT.

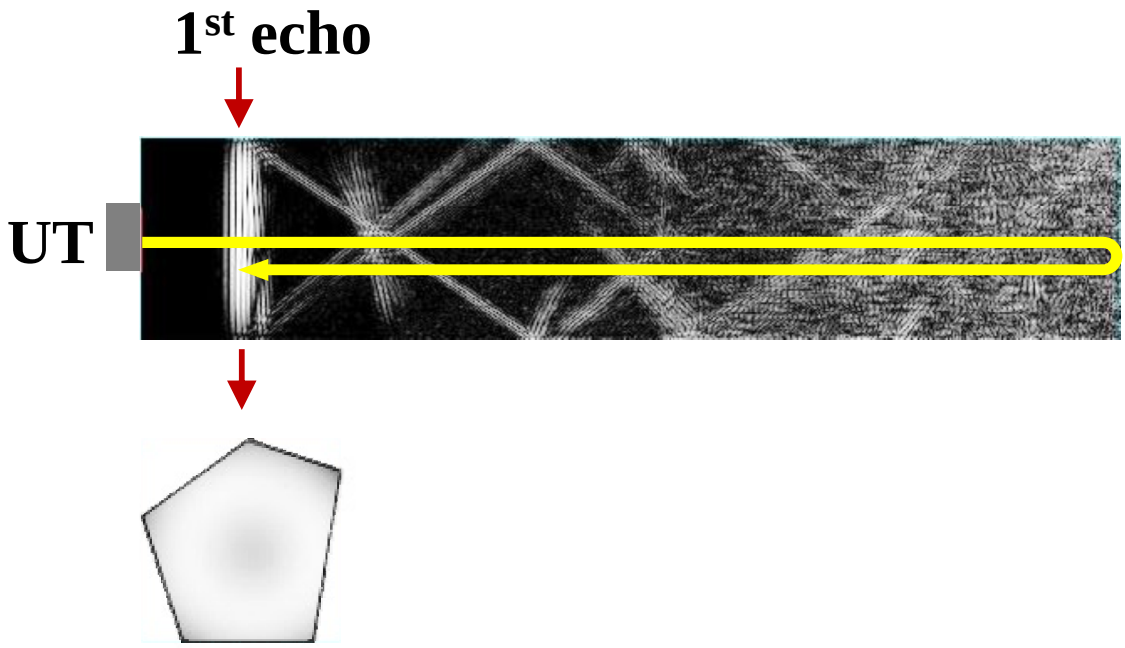

Figure 5-24: Captured images of one round-trip ultrasonic pulsed echo for a 100 mm length irregular pentagon buffer rod.

For the irregular hexagon buffer rod, as expected, significant trailing echoes are still generated due to the parallel sides that are still remained although half of the regular hexagon has been distorted. As shown by the captured images in Figure 5-25, the first and second trailing echoes are easily distinguished due to their brightness. The mechanism for generating the trailing echoes for the irregular hexagon is also verified by the wave propagation studies on the cross-sectional shape of irregular hexagon buffer rod. Figure

5-26 shows that indeed, the first reflection of shear waves (S_1) are parallel to the rod boundary, as depicted in oval.

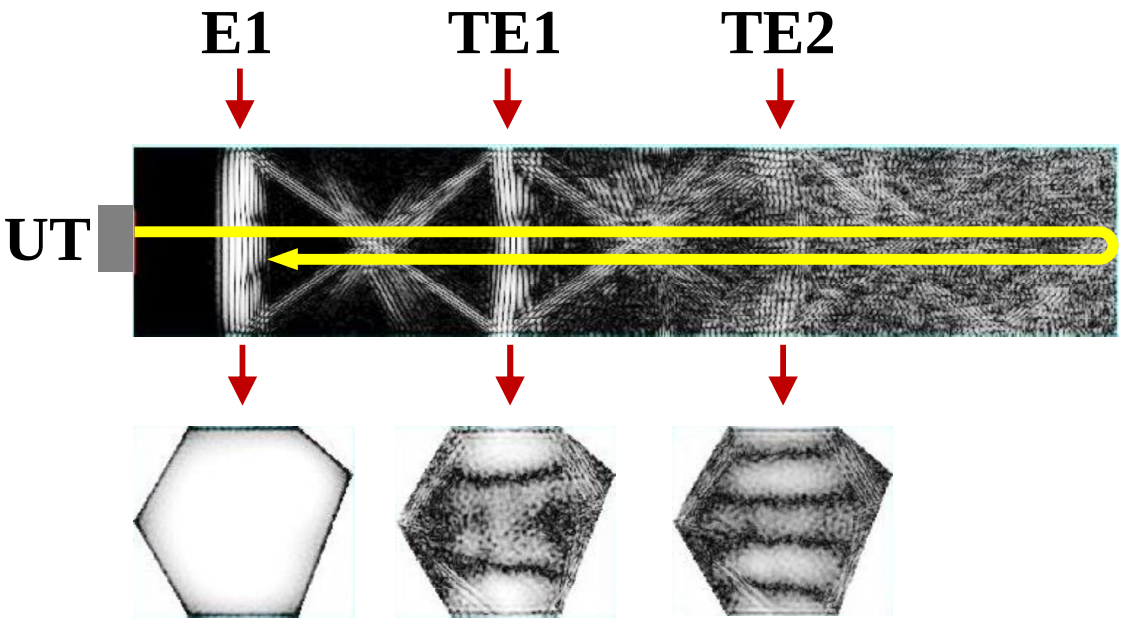

Figure 5-25: Captured images of one round-trip ultrasonic pulsed echo for a 100 mm length irregular hexagon buffer rod.

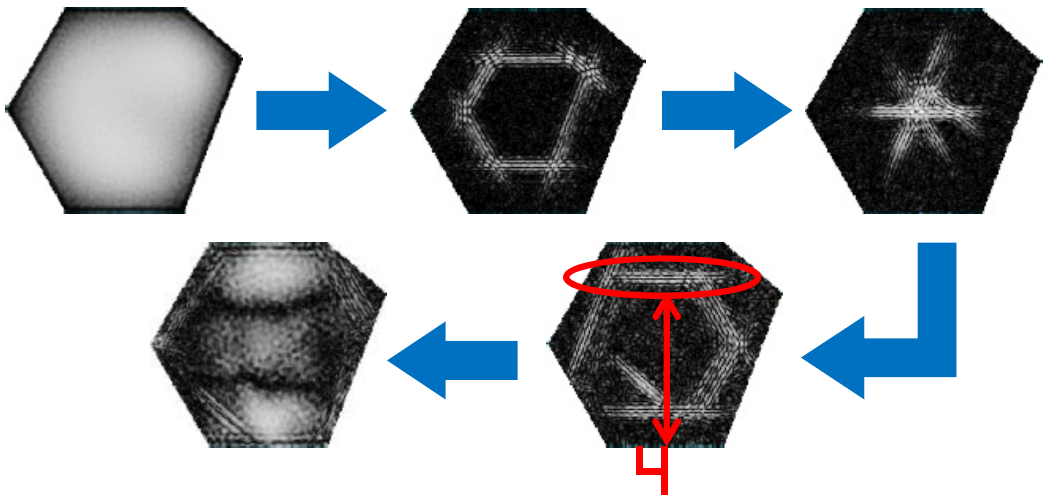

Figure 5-26: Wave propagation shows that the first trailing echo is generated by the first reflection of shear waves (S_1), as depicted in oval.

In addition, it is found that the SNR for both regular and irregular hexagon are almost the same. Such similarity is due to the influence of the location of the parallel sides. If the parallel sides that are designed for the irregular hexagon are not the inclined surface, the amplitude of trailing echo may be smaller due to diffuse reflection, which has been explained in the previous chapter. Therefore, the SNR will be increased since the amplitude of trailing echo is reduced. A similar tendency of small improvement on the SNR is also observed for the irregular heptagon. This is expected due to the influence of parallel sides when only one vertex of a regular heptagon is distorted. As stated earlier, in order to overcome such influence, two vertices need to be distorted. Figure 5-27 shows the simulated waveforms for both irregular heptagon with one vertex distorted (top waveform) and irregular heptagon with 2 vertices distorted (bottom waveform). It is observed that the trailing echoes are reduced and the SNR is improved.

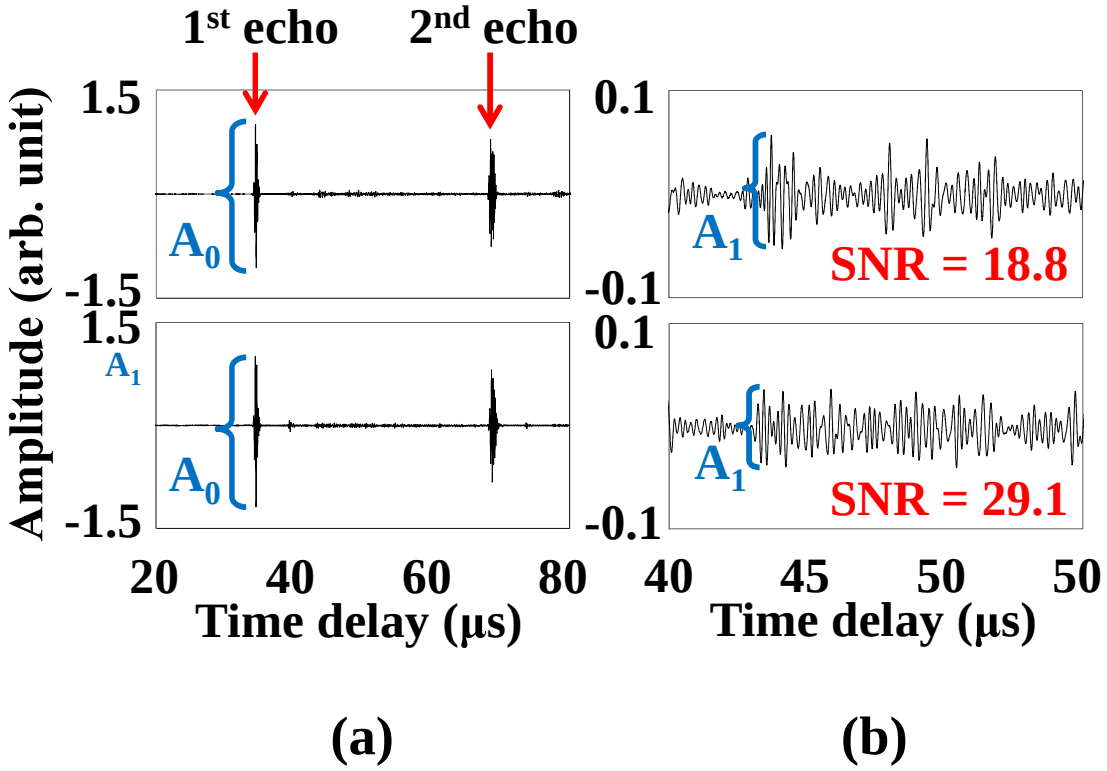

Figure 5-27: Simulated waveforms for the irregular heptagon with one vertex distorted (top) and irregular heptagon with two vertices distorted (bottom).

5.4 Experiment on the irregular polygonal buffer rods

Based on the simulation results, all the proposed irregular polygonal buffer rods, except for the irregular hexagon and irregular heptagon with only one vertex distorted, are fabricated using steel S45C. It is noted that irregular hexagon was not fabricated due to no improvement on the SNR. Meanwhile, for the irregular heptagon, irregular heptagon with two vertices distorted shows better performance in terms of smaller trailing echoes and higher SNR. Figure 5-28 shows the fabricated irregular polygonal buffer rods having different cross-sectional shapes such as (a) triangle, (b) square, (c) pentagon and (d) heptagon, respectively. The length and area for all irregular polygonal buffer rods are kept constant, for a fair comparison with the regular polygonal buffer rods and based on the guidelines during designing an irregular polygon. Each of the fabricated irregular polygonal buffer rods is then experimentally investigated with a 5 MHz ultrasonic transducer having diameter of 6.35 mm.

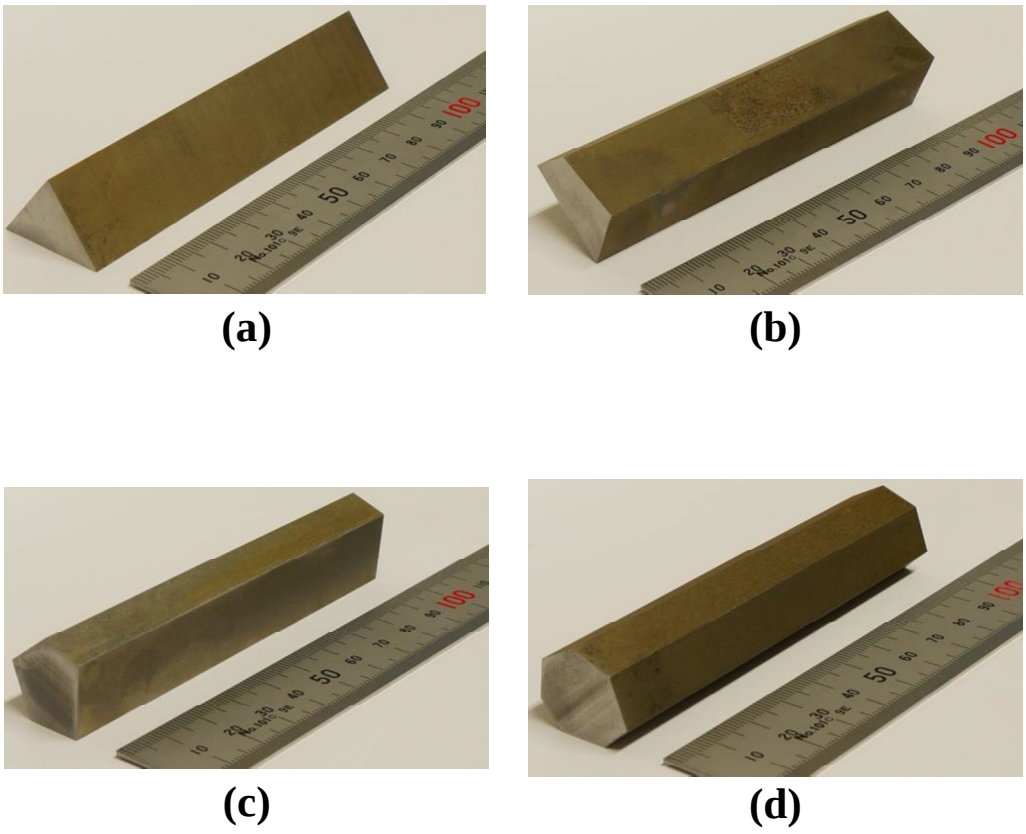

Figure 5-28: Fabricated irregular polygonal buffer rods having different cross-sectional shapes such as (a) triangle, (b) square (c) pentagon and (d) heptagon

5.4.1 Experimental results and discussions

Figure 5-29 shows the measured waveform for (a) regular polygons and (b) irregular polygons where the polygons are triangle, square, pentagon and heptagon. It is observed that for the irregular polygonal buffer rods, the tendency of trailing echoes is similar for both simulated and experiment waveforms. However, based on the measured waveforms for both regular and irregular heptagon, only small improvement on reducing the amplitude of trailing echoes is observed. Therefore, although the new design of irregular heptagon with two vertices distorted has been proposed, the amplitude of the trailing echoes for both regular and irregular heptagon are almost the same. Meanwhile, as predicted, the irregular pentagon shows a significant performance on preventing the generation of trailing echoes where the SNR is the highest compared to other irregular polygons, as shown in Figure 5-30.

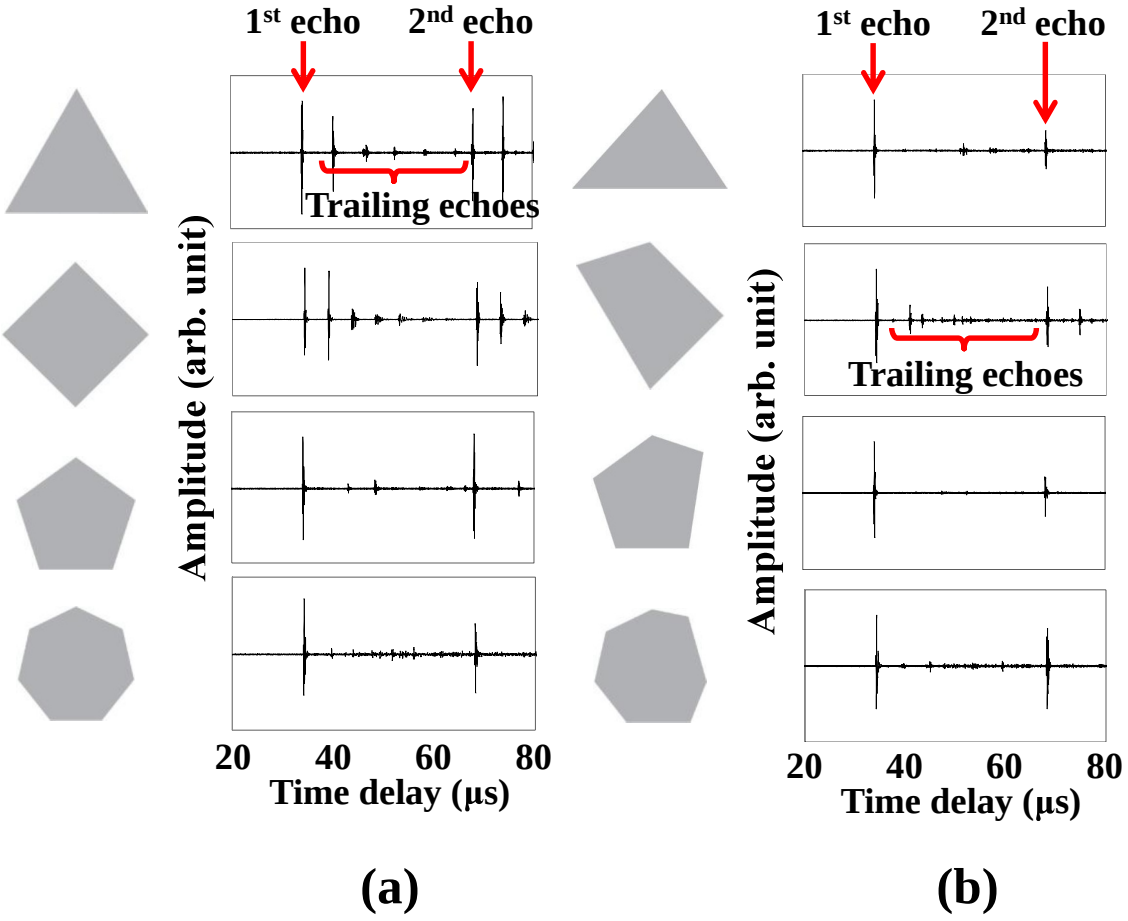

Figure 5-29: Measured waveforms for (a) regular polygonal buffer rods and (b) irregular polygonal buffer rods

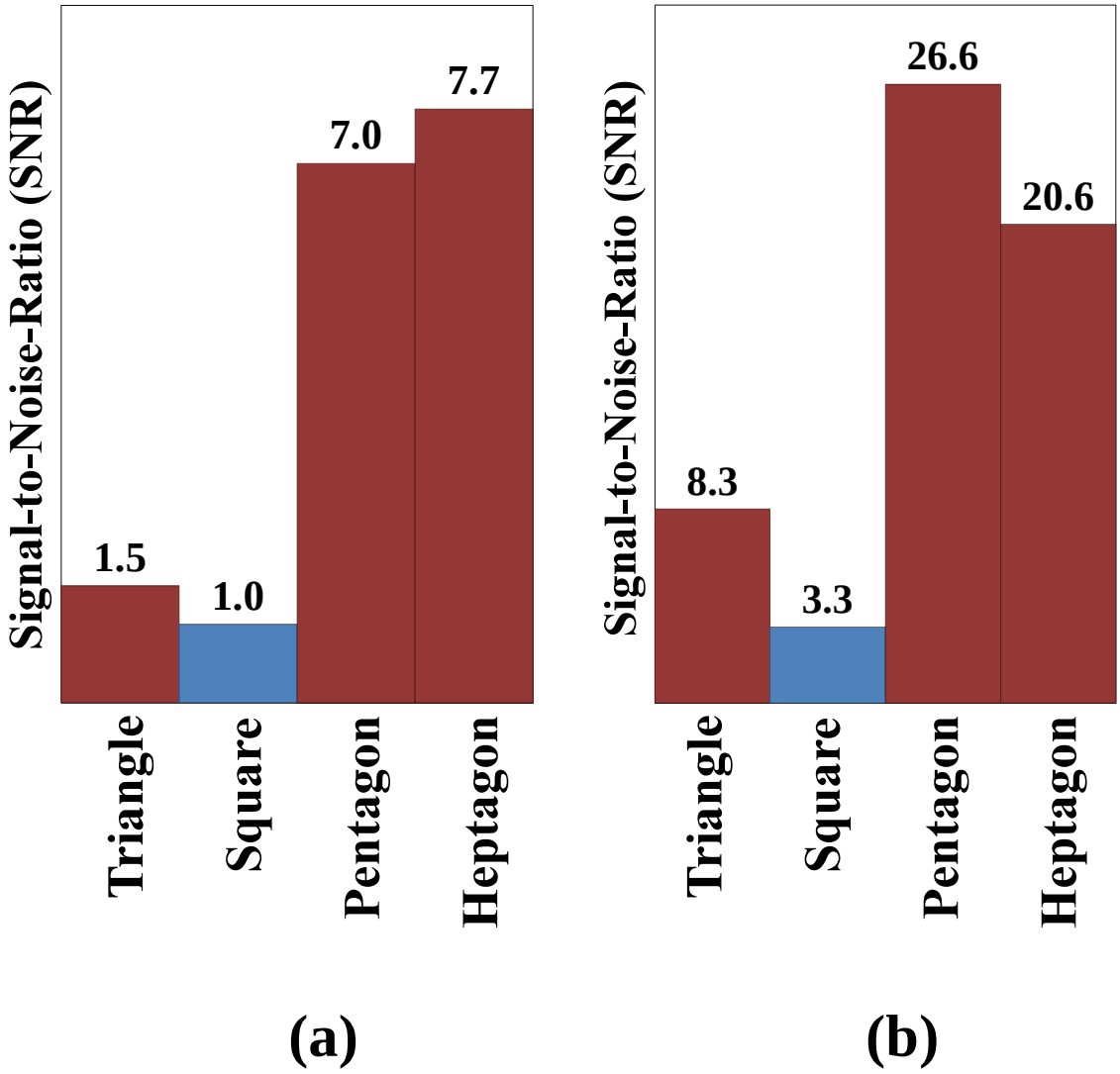

Figure 5-30: Signal-to-noise ratio (SNR) for (a) regular polygonal buffer rods and (b) irregular polygonal buffer rods based on the measured waveforms

5.5 Conclusions

The effectiveness of irregular polygon as the cross-sectional buffer rod in restraining the generation of trailing echoes has been investigated. It is found that:

1) The current guidelines that distorts only one vertex of a regular polygon is not suitable for even polygons that have six edges and more since the influence of parallel sides will still be remained. In addition, by such distortion, the second reflected shear waves (S_2) can still arrive at the side wall of the rod perpendicularly, as observed for the irregular square and irregular heptagon.

2) In order to overcome such problems, two vertices of a regular polygon should be distorted. The distortion point for these two vertices must be far from the initial regular points.

3) The new guidelines are:
   a) The influence of symmetry is eliminated by distorting two vertices of the regular polygon. The two vertices should be distorted at a point that is far from the initial regular points.
   b) For a fair comparison with the regular polygons, the two vertices should be distorted at a point where the area for both the regular and irregular polygons is constant. Therefore, the selection of which vertices that need to be distorted is important so that the area is constant.
   c) The influence of the parallel sides in the regular polygons is eliminated by the distortion on two vertices
   d) No new pairs of parallel sides are created by such distortion

4) The mechanism that shows the propagation of shear waves from each of the irregular polygons is verified from the wave propagation studies conducted during the numerical simulations.

5) Based on the proposed irregular polygons, the highest SNR is given by the irregular pentagon. Therefore, it can be concluded that although the current guidelines result to some obstacles, the current guidelines have successfully designed an irregular polygonal buffer rod with high SNR.

Chapter 6

General Conclusions and Future Works

The overall results from the three-dimensional numerical simulations and pulse-echo measurements on buffer rods having different cross-sectional shapes such as circle, regular polygons and irregular polygons are summarized. In addition, the obstacles that are found throughout this work are also addressed in this chapter. Further investigation for better outcome is also proposed.

6.1 General conclusions

1) Generation of trailing echoes

It is found that the generation of trailing echoes can be depicted from the cross-sectional shape itself where a trailing echo will be generated if the mode converted shear waves arrive at the side wall of the rod perpendicularly. Such arrival will produces longitudinal waves that are in-phase with the ultrasonic transducer. Therefore, interference will occur at the ultrasonic transducer and give the main signals such as main echoes and trailing echoes. Figure 6-1 shows how the first trailing echoes are generated for a cylindrical buffer rod where the first reflected shear waves (S_1) arrived at the side wall of the rod perpendicularly from the cross-sectional view. In addition, it is observed that S_1 are parallel to each other due to the geometry of circle.

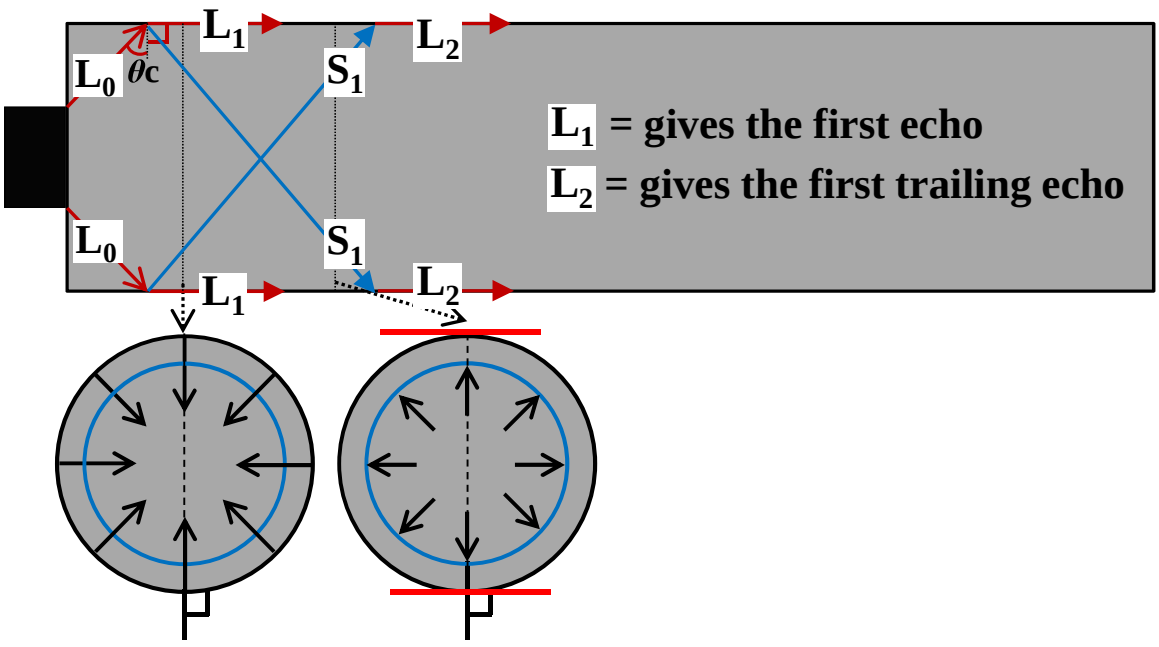

Figure 6-1: Mechanism to generate the first main echo and the first trailing echo for a cylindrical buffer rod, from the side view and cross-sectional view.

2) Regular polygonal buffer rods

It is found that odd polygons are better than even polygons since the first reflected shear waves are able to arrive at the side wall of the rod perpendicularly. Therefore, the generation of trailing echoes is restrained during the first reflection of shear waves. However, due to the bilateral symmetry shapes for all the odd regular polygons, trailing echoes can still be generated where the second reflected shear waves (S_2) arrived at the side wall of the rod and generate the first trailing echo. However, since the trailing echo is generated by S_2 rather than S_1, the amplitude of the trailing echo is expected to be small due to wave attenuation. Figure 6-2 shows the mechanism to generate the first trailing echo for a regular triangle (left) and a regular square (right). For triangle, the first trailing echo can only be generated by the second reflected shear wave (S_2) since the first reflected shear wave (S_1) did not arrive at the side wall of the rod perpendicularly. Meanwhile for square, it is observed that the first trailing echo is generated when the first reflected shear wave (S_1) arrived at the side wall of the rod perpendicularly. Therefore, based on this figure, it clearly shows why the regular odd polygons are better than the regular even polygons in improving the signal-to-noise ratio (SNR) although the generation of trailing echoes is still possible.

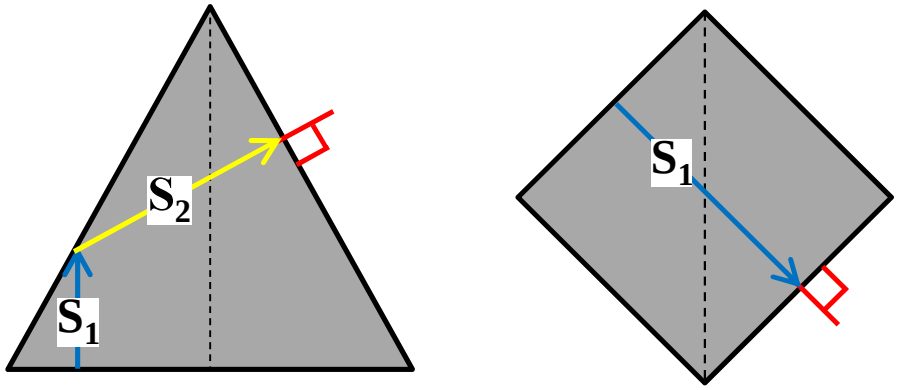

Figure 6-2: Generation of the first trailing echo due to the arrival of shear waves to the side wall of the rod perpendicularly for regular triangle (left) and regular square (right).

3) Irregular polygonal buffer rods

The signal-to-noise ratio (SNR) of the irregular polygonal buffer rods are improved except for the irregular hexagon due to some problems that arose based on the guidelines used in this work. The problems are:

a) The guidelines did not consider the propagation of the reflected shear waves after the first reflection, to the side wall of the rod. This is because it is found that some of the reflected shear waves can arrive at the side wall of the rod perpendicularly and generate the trailing echoes

b) The arrival of such problem stated in (a) is due to only one vertex of the regular polygon is distorted. In order to overcome such problem, two vertices of a regular polygon should be distorted so that the arrival of the reflected shear waves to the side wall of the rod perpendicularly can be restrained. In addition, by distorting only one vertex, the parallel sides in the regular even polygons that have the number of edge of six or more, will still be remained. Therefore, the new guidelines for designing the irregular polygons are:

i) The influence of symmetry is eliminated by distorting two vertices of a regular polygon

ii) The distortion point for these two vertices should be far from their initial regular point

iii) The influence of parallel sides is eliminated by such distortion

iv) The area is kept constant by choosing two vertices that will not alter the area of the irregular polygons.

v) No new parallel sides are generated by such distortion in (i).

The effectiveness of irregular polygons having two distorted vertices on improving the SNR is shown by the irregular heptagon. In addition, it is noteworthy to state that the current guidelines are good enough for producing an irregular polygonal buffer rod that can improve the SNR significantly. Such high performance irregular polygonal buffer rod is shown by the irregular pentagon where the value is five times higher than the regular pentagon buffer rod (simulation result).

4) Clad polygonal buffer rods

The SNR is significantly improved when the velocity of the clad is faster than that of the core where the mode converted shear waves are confined in the cladding region and restrained the generation of trailing echoes. The highest SNR is obtained when V_{clad} = 120% V_{core} and ρ_{clad} = 70% ρ_{core}. In addition, an interesting plateau of high SNR is obtained when the V_{clad} = 110% V_{core} and ρ_{clad} = 70 ~ 150% ρ_{core}. The validity of the findings is verified with materials that have faster velocity than the core which is steel. The materials for the cladding layer are zirconium oxide, molybdenum and titanium. Based on these clad materials, the highest SNR is shown by zirconium oxide since its material properties is V_{clad} = 119% V_{core} and ρ_{clad} = 73% ρ_{core} where closest to the clad properties that gives the highest SNR. Based on this verification, a cladding layer of zirconium oxide is applied on the regular polygonal buffer rods for improving the SNR. It is found that the SNR for all clad regular polygonal buffer rod improved tremendously.

Based on the findings that are obtained from the simulation and experimental works, it is proven that polygonal buffer rods can be a promising tool for improving the SNR. In addition, the mechanisms for preventing the trailing echoes and the appropriate cladding condition presented in this work can be useful for designing the optimum buffer rod.

6.2 Future works

1) It has been mentioned that the current guidelines in designing an irregular polygon is not suitable for the even polygons such as hexagon. Therefore, a new guideline is necessary for preventing the generation of trailing echoes in polygonal buffer rods completely. It has been mentioned that the new guideline should not focus on maintaining the half side of the regular polygon. The new guidelines:

(1) The influence of symmetry is eliminated by distorting two vertices of the regular polygon
(2) Such distortion in (1) is to prevent any of the reflected shear waves propagate to the side wall of the rod perpendicularly.
(3) By distorting two vertices of the regular polygons, the area is kept constant (if possible), so that the comparison between the regular and irregular polygons is fair.

2) The theoretical equation for estimating the time delay between the main echoes and trailing echoes in a cylindrical buffer rod is well known. The calculation on such time delay is possible if the velocity and diameter of the rod are known. In this work, it has been mentioned in Chapter 5 that such time delay obtained for a 100 mm length cylindrical buffer rod is used as a reference in predicting the arrival time of the first trailing echoes for the polygonal buffer rods. Although the path for generation the first trailing echoes was measured and compared between the polygonal buffer rods, such approach is not optimized. Therefore, a theoretical equation is needed for estimating the arrival time of a trailing echo in the polygonal buffer rods.

2) It has been proven that irregular polygonal buffer rods are effective in preventing the trailing echoes. Therefore, it would be interesting to apply the irregular polygonal buffer rods for the material characterization or process monitoring at high temperature. However, it may be some difficulty in mounting the irregular polygonal buffer rod in the machinery section due to sharp edges of polygonal rods. An additional layer is needed for the

threading purpose so that the irregular polygonal buffer rods can be mounted easily. By introducing a cladding layer, the small amplitudes are expected to be eliminated completely since the ultrasonic pulsed echoes in the core are well guided. Since the core is made of steel (S45C), the appropriate cladding material would be stainless steel where the pairing of steel and stainless steel has been used widely in many application at high temperature.

研究業績 (Research Achievements)

受賞(Awards)

[1] Won the 'Poster Award' by The Japanese Society for Non-Destructive Inspection (JSNDI) for her research on 'Numerical Study on the Cladding Effect in Ultrasonic Pulse-Echoes Propagating through Buffer Rods' at 21st Symposium on Ultrasonic Testing (2014.1.20)

[2] Won the 'New Research Award' by The Japanese Society for Non-Destructive Inspection (JSNDI) for her research on 'Designing the Polygonal Buffer Rods for Improving the Signal-to-Noise Ratio in Ultrasonic Pulse-Echo Measurements' at 22nd Symposium on Ultrasonic Testing (2015.1.30)

[3] Won the 'Best Oral Presentation Award' for her research on 'Newly Designed Waveguide Probes for Ultrasonic Pulse-Echo Measurements' at Malaysia-Japan Joint International Conference (MJJIC) (2015.11.15)

学術論文 (Academic Papers)

[1] Farhana Mohd Foudzi and Ikuo Ihara: Development of Polygonal Buffer Rods for Ultrasonic Pulse-Echo Measurements, *Journal of Physics: Conference Series*, IOP Publishing, vol.520, No. 1 (2014) pp. 012025-1-4.

[2] Farhana Mohd Foudzi and Ikuo Ihara: Numerical Study on Optimum Design of a Clad Waveguide for Ultrasonic Pulse-Echo Measurements with High Signal-to-Noise Ratio, *Mechanical Engineering Letters*, vol.2 (2016) pp. 15-00727-1-8.

講演論文 (Lecture paper)
国際会議（査読あり）(International Conference, peer review)

[1] Farhana Mohd Foudzi and Ikuo Ihara: Development of Polygonal Buffer Rods for Ultrasonic Pulse-Echo Measurements, 3rd International Symposium on Laser Ultrasonics and Advanced Sensing (LU2013), pp. 71, 2013.6.25-28. (Yokohama, Japan).

国際会議（査読なし）(International Conference, no peer review)

[1] Farhana Mohd Foudzi and Ikuo Ihara: Optimized Buffer Rods for High Temperature Monitoring in Ultrasonic Pulse-Echo Measurement, 4th International GIGAKU Conference in Nagaoka (IGCN), pp. 80 2015.6.19-21 (Nagaoka, Japan)

[2] Farhana Mohd Foudzi and Ikuo Ihara: Newly Designed Waveguide Probes for Ultrasonic Pulse-Echo Measurements, Malaysia-Japan Joint International Conference (MJJIC2015), 2015.11.13-15 (Yamaguchi, Japan)

国内学会

[1] Farhana Mohd Foudzi and Ikuo Ihara: Optimized Buffer Rods for High Temperature Monitoring in Ultrasonic Pulse-Echo Measurement, USE2013 Symposium on Ultrasonic Electronics, pp. 241-242, 2013.11.20-22, (Kyoto)

[2] Farhana Mohd Foudzi and Ikuo Ihara: Numerical Study on the Cladding Effect in Ultrasonic Pulse-Echoes Propagating through Buffer Rods, 21st Symposium on Ultrasonic Testing, pp. 69-70, 2014.1.20-21, (Tokyo)

[3] Farhana Mohd Foudzi and Ikuo Ihara: Polygonal Buffer Rods having Irregular Cross-Sectional Shapes for Improving the SNR in Ultrasonic Pulse-Echo Measurements, USE2014 Symposium on Ultrasonic Electronics, pp. 231-232, 2014.12.3-5, (Tokyo)

[4] Farhana Mohd Foudzi and Ikuo Ihara: Designing the Polygonal Buffer Rods for Improving the Signal-to-Noise Ratio in Ultrasonic Pulse-Echo Measurements, 22nd Symposium on Ultrasonic Testing, pp. 89 – 90, 2015.1.29-30, (Tokyo)

[5] Farhana Mohd Foudzi and Ikuo Ihara: Designing the Ultrasonic Waveguide Probes with High S/N Ratio for Materials and Process Monitoring, 23rd Mechanical and Materials Processing, 4 pages, 2015.11.13-15, (Hiroshima)

- 受賞 (Awards) : 3
- 学術論文 (Academic Papers) : 2
- 国際会議講演論文（査読有り） : 1
- 国際会議講演論文（査読なし）: 2
- 国内学会講演論文 : 5